AD-A248 132

WL-TR-91-2106

2

WRIGHT LABORATORY

A NUMERICAL AND EXPERIMENTAL INVESTIGATION OF AN INNOVATIVE AND EFFICIENT ENERGY RELEASE/STORAGE SYSTEM

Kambiz Vafai
Department of Mechanical Engineering
The Ohio State University
206 West 18th Avenue
Columbus, OH 43210-1107

30 December 1991

Final Report for Period Sept 89 - Jan 91

Approved for public release; distribution is unlimited

PROPULSION & POWER DIRECTORATE
WRIGHT LABORATORY
AIR FORCE SYSTEMS COMMAND
WRIGHT PATTERSON AIR FORCE BASE, OHIO 45433-6563

Best
Available
Copy

NOTICE

When Government drawings, specifications, or other data are used for any purpose other than in connection with a definitely Government-related procurement, the United States Government incurs no responsibility or any obligation whatsoever. The fact that the government may have formulated or in any way supplied the said drawings, specifications, or other data, is not to be regarded by implication, or otherwise in any manner construed, as licensing the holder, or any other person or corporation; or as conveying any rights or permission to manufacture, use, or sell any patented invention that may in any way be related thereto.

This report is releasable to the National Technical Information Service (NTIS). At NTIS, it will be available to the general public, including foreign nations.

This technical report has been reviewed and is approved for publication.

Won S. Chang

WON S. CHANG
Project Engineer

Jerry E. Beam

JERRY E. BEAM, TAM
Power Technology Branch
Aerospace Power Division
Aero Propulsion and Power Laboratory

William U. Borger

WILLIAM U. BORGER
Chief, Aerospace Power Division
Aero Propulsion & Power Laboratory

If your address has changed, if you wish to be removed from our mailing list, or if the addressee is no longer employed by your organization please notify WL/POOS, WPAFB, OH 45433-6563 to help us maintain a current mailing list.

Copies of this report should not be returned unless return is required by security considerations, contractual obligations, or notice on a specific document.

REPORT DOCUMENTATION PAGE

Form Approved
OMB No. 0704-0188

1a. REPORT SECURITY CLASSIFICATION: Unclassified

1b. RESTRICTIVE MARKINGS:

2a. SECURITY CLASSIFICATION AUTHORITY:

2b. DECLASSIFICATION/DOWNGRADING SCHEDULE:

3. DISTRIBUTION/AVAILABILITY OF REPORT: Approved for public release, distribution is unlimited

4. PERFORMING ORGANIZATION REPORT NUMBER(S): RF Project No. 767829/722598

5. MONITORING ORGANIZATION REPORT NUMBER(S): WL-TR-91-2106

6a. NAME OF PERFORMING ORGANIZATION: The Ohio State University Research Foundation

6b. OFFICE SYMBOL (If applicable): OSURF

6c. ADDRESS (City, State, and ZIP Code): 1960 Kenny Road, Columbus, OH 43210-1063

7a. NAME OF MONITORING ORGANIZATION: Aero Propulsion & Power Dir (WL/POOS) Wright Laboratory

7b. ADDRESS (City, State, and ZIP Code): Wright-Patterson AFB, OH 45433-6563

8a. NAME OF FUNDING/SPONSORING ORGANIZATION: Department of the Air Force

8b. OFFICE SYMBOL (If applicable): AFSC

8c. ADDRESS (City, State, and ZIP Code): Air Force Systems Command, Aeronautical Systems Division, Wright-Patterson Air Force Base, OH 45433

9. PROCUREMENT INSTRUMENT IDENTIFICATION NUMBER: F33615-89-C-2949

10. SOURCE OF FUNDING NUMBERS

PROGRAM ELEMENT NO.	PROJECT NO.	TASK NO	WORK UNIT ACCESSION NO.
63221C	D812	00	18

11. TITLE (Include Security Classification): A Numerical and Experimental Investigation of an Innovative and Efficient Energy Release/Storage System

12. PERSONAL AUTHOR(S): Kambiz Vafai

13a. TYPE OF REPORT: Final

13b. TIME COVERED: FROM Sept 89 TO Jan

14. DATE OF REPORT (Year, Month, Day):

15. PAGE COUNT: 167

16. SUPPLEMENTARY NOTATION:

17. COSATI CODES

FIELD	GROUP	SUB-GROUP

18. SUBJECT TERMS (Continue on reverse if necessary and identify by block number)

19. ABSTRACT (Continue on reverse if necessary and identify by block number)

This work is composed of a set of investigations related to the single and multiphase transport processes in packed beds, and the behavior of sensible and latent heat storage packed beds. The main objective of this work was to analyze different aspects of the applications of packed beds by considering a set of problems which were designed to provide physical insight for a number of outstanding points related to transport phenomena in porous media as well as different packed bed energy storage systems including sensible heat storage and latent heat storage ones.

20. DISTRIBUTION/AVAILABILITY OF ABSTRACT: ☒ UNCLASSIFIED/UNLIMITED ☐ SAME AS RPT ☐ DTIC USERS

21. ABSTRACT SECURITY CLASSIFICATION: Unclassified

22a. NAME OF RESPONSIBLE INDIVIDUAL: W. S. Chang

22b. TELEPHONE (Include Area Code): 513-255-2922

22c. OFFICE SYMBOL: WL/POOS

FOREWORD

The information in this report was assembled for contract #F33615-89-C-2949 with the Aero Propulsion and Power Directorate. This is the final report on this contract. The work was carried out at the Department of Mechanical Engineering at The Ohio State University.

Five tasks were performed as outlined in the Table of Contents. The work was composed of a set of investigations related to the single and multiphase transport processes in packed beds, and the behavior of sensible and latent heat storage packed beds. The main objective of this work was to analyze different aspects of the applications of packed beds by considering a set of problems which were designed to provide physical insight for a number of outstanding points related to transport phenomena in porous media as well as different packed bed energy storage systems including sensible heat storage and latent heat storage. Five journal publications related to the present work are now available in the open literature. The graduate research assistant involved in different parts of this work was Mr. M. Sozen. Dr. Won Chang from Wright Laboratory was the technical supervisor for this contract and the author is grateful to him for his discussions and comments. Support from Dr. Jerry Beam and Dr. Tom Mahefkey from Wright Laboratory is also greatly appreciated.

TABLE OF CONTENTS

LIST OF FIGURES

NOMENCLATURE

a_{sv}	specific surface area common to solid and vapor phases, $m^2\ m^{-3}$
$a_{\sigma\beta}$	specific surface area common to σ and β phases, $m^2\ m^{-3}$
$a_{\sigma\gamma}$	specific surface area common to σ and γ phases, $m^2\ m^{-3}$
A	constant in equation (3.9), 23.4851064
A	amplitude of pressure oscillation, kPa (Section VI)
B	constant in equation (3.9), 2969.2287, K^{-1}
B	amplitude of temperature oscillation, K (Section VI)
c_p	specific heat at constant pressure, $J\ kg^{-1}\ K^{-1}$
d_p	particle diameter, m
Da	Darcy number, K/H^2
f	frequency of oscillation, Hz
F	geometric factor defined in equation (2.10)
$\vec{g}$	gravitational acceleration, $m\ s^{-2}$
G	mass velocity, $kg\ m^{-2}\ s^{-1}$
h_{sv}	fluid-to-particle heat transfer coefficient, $W\ m^{-2}\ K^{-1}$
h_{sf}	specific latent heat of fusion, $J\ kg^{-1}$
$h_{\sigma\beta}$	fluid-to-particle heat transfer coefficient between σ and β phases, $W\ m^{-2}\ K^{-1}$
$h_{\sigma\gamma}$	fluid-to-particle heat transfer coefficient between σ and γ phases, $W\ m^{-2}\ K^{-1}$
H	height of the packed bed, m
k	thermal conductivity, $W\ m^{-1}\ K^{-1}$
$k_{r\beta}$	relative permeability for fluid phase
$k_{<T>}$	coefficient of capillary pressure gradient with respect to temperature, $N\ m^{-2}$
k_{ε}	coefficient of capillary pressure with respect to liquid volume fraction, $N\ m^{-2}$
K	permeability, m^2

L	length of the packed bed, m
LHSPB	latent heat storage packed bed
LTE	local thermal equilibrium
$\dot{m}$	condensation rate, kg m^{-3} s^{-1}
P	pressure, N m^{-2}
PCM	phase change material
R	gas constant for refrigerant-12, J kg^{-1} K^{-1}
Re_p	particle Reynolds number, $\rho_\gamma v^* d_p/\mu_\gamma$
s	saturation, $\varepsilon_\beta/\varepsilon$
S	normalized saturation, $(s-s_{im})/(1-s_{im})$
SHSPB	sensible heat storage packed bed
t	time, s
T	temperature, K
T_{melt}	melting temperature of PCM, K
u	velocity component in x-direction, m s^{-1}
V	volume, m^3
$\vec{v}$	velocity vector, m s^{-1}
α	thermal diffusivity, m^2 s^{-1}
ε	porosity
ε_β	volume fraction of liquid phase
ε_γ	volume fraction of vapor phase
ε_σ	volume fraction of solid phase
Δh_{vap}	latent heat of vaporization for Refrigerant-12, J kg^{-1}
Θ	dimensionless temperature, $(T-T_o)/(T_{in}-T_o)$
μ	absolute viscosity, kg m^{-1} s^{-1}

ρ	density, kg m^{-3}
$\rho_{\gamma,s}$	saturation vapor density, kg m^{-3}
τ	dimensionless time, tu*/L

<u>Subscripts</u>

av	average inlet
f	fluid (liquid+vapor)
feff	effective property for fluid
in	inlet
o	initial
s	solid
seff	effective property of solid
v	vapor
veff	effective property of vapor
β	liquid
γ	vapor
σ	solid
σeff	effective property for solid

<u>Superscripts</u>

f	fluid (liquid+vapor)
s	solid
v	vapor
β	liquid
γ	vapor
σ	solid

*	reference

Symbols

< >	"local volume average" of a quantity

SECTION I

1.1 Objectives

This report presents a series of investigations that have been carried out for the application of a packed bed (with encapsulated phase change material-PCM) as an energy storage/release unit for spacecraft thermal management systems. In this regard, relevant studies performed in the Department of Mechanical Engineering at The Ohio State University before and during the course of the Contract F33615-89-C-2949 have been assembled in this report for integrity of the material presented. The fundamental studies performed form an integral part of the preliminary investigations for the actual application, and these will be presented sequentially in the present report.

A set of investigations related to the single and multiphase transport processes in packed beds, and the behavior of sensible and latent heat storage packed beds was carried out. The main objective of this work was to analyze different aspects of the applications of packed beds by considering a set of problems which were designed to provide physical insight for a number of outstanding points related to transport phenomena in porous media as well as different packed bed energy storage systems including sensible heat storage and latent heat storage ones.

1.2 Introduction

Packed beds with single-phase flow have been analyzed in applications ranging from chemical catalytic reactors and pebble bed or rock pile heat storage units to fixed-bed nuclear propulsion systems and spacecraft thermal management systems employing packed beds of encapsulated phase change materials. A major part of the studies conducted to date

on packed bed applications with single-phase flow concentrates on utilizing incompressible fluids, liquid or gas, as the heat transporting medium. In these investigations a constant mass flow rate is assumed at every cross section of the packed bed and, therefore, there is no need for solving any continuity or momentum equations. The problem reduces to solving the governing energy equations for the solid and fluid phases. For this category of problems, the two commonly employed models are the so called single-phase conductivity and two-phase Schumann models. The main distinction between these two models is that, where local thermal equilibrium is assumed to prevail between the solid and the fluid phases in the single-phase model, no such assumption is made in the two-phase model. Therefore, the single phase conductivity model reduces to one governing energy equation in which conduction in both phases is taken care of by the use of an effective thermal conductivity, where in the two-phase model there are two governing energy equations, each of them possessing a fluid-to-solid convective heat transfer term. The origin of the two-phase models is the classical Schumann model (Schumann, 1929). Riaz (1977) presented an investigation and comparison of both the single-phase conductivity model as well as the two-phase Schumann model. From a theoretical point of view, both of these models are quite inadequate because they incorporate many simplifying assumptions, such as neglecting the transient heat storage and the conduction terms in the fluid phase.

The second major class of problems dealing with the single-phase flow through porous media studied to date concentrates on the compressible gas flow through a porous medium. It is essential to consider a compressible working fluid--hence, an equation of state for the vapor phase--in studying multiphase flow with phase change in porous media. In this category of problems too, there is a lack of analysis of the complete transient, non-isothermal and nonthermal equilibrium flow of a compressible gas. One-dimensional, transient, isothermal flow of an ideal gas through a porous medium has been studied

analytically by the use of perturbation methods by Kidder (1957). Morrison (1972) also obtained analytical solutions by perturbation methods for one-dimensional isothermal and adiabatic flows of an ideal gas. In both of these investigations Darcy's formulation has been used for fluid flow. Nilson (1981), on the other hand, obtained an analytical solution for one-dimensional isothermal flow through a porous medium in a study which utilized Ergun's equation (Ergun, 1952) to account for the inertial effects. In all of these investigations it was assumed that the gas phase was in local thermal equilibrium with the solid phase. Goldstein and Siegel (1971) performed an analytical investigation on a steady, nonisothermal ideal gas flow in a porous medium. They also utilized the local thermal equilibrium assumption in the governing energy equation and Darcy's formulation for fluid flow. Most of these studies which incorporated Darcy's formulation for fluid motion have the drawback of not being applicable to high speed flows in which the inertia effects have to be accounted for.

It can be seen that the models used in both categories of problems described above are incomplete in one aspect or another since they concentrate on either the momentum transport in an isothermal or adiabatic flow or the energy transport in an incompressible flow. In addition they incorporate some simplifying assumptions such as local thermal equilibrium between the solid and the fluid phases, neglect of conduction and transient storage terms in the gas phase energy equation, and neglect of inertial effects in the fluid phase momentum equations. Therefore, their application is limited to certain special cases. These cause a need for a more rigorous formulation of the transport processes in a porous medium for establishing a more flexible and reliable model with a wide range of applicability. The main objective of Section II is to present a rigorous analysis and investigation for transient transport processes in a compressible gas flow through a packed bed with no assumption of local thermal equilibrium between the solid and fluid phases.

Ergun-Forchheimer relation will be employed as the vapor phase momentum equation in order to account for the inertia effects in addition to the viscous effects. This is very essential for non-Darcy regime flows in porous media. More specifically, it is essential in flows with particle Reynolds numbers greater than 0.1 in which Darcy formulation becomes inaccurate. This point has been neglected in many of the previous studies dealing with single and multiphase transport phenomena in porous media. Likewise, the majority of the previous works on multiphase transport in porous media almost exclusively employ local thermal equilibrium (LTE) between the solid and fluid phases considered. This assumption is usually not satisfactory for the step change problems in which, during the early stages of the transport processes, there may be considerable difference between the temperatures of the flowing fluid and solid particles. This is also true even during the later stages of the transport processes in high-speed flows or high permeability porous media in which the fluid-to-solid interaction time or interaction surface area respectively may not be large enough for the temperatures of the fluid and solid phases to become close enough for LTE to be a reasonable assumption. The thermal interactions between the vapor and the solid phases, and how the fluid flow as well as the pressure and density fields are affected by these interactions will be analyzed in detail. Another objective of Section II is to gain a better understanding of the situations under which the local thermal equilibrium assumption and one- or two-dimensional consideration of certain field variables would be justifiable. In this regard the effect of certain characteristic nondimensional parameters, such as the particle Reynolds number, the Darcy number and certain thermophysical parameters, on the general qualitative behavior of the transport phenomena in packed beds will be investigated thoroughly.

One further step into these studies leads to multiphase flow of a single pure substance in liquid and vapor form, and the accompanying transport processes in packed beds. The

flow of a mixture of a vapor and noncondensible gases, such as air and water vapor, through a porous medium, and the accompanying phase change (condensation) and the multiphase transport processes involved have received considerable attention in a number of investigations related to different applications. These include phase change in building insulation materials (Vafai and Whitaker, 1986; Vafai and Sarkar, 1986; Ogniewicz and Tien, 1981), heat pipe technology (Udell, 1985), drying of different porous materials (Berger and Pei, 1973; Plumb *et al.*, 1985), and phase change in porous media (Eckert and Pfender, 1980; Motakef and El-Masri, 1986). The condensing flow of a single vapor through a porous medium, on the other hand, received relatively little attention (Nilson and Montoya, 1980). A rigorous model which includes the basic thermodynamics of the condensation process and the concept of nonthermal equilibrium between the solid and the fluid phases under condensing conditions seem to be completely absent. This fact is the main motivation for the investigation in Section III, which is aimed at analyzing the forced convective condensing flow of a vapor through a packed bed. This is an essential fundamental study for the application of thermal energy storage/release system for rejection of heat in pulsed space power supplies and some conceptual spacecraft thermal management systems. The operating conditions of the packed beds for such applications may require gas/vapor flow at high speeds as well as high pressures, which in turn will dictate condensation of the working fluid. This may actually be desirable in order to enhance the amount of thermal energy stored in the packed bed.

For analyzing the problem in Section III, the model established for single-phase vapor flow in Section II will be expanded such that it will accommodate the liquid phase in addition to the vapor phase of the working fluid. This will be carried out by additional conservation equations for the liquid phase as well as accommodations for the phase change terms in the already available conservation equations for the vapor phase.

Moreover, the thermodynamic aspects of the condensation process which will introduce an additional coupling relation will be presented.

A further stage of this study is concerned with the application of an encapsulated phase change material (PCM) as an energy storage medium in packed beds. This problem will be taken up in Section IV. The earlier forms of the packed bed energy storage units solely relied on the sensible heat capacity of the solid bed particles for storing thermal energy. This form has been satisfactorily employed for various applications. However, certain applications may impose a limitation on the size and the weight of the packed bed system utilized. For instance, the present application of a heat rejection system in pulsed space power supplies which incorporate packed beds, the reduction of the mass and volume is of utmost importance. In such cases, utilization of only the sensible heat capacity of a certain material for energy storage will most likely prove to be inefficient. The remedy to this can be found in the utilization of latent heat in the process of energy storage. Recently, encapsulated phase change materials (PCM) have received considerable attention as energy storage materials. The use of an encapsulated PCM is very appealing since it makes the utilization of latent heat storage capacity possible. This is achieved by using a PCM which has a melting temperature within the temperature range of operation of the system incorporating the packed bed. The principal advantage of PCMs in packed beds is that the energy storage density of the bed is increased significantly and thus, the size and mass of the storage system required for a particular application are reduced proportionally.

Different PCMs have been considered for use in the packed bed energy storage units in different applications. For applications over 450^{o}C significant consideration was given to salts by Marianowski and Maru (1977). The physical properties of different PCMs considered for storage of solar energy have been presented by Lane (1986). A number of

studies have been carried out on the analysis of latent heat storage packed beds by different researchers. Ananthanarayanan *et al.* (1987) investigated the dynamic behavior of a packed bed which utilized encapsulated Al-Si shots which have a melting temperature of 577°C. Air was used as the energy transporting fluid in their study. Pitts and Hong (1987) presented another study on transient thermal behavior of a latent heat storage packed bed which utilized an inorganic compound hydrate PCM, namely $Na_2HPO_3.12H_2O$, as the heat storage medium. Torab and Chang (1988) investigated the use of encapsulated phase change materials for thermal energy storage units in space power systems. They reported an analysis of a latent heat storage packed bed which utilized lithium hydride as the PCM, and lithium as the transport fluid.

In the majority of models employed in the analysis of this category of problems, the superficial velocity of the working fluid is assumed to be constant. This reduces the system of governing equations to a set of energy equations for the working fluid and for the PCM respectively. As pointed out before, although this is a satisfactory approach when the working fluid is incompressible, it is not so when the working fluid is a gas or vapor under high pressures. Moreover, when the working fluid itself undergoes phase change (condensation), a rigorous model which consists of the governing energy, mass and momentum balance equations in addition to the relevant coupling thermodynamic relations has to be employed for analyzing any phase change and the corresponding transport phenomena. In Section IV the analysis of such a problem with a rigorous model which will basically be the expansion of the model developed in Section III will be presented. The physical aspects of the phase change process in the PCM will be modeled and analyzed.

The main objective of Section IV is to analyze the energy storage characteristics of packed beds which utilize phase change materials in the bed particles. Time history of the crucial field variables such as the temperature profiles of the working fluid and the bed particles, and the velocity, density and pressure of the working fluid will be determined. The determination of these quantities is important since the amount of energy flowing into and out of the packed bed, and hence the amount of energy stored in the packed bed as a function of time, can be determined from the time histories of these variables.

The operation of the packed bed as an energy storage/release system requires the analysis of the transient behavior of the packed bed in thermal charging and thermal discharging modes. This behavior for both sensible and latent heat storage packed beds is investigated in Section V in order to determine the qualitative and quantitative characteristics of the two types of packed beds and the difference between their characteristics. This is performed by extending the analysis in Section IV to include the thermal discharging mode operation of both types of packed beds.

The final section of the report deals with the analysis of oscillating flow through a packed bed. This investigation is carried out in order to determine the characteristics of the packed bed systems under more realistic boundary conditions than the ideal conditions. For this reason, oscillating temperature or pressure inlet boundary conditions are employed in the case studies in Section VI. The importance of such boundary conditions on the energy storage behavior of the packed bed system is investigated.

SECTION II

ANALYSIS OF TRANSPORT PHENOMENA IN A SINGLE-PHASE FLOW OF A GAS IN A PACKED BED

In this section, the model developed for analyzing the single-phase fluid flow and transport processes in a packed bed is presented. The numerical method of solution is discussed. A benchmarking that was carried out for verification of the results of the numerical code developed in the present work is also presented. This is followed by the presentation and a thorough discussion of the case studies performed and the result obtained.

2.1 Statement of the problem

The problem that will be investigated in this section is the transfer and storage of heat from a high temperature reservoir into a packed bed which consists of randomly packed spherical particles of uniform size. The schematic diagram of the problem considered is depicted in Figure 2.1. The extent of the packed bed in the z-direction is assumed to be large enough so that the problem will essentially be two-dimensional. Superheated Refrigerant-12 is used as the energy transport medium, i.e., the fluid phase flowing through the packed bed. Refrigerant-12 (known as R-12, or dichloro-difluoro-methane) was chosen as the vapor phase because it is a highly inert and stable compound whose critical point is well above the range of temperatures considered in the present study. Moreover, it has a relatively high vapor density making it capable of carrying more thermal energy, and thus requiring smaller volume flow rate for a certain application, than the

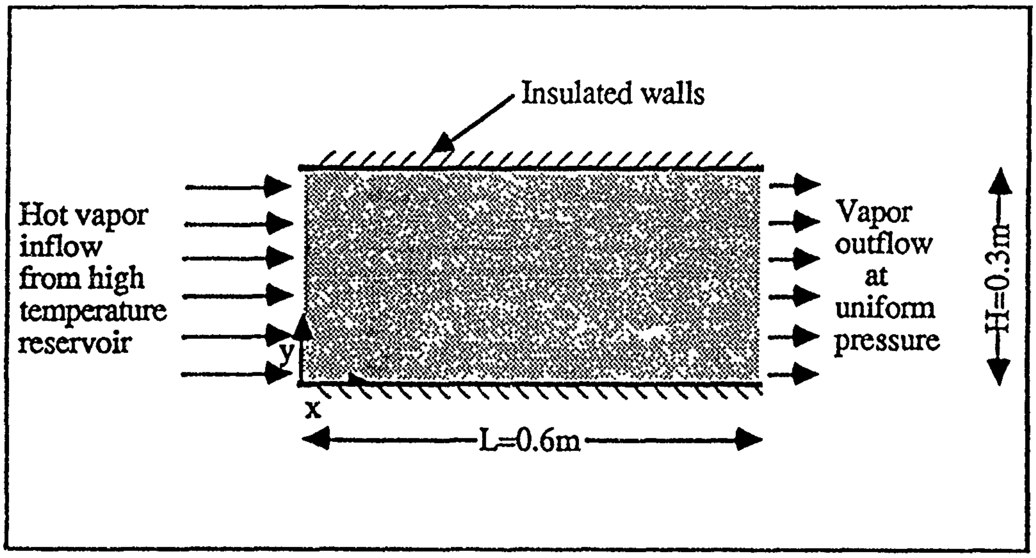

Figure 2.1: Schematic diagram of the problem

typical gases such as air. Different materials will be considered for solid particles in order to determine the effect of different thermophysical parameters on the associated transport processes. In this problem, the high temperature vapor in the reservoir is suddenly allowed to flow through the packed bed initially filled by R -12 which is also initially at a uniform temperature and pressure throughout the packed bed. The pressure in the reservoir is higher than the initial pressure in the packed bed and it remains unchanged. A uniform pressure equal to the initial pressure in the packed bed is maintained at the exit of the bed so that there is always a pressure difference between the left hand and the right-hand sides of the bed, thus sustaining the vapor flow. In essence this is a forced convection flow through a packed bed. Therefore, relatively higher particle Reynolds number flows than the Darcy regime flows are considered. Since the Darcy formulation would fail for these flows, Ergun-Forchheimer relation is employed instead, in order to account for the inertial effects as well as the viscous effects. The problem is analyzed for the case in which the two horizontal walls of the packed bed are maintained at constant temperature.

2.2 Mathematical model

The governing equations for the transport processes in porous media are developed here by using the "local volume averaging" technique. This method enables us to express the governing equations in a localized macroscopic sense for the porous media, which would otherwise require a very complex microscopic analysis that does not seem to be feasible even with the most advanced computational facilities. The fundamentals of the application of this technique to porous media are outlined by Whitaker (1977) in his work on drying of porous media. In this work the governing conservation equations have been derived for Darcy flow cases. Gray (1975) also presented an extension on the application

of the volume averaging technique to convective and diffusive terms in the governing equations. The volume averaging process is performed by associating a small volume V closed by a surface S with every point in the porous medium. The two important averages of a quantity frequently encountered in the governing equations are the so called local volume average and the intrinsic phase average. The local volume average of a quantity Φ associated with phase Ψ is defined as:

$$< \Phi > = \frac{1}{V} \int_{V_\Psi} \Phi \, dV \tag{2.1}$$

while the intrinsic phase average of a quantity Φ associated with phase Ψ is defined as:

$$< \Phi >^{\Psi} = \frac{1}{V_\Psi} \int_{V_\Psi} \Phi \, dV \tag{2.2}$$

where V_Ψ is the volume associated with phase Ψ. With this formulation it becomes reasonable to represent the intrinsic properties such as the temperature and the density of a phase by the intrinsic phase averaged quantities, and to represent the frequently used "superficial velocity" by the local volume averaged quantity.

Considerable information regarding the application of the spatial-averaging theorem for establishing the local volume averaged forms of the conservation equations for the convective and diffusive flows in porous media, and the models formed by using this principle for such problems can be found in the works of Vafai and Whitaker (1986), and Vafai and Tien (1981). The same methodology is used in the present work for establishing the model for analyzing the energy and momentum transfer in the packed bed with forced convective flow. The major assumptions and simplifications that are employed in this study are:

(1) Refrigerant-12 used as the vapor phase obeys the ideal gas equation of state, and the operation range is chosen such that it is always in the superheated form.

(2) Natural convection effects are negligible. This is a very reasonable assumption based on the fact that the bed is dominated by forced convection.

(3) The solid phase is incompressible, and the packed bed is assumed to have uniform porosity and to be isotropic.

(4) Boundary and variable permeability effects are neglected in the vapor phase momentum equation.

(5) The temperature range used in the analysis of the problem is relatively small (20K); therefore, the variation of physical properties, such as thermal conductivity, viscosity and specific heat capacity, with temperature is neglected.

(6) Due to the relatively low temperature range considered in the present study the inter-particle and intra-particle radiation heat transfer is negligible.

With these points taken into consideration the volume-averaged governing equations can be established in the following form by applying the volume averaging technique to the fundamental flow and energy equations in a porous medium:

Vapor phase continuity equation:

The volume averaged form of the vapor continuity equation for a compressible fluid takes the following form:

$$\frac{\partial}{\partial t}(\varepsilon < \rho_v >^v) + \nabla.(< \rho_v >^v < \vec{v}_v >) = 0 \qquad (2.3)$$

Vapor phase momentum equation:

The vapor phase momentum equation which incorporates the inertia effects as well as viscous effects by the use of Ergun-Forchheimer relation can be written as (Vafai, 1984):

$$\nabla < P_v >^v = -\frac{< \rho_v >^v F\varepsilon}{K_v^{1/2}}[< \vec{v}_v > . < \vec{v}_v >]\frac{\vec{v}_v}{|\vec{v}_v|} - \frac{\mu_v}{K_v} < \vec{v}_v > \tag{2.4}$$

In this equation, the first term on the right-hand side represents the inertia effects or the pressure drop due to form drag resistance of the packed bed, while the second term represents the pressure drop due to viscous effects. Without the first term, the equation reduces to Darcy equation.

When assumption (2) above is incorporated into this equation, the vapor flow essentially becomes one-dimensional and it assumes the following form:

$$\frac{\partial < P_v >^v}{\partial x} = -\frac{< \rho_v >^v F\varepsilon}{K_v^{1/2}} < u_v >^2 - \frac{\mu_v}{K_v} < u_v > \tag{2.4a}$$

Vapor phase energy equation:

$$\begin{aligned} &\varepsilon < \rho_v >^v c_{p_v} \frac{\partial < T_v >^v}{\partial t} + c_{p_v} < \rho_v >^v < \vec{v}_v > . \nabla < T_v >^v \\ &= \nabla . \left\{ k_{veff} \nabla < T_v >^v \right\} + h_{sv} a_{sv} (< T_s >^s - < T_v >^v) \end{aligned} \tag{2.5}$$

This equation accounts for conduction and transient storage of energy in the vapor phase as well as the transport of sensible heat by the vapor motion. Vapor-to-solid heat transfer is modeled by a convective heat transfer term by the use of a fluid-to-solid heat transfer coefficient.

Solid phase energy equation:

$$(1-\varepsilon)\rho_s c_{p_s} \frac{\partial \langle T_s \rangle^s}{\partial t} = \nabla . \left\{ k_{seff} \nabla \langle T_s \rangle^s \right\} - h_{sv} a_{sv} \left(\langle T_s \rangle^s - \langle T_v \rangle^v \right) \tag{2.6}$$

This equation follows similarly as in the case of the vapor phase energy equation except that there is no sensible energy transport due to motion.

Vapor phase equation of state:

From the ideal gas law, the equation of state can be written as:

$$\langle P_v \rangle^v = \langle \rho_v \rangle^v R_v \langle T_v \rangle^v \tag{2.7}$$

In the equations presented above, the effective thermal conductivities for the solid and the vapor phases were modeled in the following form:

$$\begin{aligned} k_{veff} &= \varepsilon\, k_v \\ k_{seff} &= (1-\varepsilon)\, k_s \end{aligned} \tag{2.8}$$

The permeability of the packed bed, K_v, and the geometric function F in the vapor momentum equation can be obtained from the experimental results of Ergun (Ergun, 1952; Vafai, 1984) in terms of the porosity, ε, and the particle diameter, d_p, as follows:

$$K_v = \frac{\varepsilon^3 d_p^2}{150(1-\varepsilon)^2} \tag{2.9}$$

$$F = \frac{1.75}{\sqrt{150}\ \varepsilon^{3/2}} \tag{2.10}$$

In equations (2.5) and (2.6), a_{sv} represents the specific surface area of the packed bed, i.e., the surface area of the solid particles per unit bulk volume of the packed bed. Based on geometrical considerations, this ratio can be expressed in terms of the particle diameter and porosity as (Dullien, 1979):

$$a_{sv} = \frac{6(1-\varepsilon)}{d_p} \tag{2.11}$$

For the fluid-to-particle heat transfer coefficient, h_{sv}, it is necessary to choose an empirical correlation from a range of available experimental results. Considerable amount of experimental work has been carried out for determining this quantity for packed beds for different sizes, shapes and packing configurations of solid particles. Typical experimental investigations and some reviews on fluid-to-particle heat transfer coefficients may be found in the works of Baumeister and Bennett (1958), Bhattacharyya and Pei (1975) and Barker (1965). Considering the ranges of the particle diameter, d_p, and the particle Reynolds number, Re_p, used in this investigation, the empirical correlations established by Gamson et al. (1943) were found to be appropriate for use in the present work. These empirical correlations which were presented in terms of Colburn-Chilton j_h factors can be expressed in the following form after some manipulation:

$$h_{sv} = 1.064\, c_p G \left(\frac{c_p \mu}{k}\right)^{-2/3} \left(\frac{d_p G}{\mu}\right)^{-0.41} \quad \text{for} \quad \frac{d_p G}{\mu} \geq 350 \quad \text{(turbulent)} \tag{2.12}$$

$$h_{sv} = 18.1\, c_p G \left(\frac{c_p \mu}{k}\right)^{-2/3} \left(\frac{d_p G}{\mu}\right)^{-1} \quad \text{for} \quad \frac{d_p G}{\mu} \leq 40 \quad \text{(laminar)} \tag{2.13}$$

where G represents the rate of mass flow through a unit surface area perpendicular to the flow direction.

Thus equations (2.3) through (2.13) form the model for analyzing the energy and momentum transport in unsteady forced convection flow of a gas through a packed bed. This is basically a system of five coupled governing equations which must be solved for analyzing the five field variables, namely $<\rho_v>^v$, $<u_v>$, $<T_v>^v$, $<T_s>^s$, and $<P_v>^v$.

2.2.1 Initial and boundary conditions

In the problem under consideration, the initial conditions are mathematically expressed as:

$$
\begin{aligned}
&P_v(x,y,t=0) = P_o \\
&T_v(x,y,t=0) = T_s(x,y,t=0) = T_o \\
&u_v(x,y,t=0) = 0
\end{aligned}
\tag{2.14}
$$

The boundary conditions used are as follows:

$$
\begin{aligned}
&P_v(x=0,y,t) = P_{in}, \quad P_v(x=L,y,t) = P_o \\
&T_v(x=0,y,t) = T_{in} \qquad \text{at } t > 0^+ \\
&T_v(x,y=0,t) = T_v(x,y=H,t) = T_s(x,y=0,t) = T_s(x,y=H,t) = T_o
\end{aligned}
\tag{2.15}
$$

Constant wall temperature boundary conditions were employed in order to study the two-dimensional effects in the transport phenomena in the packed bed. This kind of boundary conditions will give an insight about the behavior of the packed bed during the energy release cycle.

2.2.2 Physical conditions for the numerical runs

To analyze the effect of different parameters on energy and momentum transport in the packed bed, different solid particle sizes and different materials for the solid phase were considered. A complete set of computations were carried out for particle diameter values of 1 mm, 2.5mm and 5 mm for the set of different materials which were considered for the solid phase. Several runs were also performed for a particle diameter of 1 cm. The three different materials considered for the solid phase in this study were lithium-nitrate-trihydrate, sandstone and 1% Carbon-steel. The main criterion in selecting these materials was to obtain a wide range of thermophysical properties and explore their effects on the qualitative behavior of the transport phenomena since the properties of the bed material may differ widely from one application to another. The average porosity was chosen to be equal to the asymptotic value of 0.39 throughout the packed bed. This is a valid assumption for all cases in which the ratio of the solid particle diameter to the characteristic global dimension of the packed bed is below a certain value as determined by Benanati and Brosilow (1962). The following physical data were used for the boundary conditions and for the properties of the materials considered in the numerical computations:

Refrigerant-12

$R = 68.7588$ J/kg.K

$c_p = 602$ J/kg.K

$k = 0.0097$ W/m.K

$\mu = 12.6 \times 10^{-6}$ Pa.s

Lithium-nitrate-trihydrate

$c_p = 2090$ J/kg.K

$k = 0.5$ W/m.K

$\rho = 1550$ kg/m^3

Sandstone

1% Carbon-steel

$c_p = 710$ J/kg.K	$c_p = 473$ J/kg.K
$k = 1.83$ W/m.K	$k = 43$ W/m.K
$\rho = 2200$ kg/m^3	$\rho = 7800$ kg/m^3

$P_0 = 100$ kPa $\quad T_{in} = 300$ K $\quad T_0 = 280$ K

The effects of three important parameters have been studied extensively in this investigation. These are the particle Reynolds number, the Darcy number and the ratio of the solid phase thermal diffusivity to liquid phase thermal diffusivity. Different Reynolds numbers were obtained by varying the pressure in the reservoir, i.e., by applying different pressure gradients across the packed bed. Different Darcy numbers resulted from different particle sizes since the permeability of the packed bed varies with the particle diameter as given in equation (2.9). The ratio of solid to vapor thermal diffusivity, (α_s/α_v), was of a different order of magnitude for each of the three materials considered for the solid phase.

2.3 The numerical code and solution procedure

A numerical code was developed for solving the system of governing equations presented in the previous section. The Beam-Warming type implicit method which is frequently used in compressible flow problems in regular media was not applicable in this case because of the nature of the equations. Therefore, it was found necessary to employ explicit schemes. In developing the finite difference forms of equations (2.3) through (2.7), central difference approximations were used for most of the spatial derivatives for the inner grid points. Spatial derivatives for the grid points on the left and right boundaries were formed by first-order forward and backward difference approximations respectively. Upwind differencing was implemented for the convective terms in the vapor energy and

continuity equations in order to ensure the stability of the numerical scheme. It was found through numerical experimentation that using central differencing in the convective term of the continuity equation did not make any appreciable change in the results.

While the vapor density at each grid point on the left boundary was determined from the equation of state by using the boundary conditions for temperature and pressure, the density at each grid point on the right boundary was determined from the equation of state by using the vapor temperature computed from equation (2.5) and the pressure given by the right boundary condition. For the rest of the grid points the density was computed by the vapor continuity equation. The velocity $< u_v >$ for all the grid points except those on the right boundary were determined by the vapor phase momentum equation which is basically a quadratic equation in $< u_v >$. The velocity at the grid points on the right boundary was computed by linear extrapolation from the preceding two grid points in x-direction. Temperatures of the solid and fluid phases were determined by the associated energy equations while the pressure was determined from the equation of state.

The numerical computations were performed on a CRAY XMP/28. As a result of vectorization the CPU time required on the CRAY for a certain run using a grid mesh of 21 x 11 was approximately 30 times smaller than the CPU time required for the same run on a VAX 8550. Due to the nature of the governing equations, small time steps had to be employed for the stability of the numerical scheme. A systematic decrease in the grid size was carried out and the corresponding stable Δt was employed until an agreement to within 1% was achieved in the solutions between the consecutive grid sizes, and the effect of reducing the Δt further did not make any appreciable change in the solutions.

A number of interesting observations were made on the stability of the numerical code. It was found that in some cases the time step used in the *early stage* could be

increased in the *later stage* by an order of magnitude without any influence on the accuracy of the results. It was observed that for a fixed particle Reynolds number, Re_p, decreasing the Darcy number, Da, consistently increased the stability of the numerical scheme in both the *early* and the *later stages*. Decreasing Da at a fixed Re_p requires using smaller particle diameter (hence smaller permeability) and a larger pressure difference across the packed bed.

On the other hand, for a fixed Da, smaller values of Re_p translate into smaller mass flow rates and smaller amounts of thermal energy flowing into the packed bed per unit time. Therefore, for small values of Re_p the CPU time required for simulating the complete charging of the packed bed becomes excessively large. For instance, for the case when lithium-nitrate-trihydrate is the solid phase and $Da=1.18\times10^{-8}$, the CRAY CPU time required for simulating the complete charging of the packed bed was of the order of 1 hour for $Re_p=1100$. For this specific case the Δt employed in the computations was 1.7647×10^{-5} sec. for the *early stage* while it was possible to push it up to 1.7647×10^{-4}sec. for the *later stage*. The CPU time was estimated to increase significantly for small Reynolds numbers. Therefore, full simulation of such cases is very costly on CRAY and would be extremely tedious on regular main frames. For this reason no attempt was made to perform the complete simulation for such cases.

2.4 Benchmark of the numerical code

In order to gain confidence in the accuracy of the results of the numerical code developed, it was necessary to perform a benchmark against some analytical solutions, experimental results or other reliable numerical results. As mentioned earlier, no complete analysis of unsteady, nonisothermal and nonequilibrium flow of a gas through a porous

medium is available in the literature. Therefore, in order to check the numerical code it was necessary to compare its results with different limiting case analytical solutions dealing with different aspects of energy and momentum transport in porous media. This benchmarking was performed in two main sections. These were namely the comparison of momentum transport (pressure and hence velocity distributions) in an isothermal flow of an ideal gas through a porous medium, and the comparison of energy transport (temperature distribution in solid and fluid phases) of an incompressible fluid flow through a porous medium with no local thermal equilibrium between the solid and vapor phases. The two sources chosen for this benchmarking were the most relevant sources that could be found for possible comparisons.

The benchmarking of the energy transport was carried out by comparing the analytical solution of the simplified Schumann model presented by Riaz (1977) against the results generated by the present numerical code. This was achieved by making the necessary adjustments to our model in order to reduce it to a system which was equivalent to the simplified Schumann model, i.e., by omitting a number of the transport terms. This comparison is depicted in Figure 2.2 for the fluid phase and solid phase temperature distributions respectively in terms of the dimensionless variables that appear in the work of Riaz (1977). As may be seen from these figures, the agreement between our numerical results and the analytical solution is excellent.

The benchmarking of the momentum transport was carried out by comparing our results with the analytical solution of a one-dimensional isothermal flow of an ideal gas through a semiinfinite porous medium presented by Kidder (1957). Although this analytical solution was obtained for a semiinfinite porous medium, it could be safely

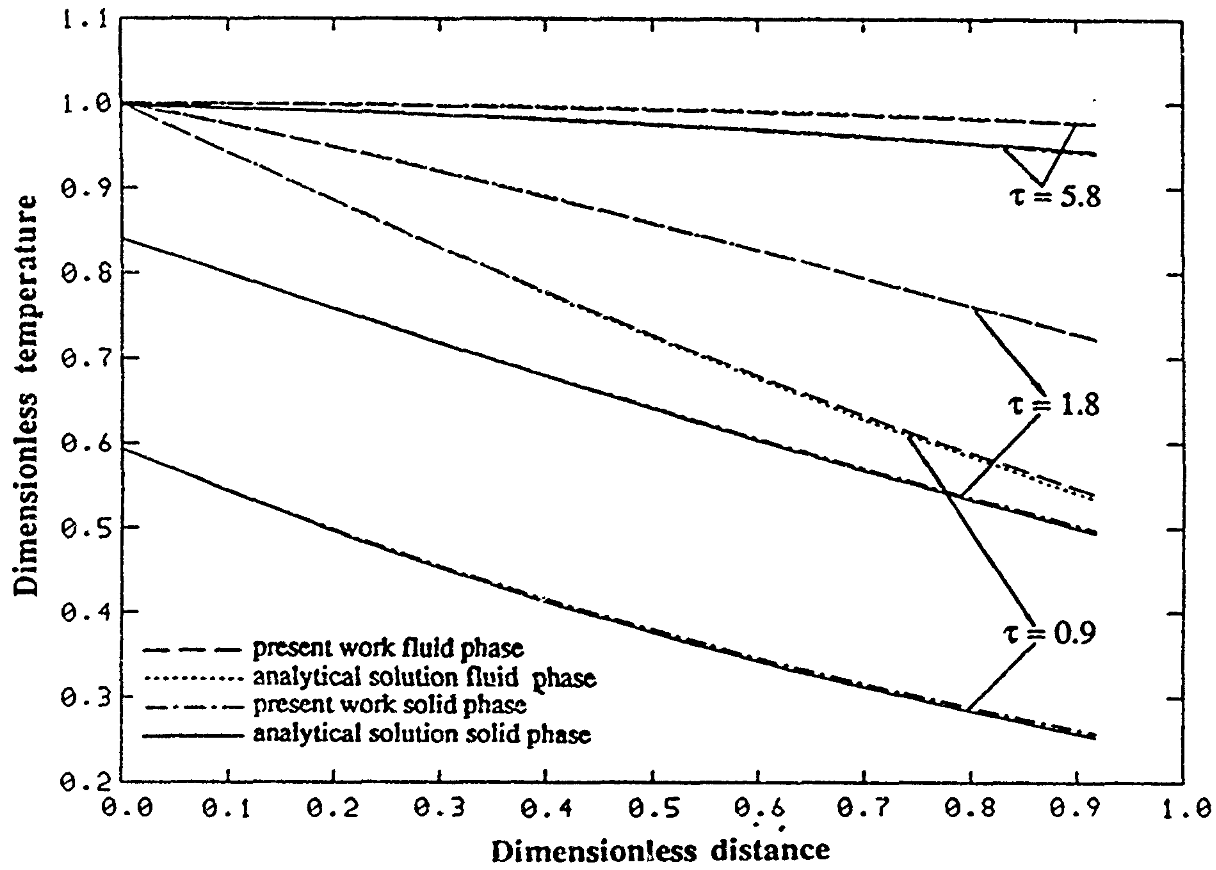

Figure 2.2: Comparison of the temperature solutions of the present work against the analytical solutions presented by Riaz (1977)

compared with our numerical results for small times, during which the information from the boundary had not reached the total length of the packed bed under consideration. The comparison of the analytical solution with the results generated by the present numerical code is shown in Figure 2.3 in terms of the dimensional distance and time and the dimensionless pressure which appears in the work of Kidder (1957). Again, a very good agreement can be observed between our numerical results and the analytical solution.

2.5 Results and discussions

For the present analysis, it was found to be appropriate to present the results in a non-dimensionalized form. The reference quantities that are used in nondimensionalizing the variables are the reference density, reference velocity and reference pressure denoted by ρ^*, u^* and P^* respectively. For convenience, the reference pressure, P^*, for each run is taken to be the average of the initial pressure P_0 and the pressure of the vapor flowing from the reservoir into the packed bed, P_{in}. Likewise, the reference density, ρ^*, is computed from the equation of state by using P^* and the average value of the initial and the vapor inflow temperatures. Finally the reference velocity, u^*, is computed from equation (2.4a) by using ρ^* and the global pressure gradient applied across the packed bed. The dimensionless time and temperature chosen for presenting the results are defined as $\tau = tu^*/L$, and $\Theta = (T-T_0)/(T_{in}-T_0)$ respectively. For each of the computational runs two distinct regimes were observed. These two regimes will be referred to as the "'*early stage*'" and the "'*Later stage*'". The *early stage* lasts for a very short period of time which starts with the application of the high temperature and high pressure boundary conditions on the left, and ends when the pressure distribution across the packed bed becomes almost linear. This process takes place extremely fast, and afterwards the pressure distribution

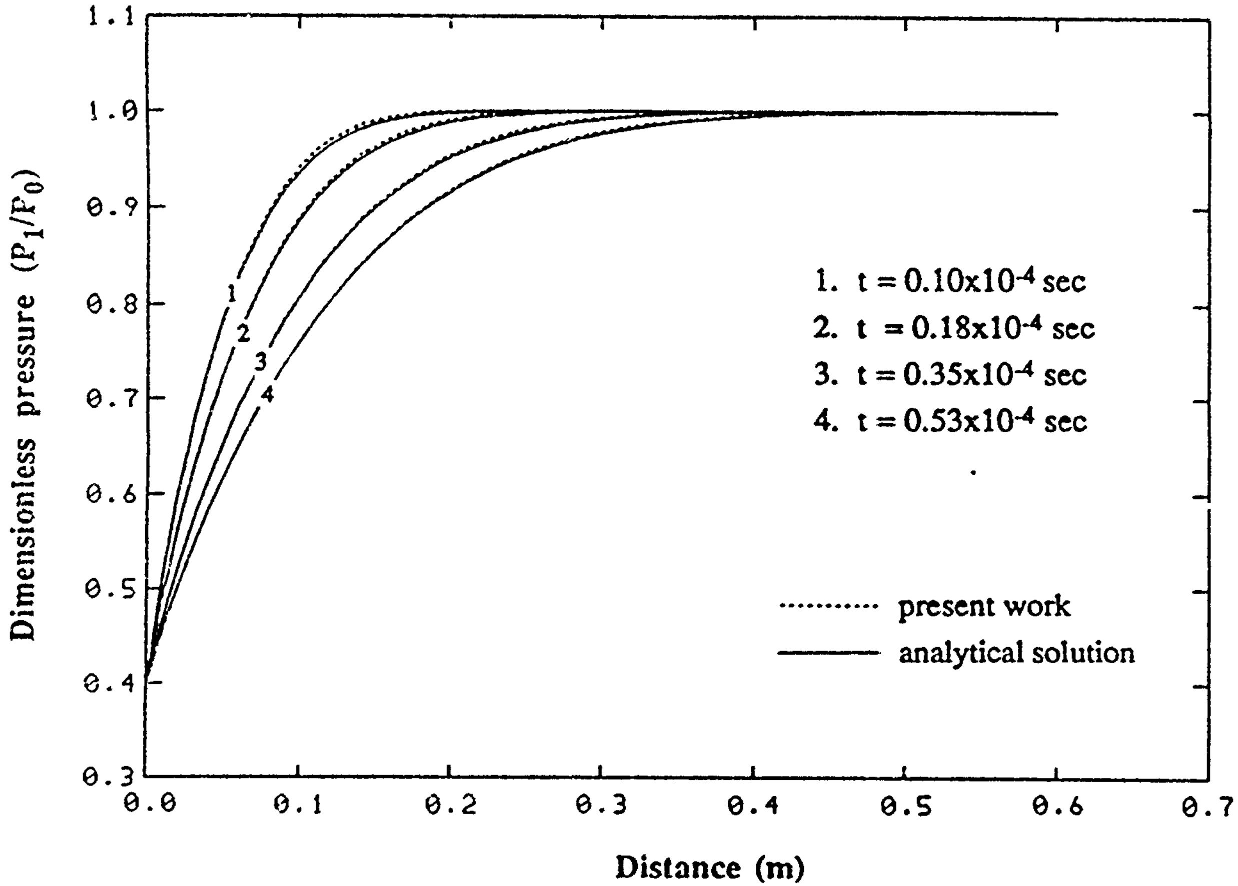

Figure 2.3: Comparison of the pressure solution of the present work with the analytical solution of Kidder (1957)

remains in a quasi-steady linear state. During the *early stage* no appreciable thermal penetration depth develops in the packed bed. The *later stage* is the period of time following the *early stage.*

The vapor velocity, density and pressure distributions along the x-direction at the midplane of the packed bed during the *early stage*, for the case where the solid phase material was lithium-nitrate-trihydrate, are depicted in Figure 2.4. It was observed that for this case the variation of different variables in the y-direction for the core region of the packed bed did not exceed 1%. Therefore, it is very reasonable to present the results for this case in one-dimensional form. The variation in the velocity distribution can be explained by the variation of the pressure. Initially when the high pressure boundary condition is applied, the large pressure gradient causes high velocities. Gradually as the pressure propagates in time and space, the large pressure gradients die away, and the velocities follow the same trend. As mentioned earlier, there is no appreciable thermal penetration depth during the *early stage*. Therefore, there is a sharp decrease in the vapor temperature near the entrance of the bed. This drop in temperature is more pronounced than the corresponding pressure drop. The resulting peak value of the vapor density close to the entrance region, therefore, follows from the equation of state. Beyond the peak region the temperature is almost constant while the pressure decreases in the x-direction. Hence, based on the equation of state the vapor density will follow the same trend as the vapor pressure. On the other hand, the temporal increase in the vapor density during the *early stage* occurs because during this period the mass flux at any point is larger than the mass flux at a point on its right, i.e., there is a continuous net mass flux into the bed. Therefore, the second term on the left-hand side of equation (2.3) has a negative value. Thus, the density has to increase in time during the *early stage* in order to satisfy the continuity equation of the vapor phase.

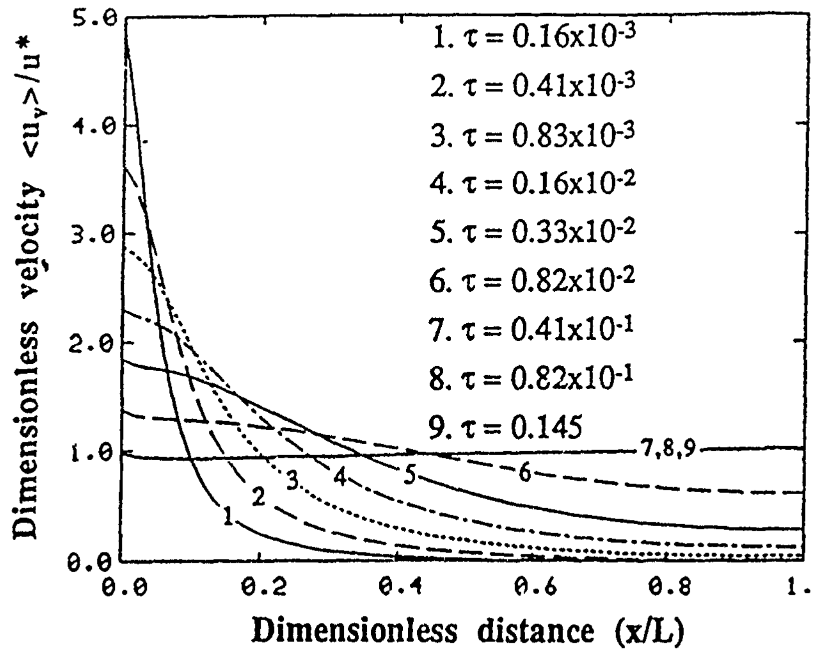

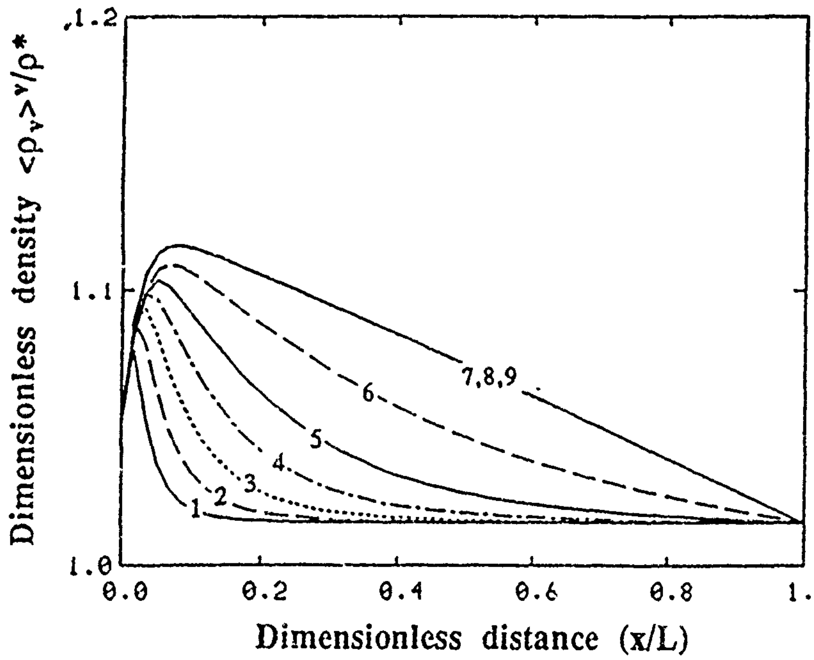

Figure 2 4: Variations of different field variable distributions at the mid-plane of the packed bed during the *early stage*

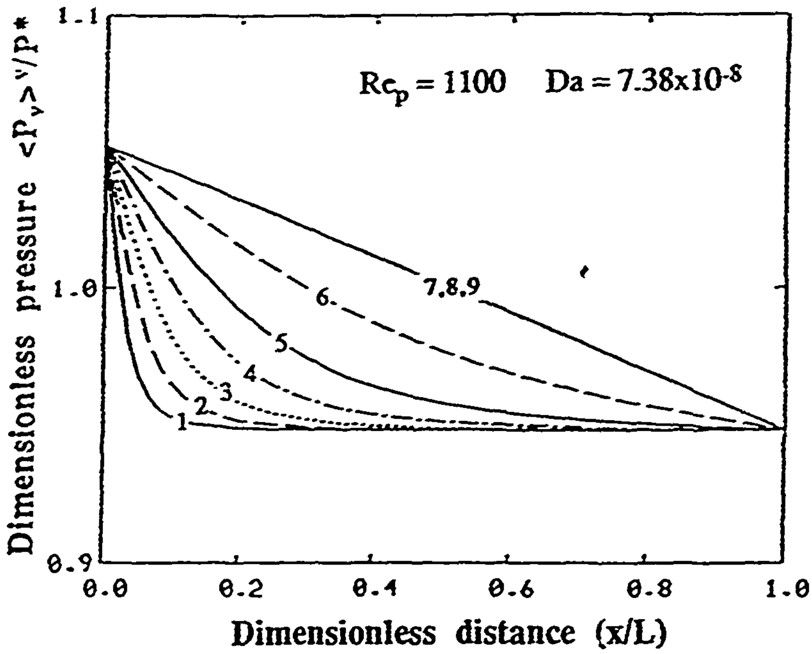

Figure 2.4 (continued)

The variations of the solid and vapor temperatures, and the density, velocity and pressure of the vapor phase during the *later stage* for the above-mentioned case are shown in Figure 2.5. It should be noted that the *later stage* starts after the pressure distribution in the packed bed becomes almost linear and remains in that quasi-steady state thereafter. During this stage the thermal penetration depth develops as shown in the figure. Since the effect of the transient term in the vapor continuity equation becomes much less pronounced at the end of the *early stage*, an almost steady-state continuity equation prevails in the *later stage*. This requires the existence of an inverse relationship between the vapor density and vapor velocity distributions. This behavior can be seen in the figure as almost a mirror image trend in the variations of the density and the velocity, i.e., as one increases the other one decreases. The vapor pressure distribution is almost linear in the x-direction and remains unchanged. Furthermore, at any time before the packed bed is fully charged, the slope of the temperature profile is much steeper than the slope of the pressure profile within a major portion of the thermal penetration depth. Therefore, during such times the vapor density increases in the x-direction within this zone. Beyond this zone the vapor temperature is almost constant and the vapor pressure decreases linearly, and so the vapor density also decreases linearly. The advancement of the thermal penetration front which translates into a temporal increase in temperature at a given x-location causes a decrease in the vapor density in time at that location. This, of course, follows from the equation of state. When ultimately a uniform temperature is reached throughout the packed bed, the density distribution becomes similar to the pressure distribution as dictated by the equation of state. From the variation of the different field variables in Figure 2.5, it becomes evident that the flow field is very much influenced by the temperature field.

A typical example run in which two-dimensional variations are very pronounced is considered next. The solid particle material considered for this case was 1% Carbon-steel.

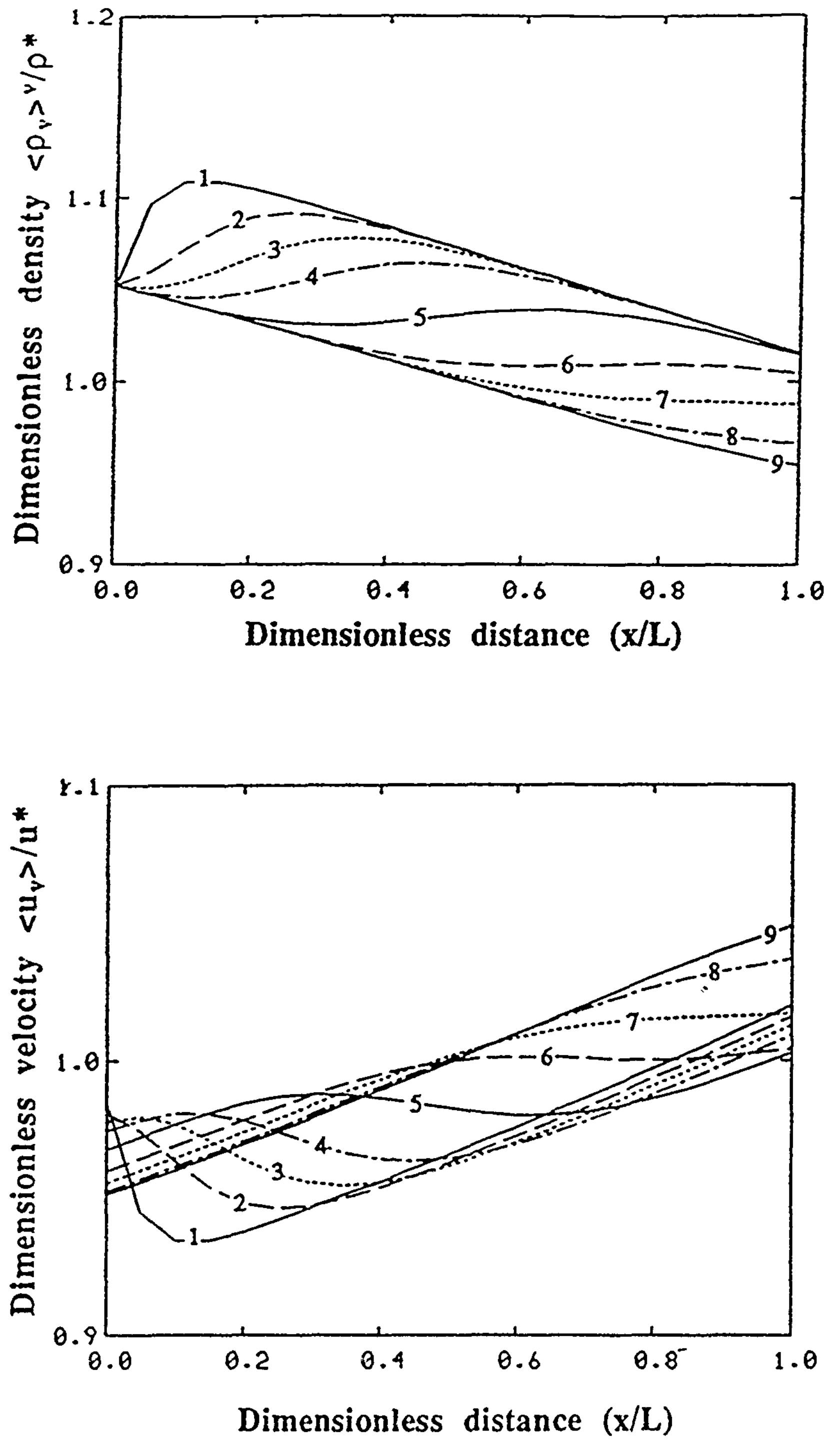

Figure 2.5: Variations of different field variable distributions at the mid-plane of the packed bed during the *later stage*

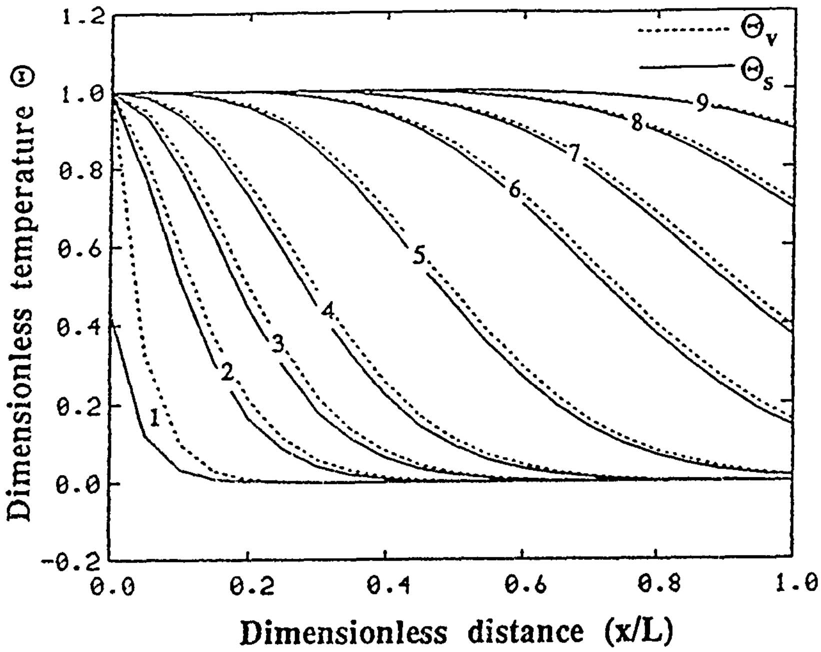

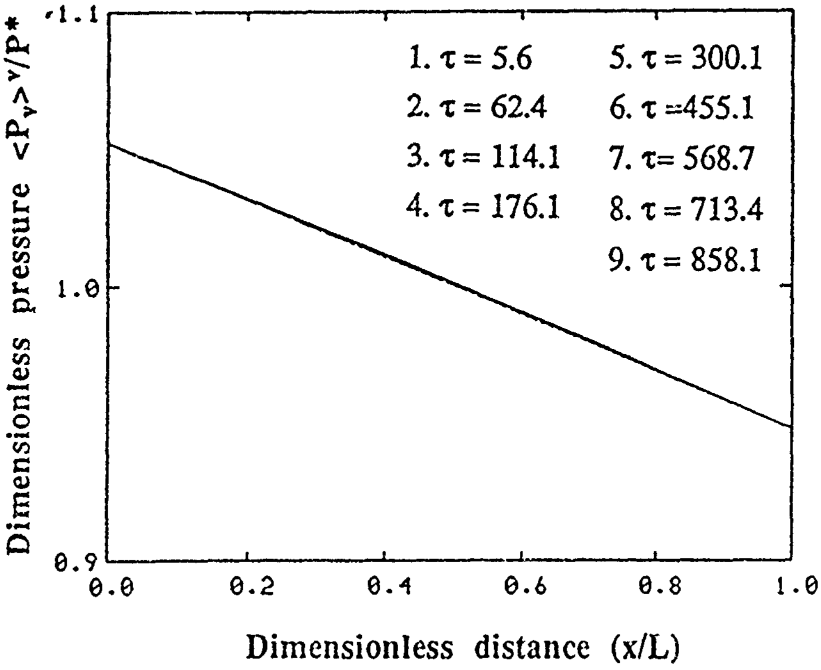

Figure 2.5 (continued)

Figures 2.6(a) and 2.6(b) depict the distributions of the solid and vapor phase temperatures, the vapor density and the vapor pressure. As may be seen from these figures, there is considerable heat loss through the horizontal walls of the packed bed due to conduction heat transfer in y-direction and a strongly two-dimensional temperature distribution exists within the packed bed. Apparently, a one-dimensional modeling for such a case will yield erroneous results. In order to better track the two-dimensional behavior of the variables a grid mesh of 21 x 21 was employed for the cases in which sandstone or steel was considered as solid material.

It was observed from the numerical computations that during the *later stage* of each run, the value of the vapor-to-solid heat transfer coefficient computed for each grid point at each time step was very stable and did not differ more than 2% from the reference vapor-to-solid heat transfer coefficient which was based on the reference density, ρ^*, and the reference velocity, u^*. This suggests that an assumption that takes this value to be a constant for all the grid points during the *later stage* would be very reasonable. Considerable CPU time can be saved in this way by eliminating the otherwise required computations from eqns (2.12) and (2.13) at each time step. However, all of the runs for this investigation were performed by using the variable heat transfer coefficient.

2.5.1 Effect of the Darcy number (Da):

In order to determine the effect of the Darcy number on energy and momentum transport in the packed bed, different cases with different Darcy numbers were compared. These comparisons were performed for a fixed particle Reynolds number of 1100 using the same solid material. Again lithium-nitrate-trihydrate was used for convenience in presenting the results, since for this material the distribution of the field variables were essentially one-dimensional in all of these cases. Figure 2.7 depicts the temperature

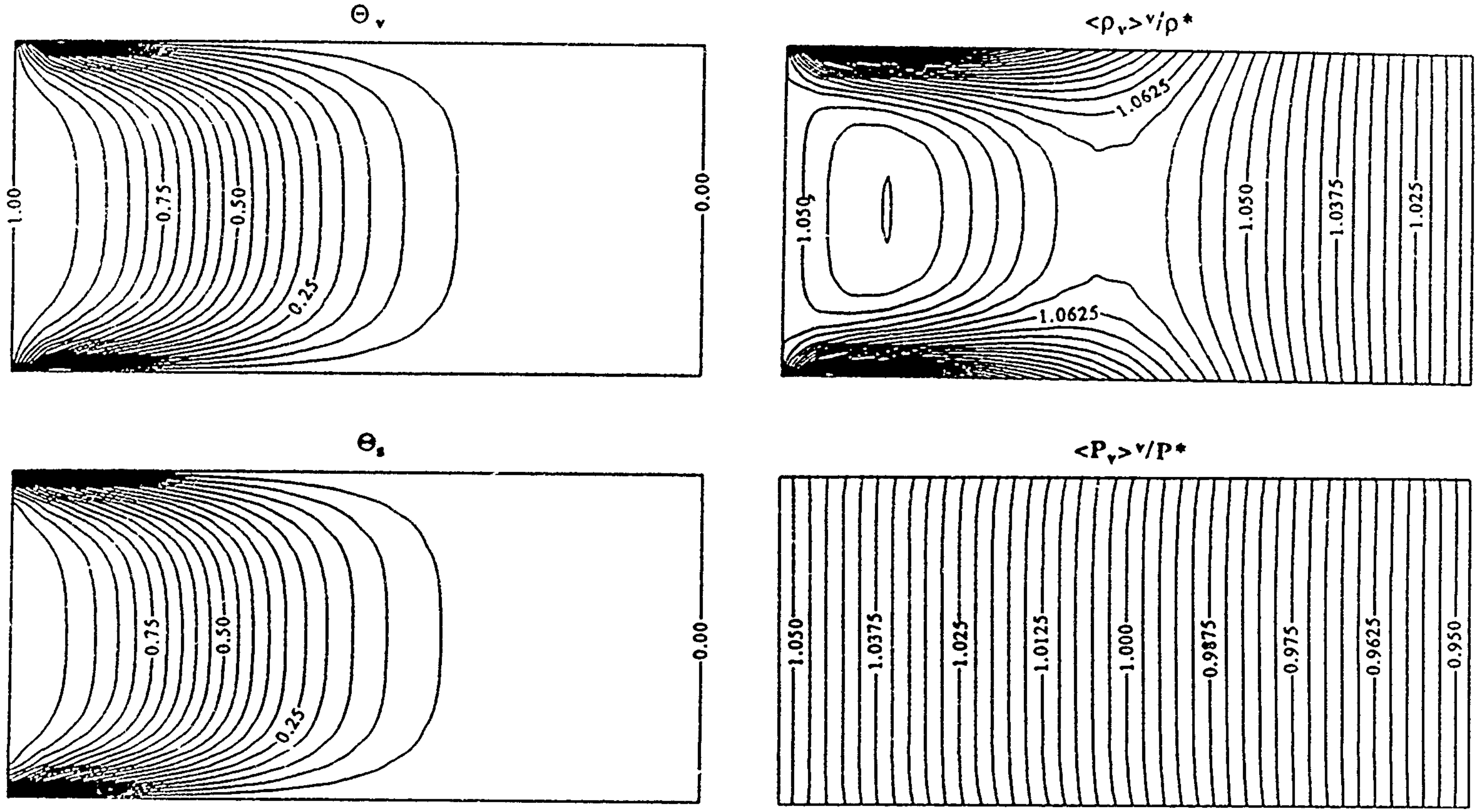

(a)

Figure 2.6: Temperature, density and pressure distribution in the packed bed for the case when the solid phase is steel, (a) at $\tau = 211.4$, (b) at $\tau = 546.2$

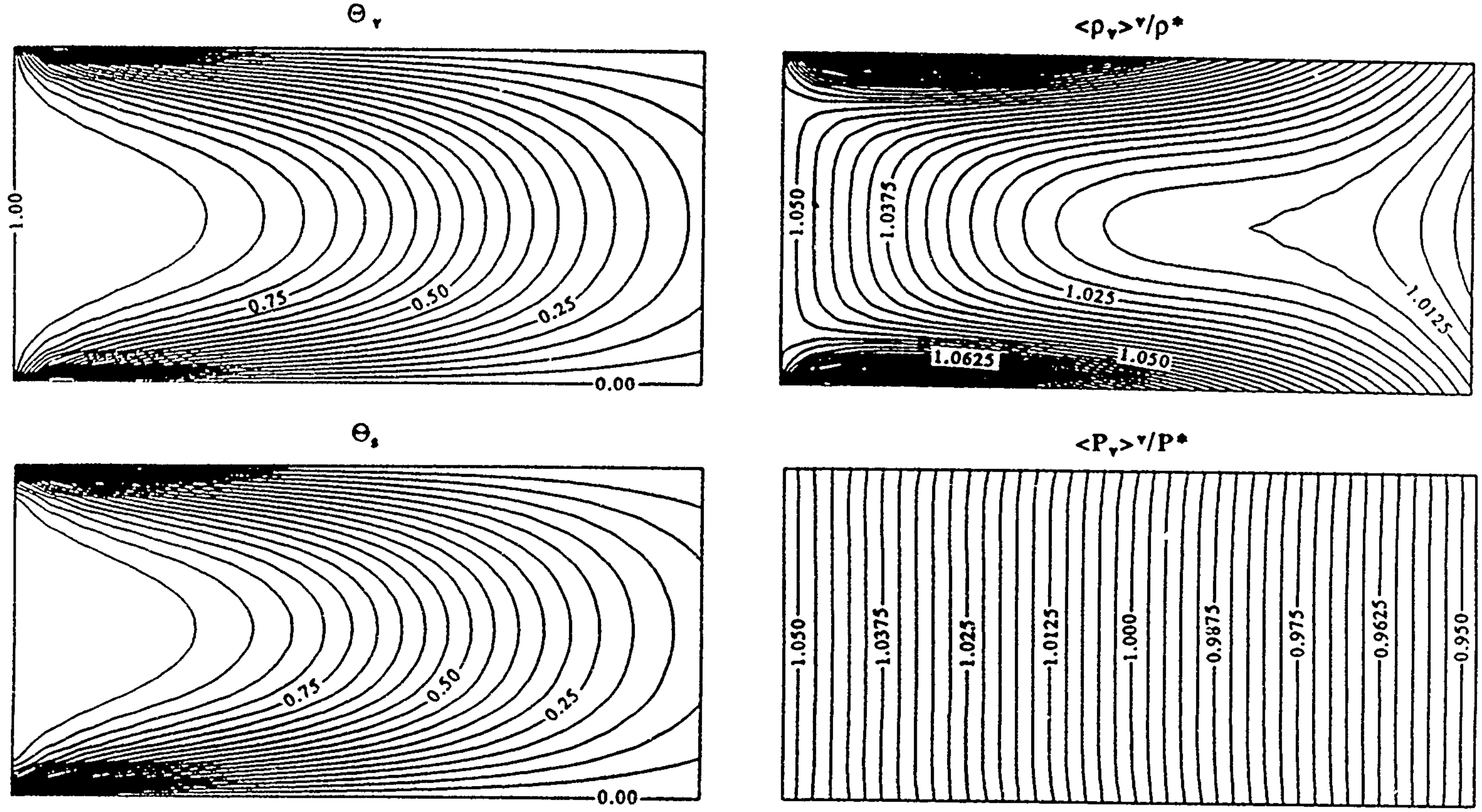

(b)

Figure 2.6 (continued)

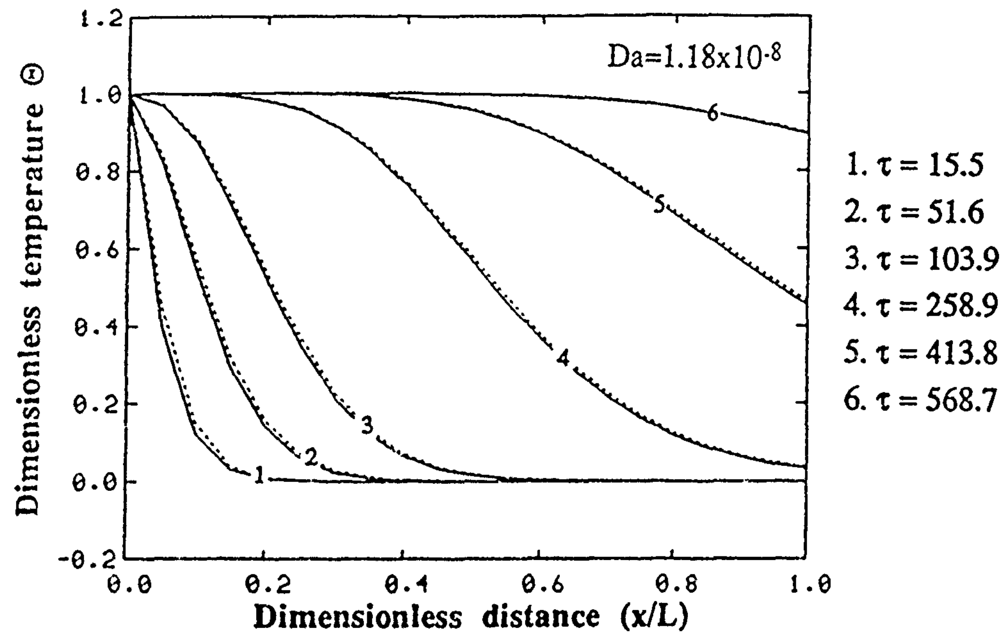

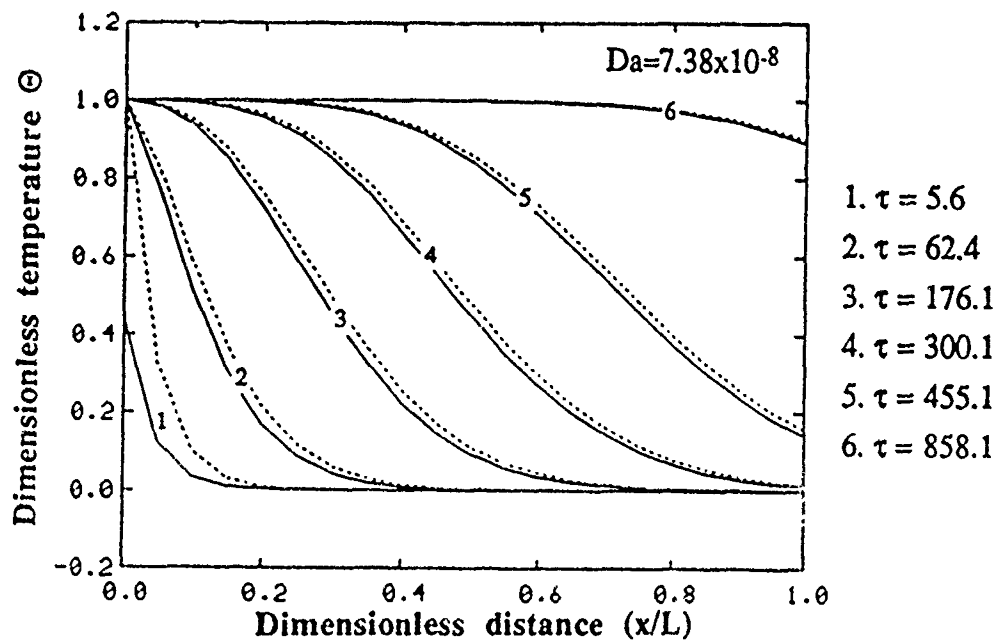

Figure 2.7: Temperature distributions in the vapor and solid phases for different Darcy numbers for a fixed particle Reynolds number

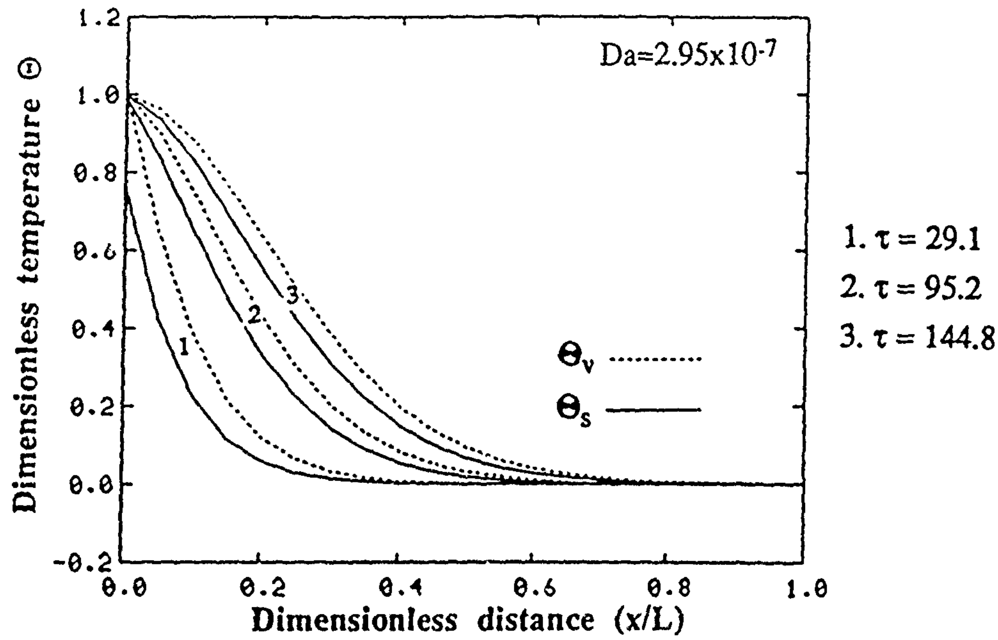

Figure 2.7 (continued)

distributions in the solid and vapor phases along the packed bed at different time levels for Darcy numbers of 1.18×10^{-8}, 7.38×10^{-8} and 2.95×10^{-7}. The time levels in this figure were chosen such that they would result in a reasonable presentation of the penetration fronts in each case. It can easily be seen that as the Darcy number decreases, the difference between the solid and vapor phase temperatures decreases. The reason for this is that a decrease in the Darcy number translates into a decrease in the particle diameter (see equation (2.9)). As the particle diameter decreases, the specific surface area, a_{sv}, of the packed bed increases, thus, increasing the vapor-to-solid heat transfer interaction by offering a larger surface area. Hence, the exchange of heat between the solid and vapor phases becomes more efficient. Therefore, the local thermal equilibrium assumption would be more justifiable at low Darcy number flows.

2.5.2 Effect of the particle Reynolds number (Re_p):

The procedure followed for determining the effect of Re_p on transport phenomena was similar to the one carried out in determining the effect of the Darcy number. This time Da was fixed at 7.38×10^{-8} for the same solid phase material while Re_p was varied. The temperature distributions for the solid and vapor phases along the x-direction at the horizontal midplane of the packed bed are shown in Figure 2.8 for Re_p of 400, 1100 and 2126. As can be seen from these figures, the difference between the temperatures of the solid and fluid phases at any point increases with an increase in Re_p. This increase should be attributed to the velocity of the flow since the specific surface area of the packed bed is the same in all of these cases. As the velocity of the flow increases, i.e., Re_p increases, the time for the solid-to vapor heat interaction decreases. This will cause a decrease in the efficiency of heat exchange between the solid and vapor phases and, hence, the deviation from the local thermal equilibrium will increase.

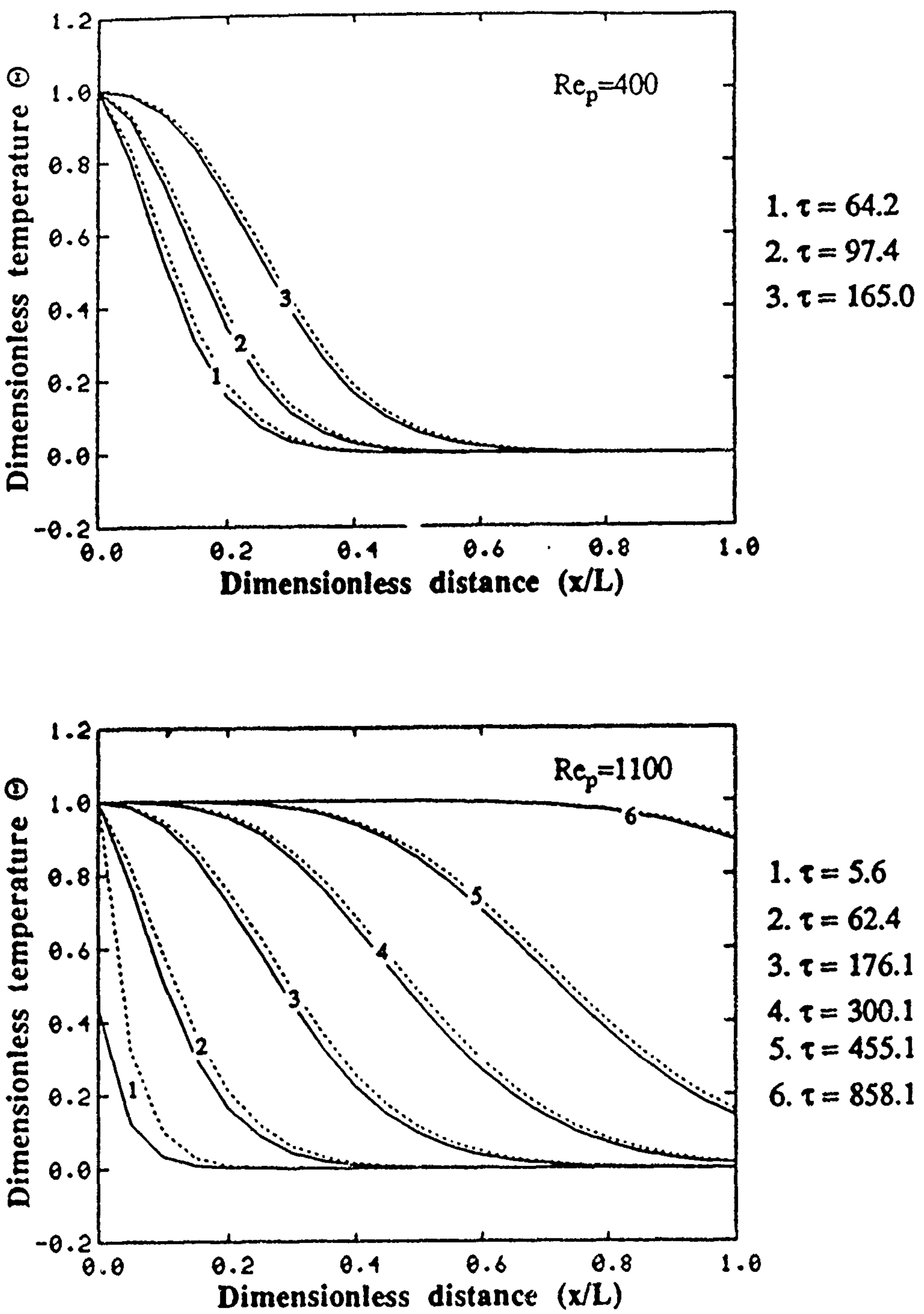

Figure 2.8: Temperature distributions in the vapor and solid phases for different particle Reynolds numbers for a fixed Darcy number

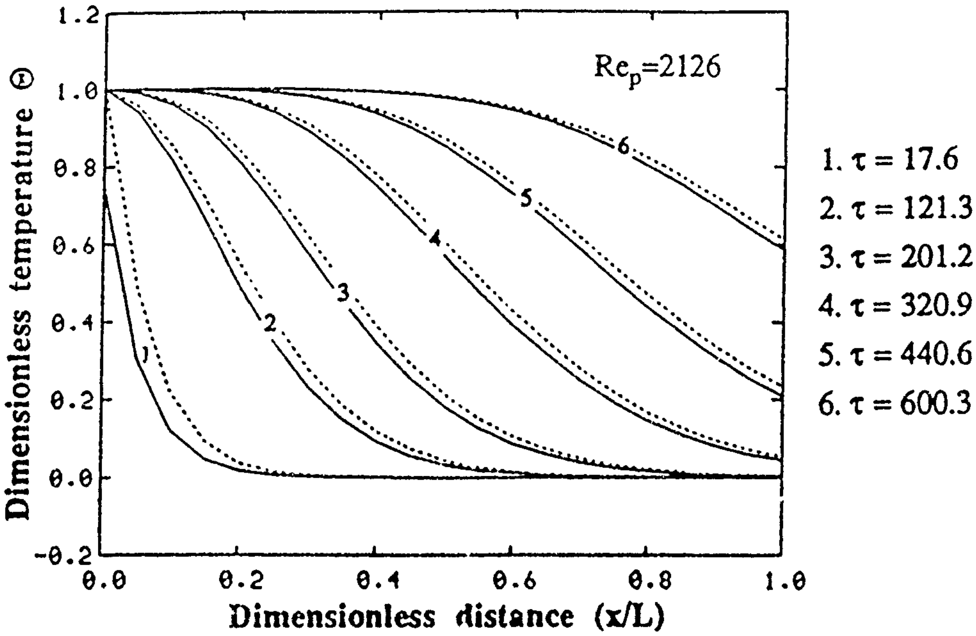

Figure 2.8 (continued)

The combined effect of increasing both Re_p and Da was found to have, as expected, a much more pronounced effect on the local thermal equilibrium assumption. It becomes evident that for high Re_p and Da flows the local thermal equilibrium assumption becomes very erroneous. Similar qualitative behavior was also found to be valid for the cases in which sandstone or steel was used as the solid phase. Lithium-nitrate-trihydrate was chosen just for its convenience in presenting the results.

2.5.3 <u>Effect of the thermal diffusivities ratio (α_s/α_v):</u>

It was found through numerical experimentations that the ratio of the solid phase thermal diffusivity to liquid phase thermal diffusivity, α_s/α_v, was the most appropriate parameter in representing the combined effects of k_s/k_v, c_{p_s}/c_{p_v} and ρ_s/ρ_v ratios, all of which are determining factors in the overall heat transfer process. Furthermore, from the numerical experimentations it was also found that one-dimensional approach was very satisfactory for all cases in which lithium-nitrate-trihydrate was used as the solid phase and for which α_s/α_v was of the order of 0.035 to 0.075, which resulted from different vapor density values corresponding to the average operating pressures applied for different runs. Therefore, the effect of α_s/α_v will be shown for cases in which sandstone and steel were used as the solid phase. The temperature distributions in the solid and fluid phases for two cases in which sandstone and steel were used respectively are shown in Figs. 2.9(a) and 2.9(b). In both of these figures the value of Re_p was 1100 and the Darcy number was chosen to be 1.18×10^{-8}. In the case of sandstone α_s/α_v was equal to 0.57 where in the case of steel it was 5.71. As can be seen from these figures the temperature distributions are strongly two dimensional in the case of steel and mildly two-dimensional in the case of sandstone for which one dimensional approach may give fairly good results. It should be noted that the same qualitative behavior was observed for all ranges of Re_p and Da

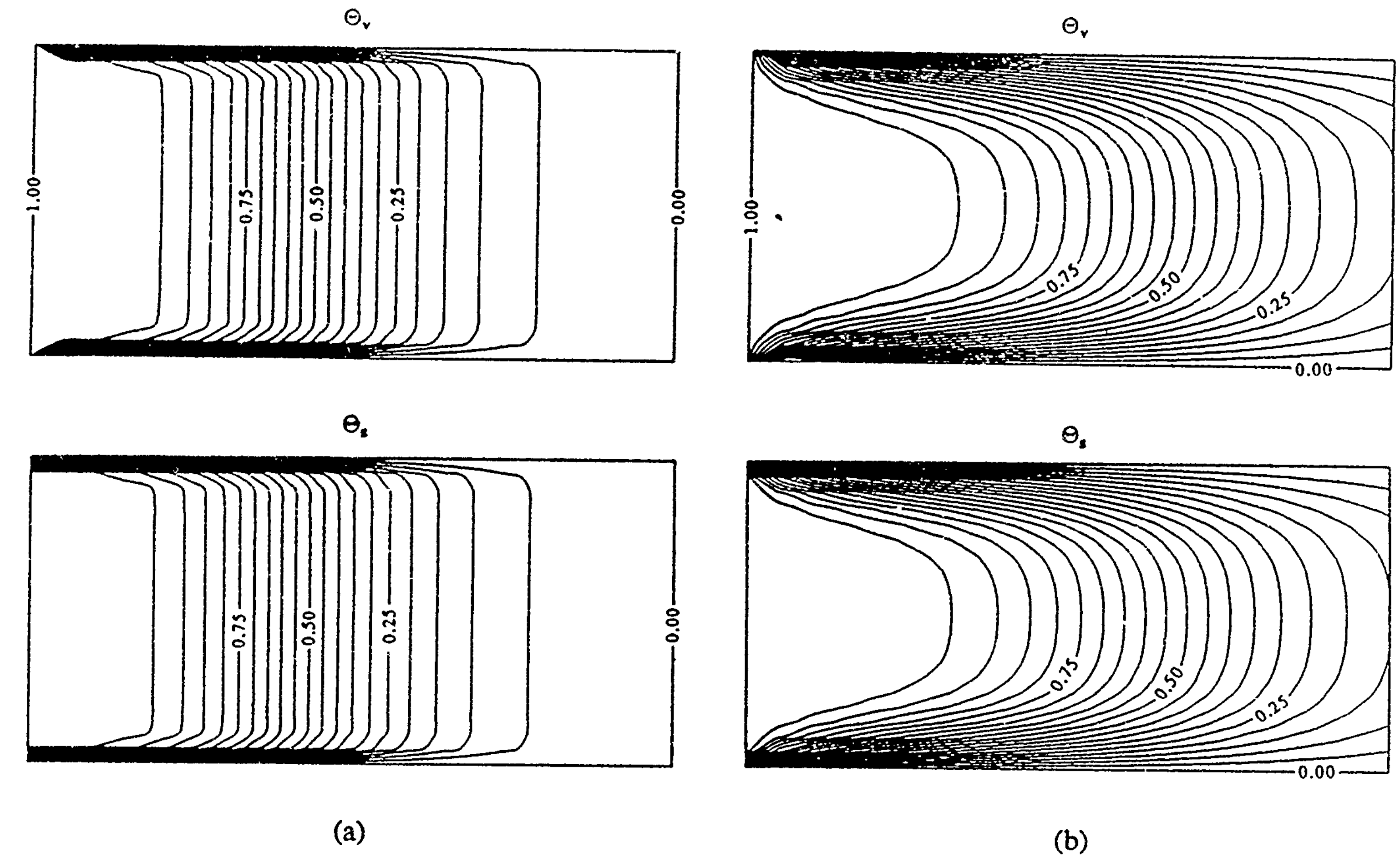

Figure 2.9: Temperature distributions in the solid and vapor phases at the mid-plane of the packed bed for $Re_p = 1100$, $Da = 1.18 \times 10^{-8}$, (a) at $\tau = 103.9$ for the case with sandstone, (b) at $\tau = 568.7$ for the case with steel

considered in this investigation which proves that two-dimensionality effects are not sensitive to the particle Reynolds number and Darcy number.

For a qualitative assessment of the validity of local thermal equilibrium assumption and the strength of the two-dimensional effects in the energy and momentum transport, the findings of the numerical computations will be presented in an integrated form. Figure 2.10 shows this assessment for the local thermal equilibrium assumption for the case of lithium-nitrate-trihydrate, sandstone and steel for the entire ranges of Re_p and Da which were considered in this work. It should be noted that for all the runs there is a difference between the solid and vapor phase temperatures at time equal to zero, and therefore, the present assessment is based on the later times during which the thermal penetration depth is developed to some appreciable position. The dividing lines in this figure were decided by the maximum difference between the solid and the vapor phase temperatures relative to the overall temperature range (difference between the inlet vapor temperature and the initial temperature, 20 K). For the qualitative ratings, the percentage difference relative to the overall temperature range falls into the following categories: very poor, more than 15%; poor, 10-15%; fair, 5-10%; good, 1-5%; very good, less than 1%. From Figure 2.10 it can be concluded that Da is the most influential parameter in determining the validity of local thermal equilibrium. The Reynolds number based on particle diameter is also a very important parameter in this regard. The local thermal equilibrium assumption becomes more viable as both Re_p and Da decrease for the reasons which were explained in the sections analyzing the effects of these parameters. This is clearly seen from the lower left corner of each figure. By the same token it is reasonable to observe the opposite behavior as Re_p and Da increase, i.e., approaching the top right corners of these figures. Also it may be seen that the thermophysical parameters have a much less pronounced influence on the local thermal equilibrium condition. Only for the case of steel were the effects of the

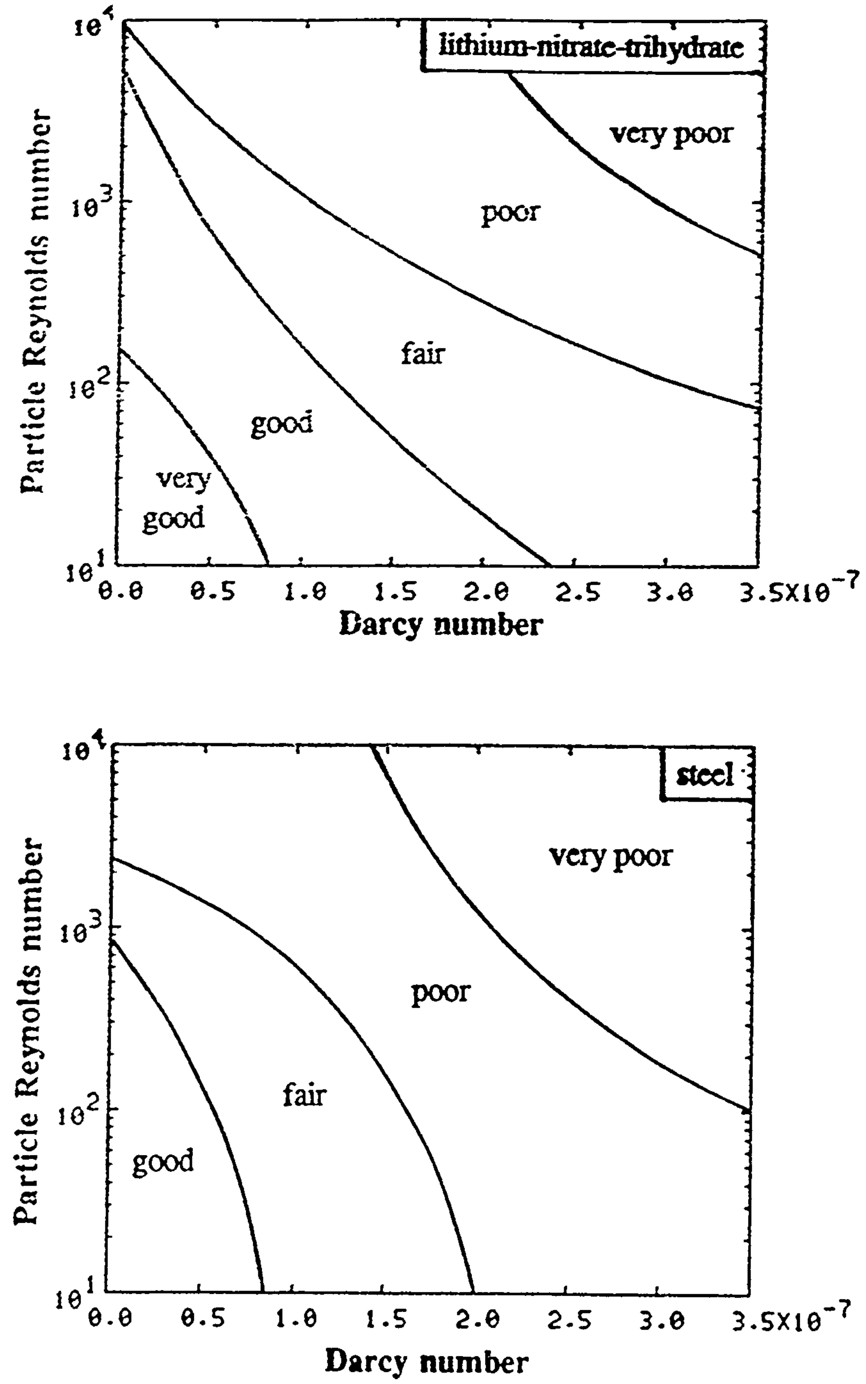

Figure 2.10: Qualitative assessment of the local thermal equilibrium for the cases with lithium-nitrate trihydrate, sandstone and steel as solid phase respectively

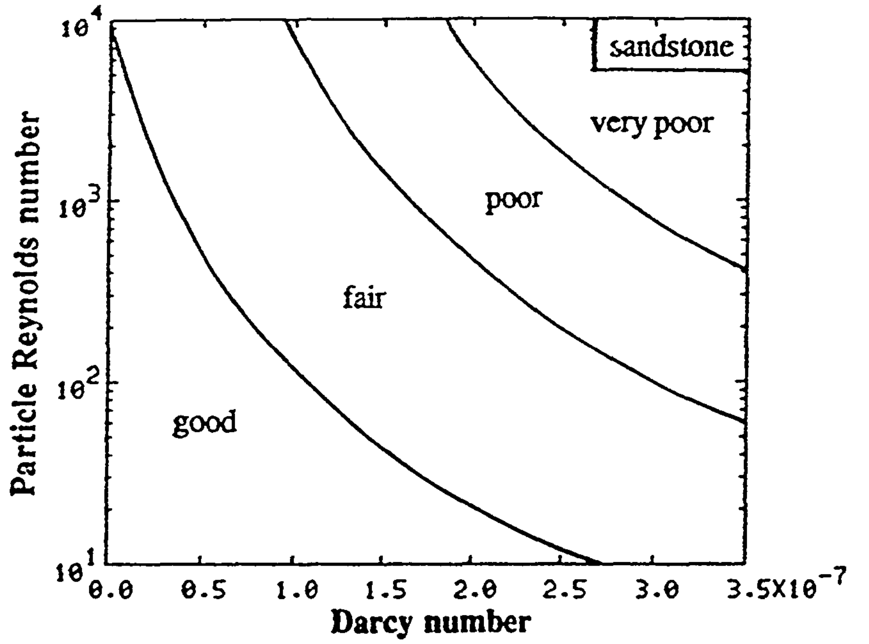

Figure 2.10 (continued)

physical parameters found to be mildly significant. This is because the conduction heat transfer becomes more dominant than the vapor-to-solid convective heat transfer in this case. Therefore, the conduction heat transfer will play an additional role in the case of steel. This was significantly absent in the cases of sandstone and lithium-nitrate-trihydrate.

In a similar manner a qualitative assessment of the strength of the two-dimensional behavior is depicted in Figure 2.11. This figure shows the behavior for a fixed Da of 7.38×10^{-8} for the entire range of Re_p used in this investigation, and the behavior for a fixed Re_p equal to 400 for the entire range of Da used in this investigation. This qualitative behavior, for each case in the figure, was found to be exactly the same for the entire ranges of the corresponding Da or Re_p which were considered in this investigation. Therefore, for brevity only these two cases are presented. The above-mentioned fact and Figure 2.11 confirm that the two-dimensionality effects are not sensitive to either Re_p or Da, but very sensitive to the α_s/α_v ratio, i.e., to the thermophysical properties of the materials which are considered for the bed.

2.6 Conclusions

Solution of the transient problem with step change boundary conditions showed the existence of two distinct stages, namely the *early stage* and the *later stage*. It was found that the *early stage* is mostly dominated by changes in the pressure distribution, and the time scale for the changes in the distribution of pressure and the dependent variables is very short during this stage. On the other hand, the time scale for changes in the field variables during the *later stage* was found to be relatively larger, and that development of the thermal penetration into the packed bed played an important role in these changes.

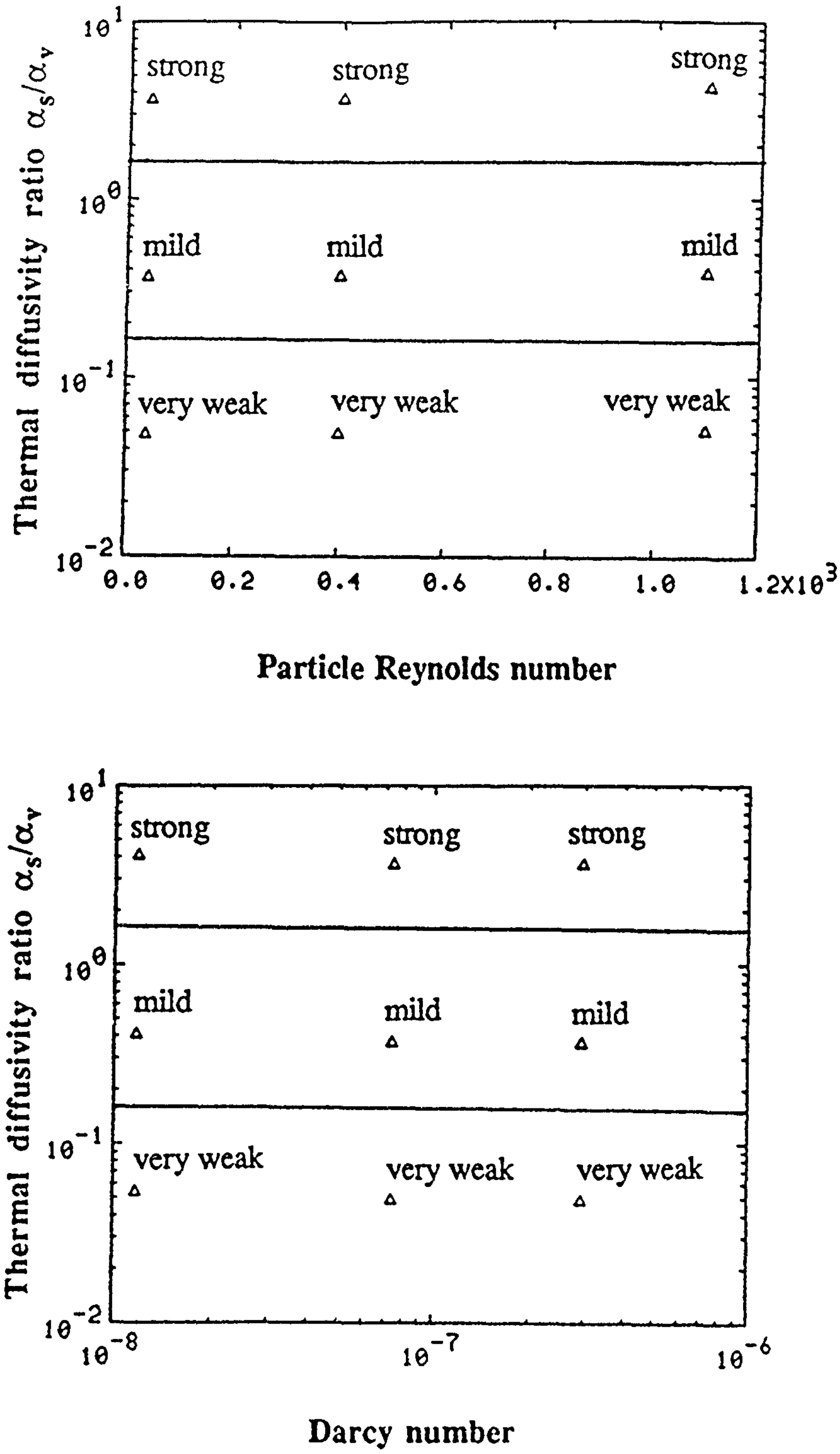

Figure 2.11: Qualitative assessment of the two-dimensionality effects

Modeling the flow of the vapor/gas by using an equation of state was found to be very useful since this way it was possible to track down the pressure evolution as well as the variations in the velocity and density of the transporting fluid during the *early stage*. These can be crucial information during the start-up procedures of certain applications. It was also shown that although no such assumption has to be made, the pressure distribution in the packed bed assumes a linear form during the *later stage*.

The results obtained in the case studies performed in Section II were also helpful in drawing a number of conclusions on the qualitative aspects of transport phenomena in packed beds generally applicable to any porous medium. The first significant outcome of these analyses was related to the local thermal equilibrium (LTE) assumption. It was clearly seen from the results obtained that higher particle Reynolds number resulted in larger differences between the solid and fluid phases, that is larger deviations from local thermal equilibrium. Similar behavior was seen with increase in the Darcy number which translates into an increase in the particle size of the packed bed. On the other hand, the effect of the thermophysical properties on LTE was found to be much less influential. Therefore, it can be concluded that the validity of LTE assumption is mostly dependent on the speed of the flow and the particle size of the porous medium.

The two-dimensional behavior in the transport processes was also examined. It was found that while the two-dimensional effects are very sensitive to the thermophysical properties of the solid and fluid phases considered, particle size or speed of flow do not have significant effect on two-dimensional behavior. The results obtained show that higher the thermal diffusivity of the solid phase relative to that of the working fluid the more pronounced are the two-dimensional effects. This is reasonable since with higher thermal

diffusivity in the solid phase the diffusion of heat in the transverse direction can reach the order of magnitude of the convective heat transfer between the solid and the fluid phases.

Numerical experimentations showed that the stability of the numerical code for the *later stage* simulations was primarily dependent on the magnitudes of the particle Reynolds number, Re_p, and Darcy number, Da. The maximum stable time step, Δt, was found to increase with an increase in Re_p or decrease in Da. While the reason for increased stability with decrease in Da can be attributed to the increased damping forces in the packed bed, the reason for increase in the stability of the numerical code with increase in Re_p should be related to the level of constraint that the flowing gas is under, or in other words the magnitude of the pressure difference applied across the packed bed.

It was found out that due to the nature of the governing equations, very small time steps have to be employed in the numerical simulation of the transport processes in compressible flow through porous media. Numerical simulation of the complete thermal charging process of the packed bed for cases with low Re_p and/or high Da requires excessive CPU time even on vector machines. For such cases, the use of regular main frames becomes highly inefficient.

One significant finding in Section II was that the use of a fluid-to-solid heat transfer coefficient based on a representative reference velocity, i.e., a nominal Re_p and a reference density throughout the *later stage* simulations would not cause a significant inaccuracy in the numerical solutions. This is of engineering importance because considerable amount of CPU time can be conserved by introducing this simplified form rather than performing computations for each grid point at each time step.

SECTION III

ANALYSIS OF MULTIPHASE TRANSPORT PHENOMENA IN A CONDENSING FLOW OF A VAPOR IN A PACKED BED

In this section, the problem analyzed in Section II is extended to cover the multi-phase transport phenomena in a packed bed. This basically involves the consideration of the same flow problem at a pressure range in which the vapor (working fluid) density may reach the saturation vapor density causing condensation. A rigorous model for analyzing the multiphase transport in the packed bed is developed by considering the basic thermodynamics of the condensation process. Numerical solution procedure is discussed in detail. This is followed by the presentation of the results of a set of case studies performed for this problem.

3.1 Statement of the problem

The problem under consideration is the transient condensing flow of a vapor through a fixed bed of regularly sized spherical solid particles packed in a two-dimensional channel. Figure 3.1. depicts the schematic diagram of the problem under consideration. The packed bed is initially filled with the working fluid (Refrigerant-12) at a slightly superheated state and the whole vapor and solid system is at uniform temperature and pressure. R-12 vapor at a higher temperature and pressure from a reservoir is suddenly allowed to flow through the packed bed, thus depositing its thermal energy to the solid particles of the bed. This basically forms a step change in the temperature and pressure at the inlet boundary. In this problem the pressures are high enough so that at certain times during the thermal charging

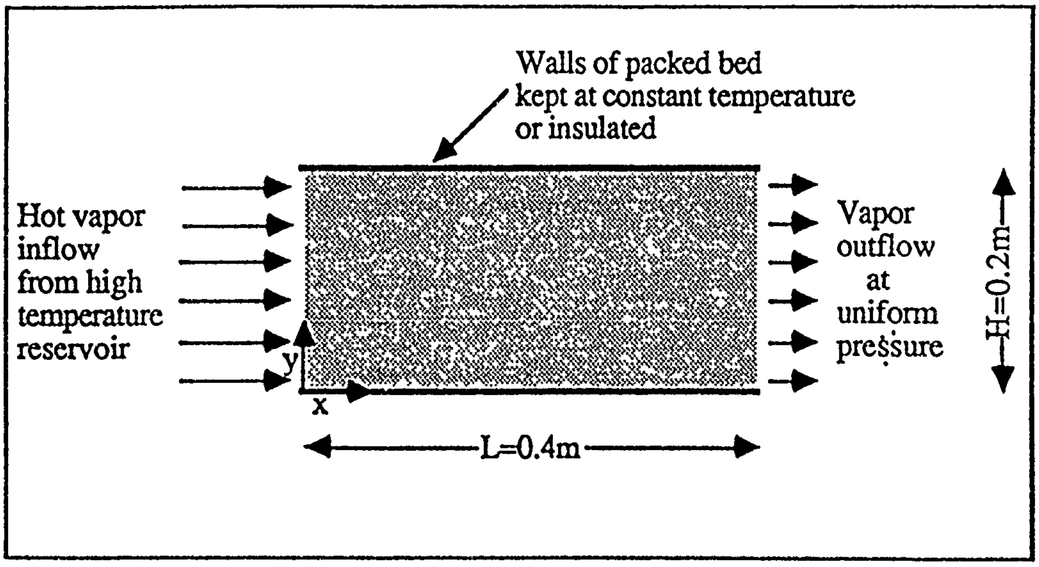

Figure 3.1: Schematic diagram of the problem

of the packed bed, the vapor at certain locations becomes compressed enough so that its density reaches the saturation vapor density at the prevailing temperature, thus causing condensation to take place.

3.2 Mathematical model

The volume averaging technique which was used in Section II will be employed in this section too in developing the governing equations for the present problem. In establishing the model for the analysis of this problem, the following assumptions and simplifications were employed:

(1) The width of the packed bed is significantly larger than the height and, therefore, the problem is essentially two-dimensional.

(2) The vapor phase always behaves as an ideal gas.

(3) There is no local thermal equilibrium (LTE) between the solid and fluid phases but there is LTE between the vapor and liquid phases when there is condensate present in the packed bed.

(4) Natural convection effects are negligible compared to the forced convection in the vapor phase. This essentially yields a one-dimensional flow in the vapor phase.

(5) The solid and the liquid phases are incompressible, and the packed bed has uniform porosity and is isotropic.

(6) Boundary and variable porosity effects are neglected.

(7) Inter-particle and intra-particle radiation heat transfer as well as thermal dispersion effects are neglected.

(8) Variations of physical properties such as thermal conductivities, specific heat capacities, viscosity and latent heat of vaporization with temperature are neglected.

With all these assumptions and simplifications taken into account, the volume averaged governing equations can be established in the following form (it should be noted that we have switched to subscripts β, γ, σ and f which denote the liquid, vapor, solid and the combined fluid (liquid+vapor) phases respectively):

Vapor phase continuity equation:

$$\frac{\partial}{\partial t}\left(\varepsilon_\gamma < \rho_\gamma >^\gamma\right) + \nabla.\left(< \rho_\gamma >^\gamma < \vec{v}_\gamma >\right) = - < \dot{m} > \tag{3.1}$$

Due to possible phase change (condensation) in the vapor phase, there is an additional source term, $< \dot{m} >$, in this equation as compared to equation (2.3). Moreover, because of phase change, the volume fractions of the vapor and the liquid phases will be functions of time. Therefore, instead of a constant porosity value, ε, in this equation we have a variable for the vapor phase volume fraction, namely $\varepsilon_\gamma(t)$.

Liquid phase continuity equation:

The volume averaged continuity equation for the noncompressible liquid phase can be established as:

$$\frac{\partial \varepsilon_\beta}{\partial t} + \nabla. < \vec{v}_\beta > - \frac{< \dot{m} >}{\rho_\beta} = 0 \tag{3.2}$$

Vapor phase equation of motion:

$$\nabla < P_\gamma >^\gamma = - \frac{< \rho_\gamma >^\gamma F \varepsilon_\gamma}{K_\gamma^{1/2}} [< \vec{v}_\gamma > . < \vec{v}_\gamma >] \frac{< \vec{v}_\gamma >}{|< \vec{v}_\gamma >|} - \frac{\mu_\gamma}{K_\gamma} < \vec{v}_\gamma > \tag{3.3}$$

This equation is similar to the one used in Section II except that ε_γ is used instead of ε, and the definitions of F and K_γ are slightly different as will be discussed later. With assumption (4) above, this equation reduces to the following one-dimensional form:

$$\frac{\partial}{\partial x} < P_\gamma >^\gamma = - \frac{< \rho_\gamma >^\gamma F \varepsilon_\gamma}{K_\gamma^{1/2}} < u_\gamma >^2 - \frac{\mu_\gamma}{K_\gamma} < u_\gamma > \tag{3.3a}$$

Liquid phase equation of motion:

The liquid phase motion is formulated by Darcy's law since any motion of the liquid will be much smaller than that of the vapor phase:

$$< \vec{v}_\beta > = - \frac{k_{r\beta} K}{\mu_\beta} \left\{ k_\varepsilon \nabla \varepsilon_\beta + k_{<T>} \nabla < T_f >^f + (\rho_\beta - < \rho_\gamma >^\gamma) \vec{g} \right\} \tag{3.4}$$

Fluid phase energy equation:

$$\left[\varepsilon_\beta \rho_\beta (c_p)_\beta + \varepsilon_\gamma < \rho_\gamma >^\gamma (c_p)_\gamma \right] \frac{\partial < T_f >^f}{\partial t} - < \dot{m} > \Delta h_{vap}$$

$$+ \left[\rho_\beta (c_p)_\beta < \vec{v}_\beta > + < \rho_\gamma >^\gamma (c_p)_\gamma < \vec{v}_\gamma > \right] . \nabla < T_f >^f = \nabla . \left[k_{feff} \nabla < T_f >^f \right]$$

$$+ h_{\sigma\beta} a_{\sigma\beta} \left[< T_\sigma >^\sigma - < T_f >^f \right] + h_{\sigma\gamma} a_{\sigma\gamma} \left[< T_\sigma >^\sigma - < T_f >^f \right] \tag{3.5}$$

Comparison of this equation with equation (2.5) shows the additional effect of the liquid phase in the transient storage term, conduction term and the sensible heat transport term due

to motion. Moreover, there is an additional term accounting for the heat transfer due to condensation as well as a convection heat transfer term accounting for the energy transport between the solid and the liquid phases.

Solid phase energy equation:

$$\varepsilon_\sigma \rho_\sigma (c_p)_\sigma \frac{\partial < T_\sigma >^\sigma}{\partial t} = \nabla.\left[k_{\sigma eff} \nabla < T_\sigma >^\sigma\right]$$

$$- h_{\sigma\beta} a_{\sigma\beta}\left[< T_\sigma >^\sigma - < T_f >^f\right] - h_{\sigma\gamma} a_{\sigma\gamma}\left[< T_\sigma >^\sigma - < T_f >^f\right] \qquad (3.6)$$

In this equation too, the energy transport term between the liquid and the solid phases is modeled by a convective heat transfer term.

Volume constraint relation:

Due to the fact that the liquid and vapor volume fractions are variable, the following volume constraint relation , ,ovides a coupling equation, namely:

$$\varepsilon_\sigma + \varepsilon_\gamma(t) + \varepsilon_\beta(t) = 1 \qquad (3.7)$$

Equation of state for vapor phase:

Following assumption (2), the equation of state for the vapor phase becomes:

$$< P_\gamma >^\gamma = < \rho_\gamma >^\gamma R_\gamma < T_f >^f \qquad (3.8)$$

Thermodynamic relation for the saturation density of vapor:

$$\rho_{\gamma,s} = \frac{\exp\left(A - \frac{B}{T_f}\right)}{R_\gamma T_f} \tag{3.9}$$

where A and B are constants, T_f is in degrees Kelvin and $\rho_{\gamma,s}$ is in kg/m^3. This relation was obtained by a least squares curve fitting method to a range of data relevant to the present study.

Equations (3.1) through (3.9) yield nine equations in nine unknowns, namely $\varepsilon_\beta(t)$, $\varepsilon_\gamma(t)$, $<\rho_\gamma>^\gamma$, $<\vec{v}_\gamma>$, $<\vec{v}_\beta>$, $<P_\gamma>^\gamma$, $<T_f>^f$, $<T_\sigma>^\sigma$, and $<\dot{m}>$.

For the present analysis the effective thermal conductivities for the solid and fluid phases were modeled as:

$$\begin{aligned} k_{\sigma eff} &= \varepsilon_\sigma k_\sigma \\ k_{feff} &= \varepsilon_\gamma k_\gamma + \varepsilon_\beta k_\beta \end{aligned} \tag{3.10}$$

The permeability of the packed bed of spherical particles is given in the following form (Ergun, 1952):

$$K = \frac{\varepsilon^3 d_p^2}{150\,(1-\varepsilon)^2} \tag{3.11}$$

where ε is the porosity and d_p is the particle diameter. Therefore, the permeability for the vapor phase, K_γ, and the geometric factor, F, in the vapor phase momentum equation can be expressed as functions of d_p and ε_γ as (Vafai, 1984):

$$K_\gamma = \frac{\varepsilon_\gamma^3 d_p^2}{150\,(1-\varepsilon_\gamma)^2} \tag{3.12}$$

$$F = \frac{1.75}{\sqrt{150}\,\varepsilon_{\gamma}^{3/2}} \tag{3.13}$$

For the relative permeability of the liquid phase, the one suggested by Udell and Fitch (1985) was used. This is modeled in the following form:

$$k_{r\beta} = S^3$$

$$\text{where:} \qquad S = \frac{s - s_{im}}{1 - s_{im}} \qquad \text{and} \qquad s = \frac{\varepsilon_\beta}{\varepsilon} = \frac{\varepsilon_\beta}{1 - \varepsilon_\sigma} \tag{3.14}$$

where S is the normalized saturation, s is the absolute saturation, and s_{im} is the "immobile" saturation. The immobile saturation, s_{im}, is the critical value of the absolute saturation. If s is greater than s_{im} then the liquid phase in the packed bed becomes mobile. For values of s lower than s_{im}, any liquid phase present in the porous system will be immobile, or in the so called pendular state. The value of 0.1 used for s_{im} in the work of Kaviany and Mittal (1987) will be used in the present work because of lack of any better experimental finding. With this value of s_{im}, the critical value of the liquid fraction at which liquid phase becomes mobile, i.e., $\varepsilon_{\beta crit}$, was computed from equation (3.14) to be 0.039, with the value of porosity of the packed bed taken to be 0.39, which is the average asymptotic value for packed beds in which the particle diameter to packed bed diameter is below a certain value (Benanati and Brosilow, 1962). For all the cases studied in the present investigation the maximum value of ε_β never reached $\varepsilon_{\beta crit}$ and, therefore, the liquid was always immobile. It should, however, be noted that the liquid was not assumed to be immobile in modeling the problem, but the fact that it turned out to be immobile was the consequence of the governing physical conditions of the problem.

The empirical correlations for the fluid-to-solid heat transfer coefficients that were used in this section are the same as those in Section II, namely:

$$h_{\sigma j} = 1.064\,(c_p)_j G_j \left[\frac{c_p\mu}{k}\right]_j^{-2/3} \left[\frac{d_p G}{\mu}\right]_j^{-0.41} \qquad \text{for} \quad \frac{d_p G}{\mu} \geq 350 \qquad \text{(turbulent)}$$

$$h_{\sigma j} = 18.1\,(c_p)_j G_j \left[\frac{c_p\mu}{k}\right]_j^{-2/3} \left[\frac{d_p G}{\mu}\right]_j^{-1} \qquad \text{for} \quad \frac{d_p G}{\mu} \leq 40 \qquad \text{(laminar)} \tag{3.15}$$

where G represents the mass flow rate through a unit surface area perpendicular to the direction of flow, and the subscript j denotes β or γ for the liquid or vapor phase respectively.

The specific surface area of the packed bed for the vapor phase is expressed in the following form:

$$a_{\sigma\gamma} = \frac{6(1 - \varepsilon_\gamma - \varepsilon_\beta)}{d_p} \tag{3.16}$$

Strictly speaking, this correlation was originally derived from geometric considerations for a fully saturated packed bed of spherical particles for a single fluid phase, in the form $a = 6(1 - \varepsilon) / d_p$ (Dullien, 1979). However, since ε_β is very small (less than 0.01) compared to ε_γ (approximately 0.38-0.39), equation (3.16) provides a very accurate estimate for $a_{\sigma\gamma}$

Also from an analysis of the representative length scales and volume scales of the liquid and vapor phases of the working fluid, one may obtain a relation between the specific surface areas $a_{\sigma\gamma}$ and $a_{\sigma\beta}$ as:

$$a_{\sigma\beta} = a_{\sigma\gamma} \left(\frac{\varepsilon_\beta}{\varepsilon_\gamma} \right)^{2/3} \tag{3.17}$$

and hence:

$$a_{\sigma\beta} = \frac{6(1-\varepsilon_\gamma-\varepsilon_\beta)}{d_p} \left(\frac{\varepsilon_\beta}{\varepsilon_\gamma} \right)^{2/3} \tag{3.18}$$

Since the liquid phase was always in pendular state and, therefore, $h_{\sigma\beta}$ was always zero, due to the fact that for the liquid phase the mass flow rate was zero, there was no real need for the above information. However, $a_{\sigma\beta}$ was modeled as given in equation (3.18) for the sake of complete modeling.

3.2.1 Initial and boundary conditions

The physical conditions initially prevailing in the packed bed are the same as those of the previous section. They are, therefore, mathematically expressed as follows:

$$\begin{aligned} &T_f(x,y,t=0) = T_\sigma(x,y,t=0) = T_o \\ &P_\gamma(x,y,t=0) = P_o \\ &u_\gamma(x,y,t=0) = 0 \end{aligned} \tag{3.19}$$

The pressure on the right boundary is kept at a value equal to the initial pressure in the packed bed while vapor at a fixed high temperature and pressure is supplied at the inlet of

the packed bed. The mathematical form of the left and right boundary conditions is as follows:

$$\begin{aligned} &T_f(x=0,y,t) = T_{in} \\ &P_\gamma(x=0,y,t) = P_{in} \qquad \text{at } t > 0^+ \\ &P_\gamma(x=L,y,t) = P_{out} = P_O \end{aligned} \tag{3.20}$$

In the present problem, both insulated top and bottom wall boundary conditions as well as constant temperature top and bottom wall boundary conditions will be investigated. For the case with insulated boundary conditions we have:

$$k_{feff} \left. \frac{\partial T_f}{\partial y} \right|_{y=0,\ y=H} = 0 \qquad \text{and} \qquad k_{\sigma eff} \left. \frac{\partial T_\sigma}{\partial y} \right|_{y=0,\ y=H} = 0 \tag{3.21}$$

For the case with constant temperature boundary conditions at the top and bottom walls, the boundary conditions can be expressed as:

$$\begin{aligned} &T_f(x,y=0,t) = T_\sigma(x,y=0,t) = T_{bot} = T_O \\ &T_f(x,y=H,t) = T_\sigma(x,y=H,t) = T_{top} = T_O \end{aligned} \tag{3.22}$$

3.2.2 Physical conditions for the numerical runs

In the present investigation too, in order to analyze the effects of different characteristic parameters, such as Re_p and Da, different particle diameters ranging from 1 mm to 5 mm, and different ranges of operating pressures were considered. Also two different solid materials were considered in the present problem for determining the effect of the thermal properties of the solid phase on transport phenomena. These materials were

lead and 1% Carbon-steel. The value of the average porosity of the packed bed was taken to be 0.39 following the arguments in Section II. The numerical values of different parameters used as initial and boundary conditions are given as follows:

$T_o = 300$ $\quad P_o = 796$ kPa $\quad T_{in} = 350$ K $\quad P_{out} = 796$ kPa

and the value of P_{in} was different for different cases ranging from 800 kPa to 866 kPa. The numerical values of the other physical data used in the numerical computations are as follows:

R-12:

k_γ=0.0097W/m.K $\quad (c_p)_\gamma$=710.J/kg.K $\quad \mu_\gamma$=12.6x10^{-6}kg/m.s $\quad R_\gamma$=0.0687588 J/kg.K
Δh_{vap}=111.3x10^3J/kg $\quad k_\beta$=0.0545 W/m.K $\quad (c_p)_\beta$=1115J/kg.K $\quad \mu_\beta$=179.2x10^{-6}kg/m.s
ρ_β=1190.35 kg/m^3

Lead:

k_σ = 35. W/m.K $\quad \rho_\sigma$ = 11340. kg/m^3 $\quad (c_p)_\sigma$ = 129. J/kg.K

1% Carbon steel:

k_σ = 43. W/m.K $\quad \rho_\sigma$ = 7800. kg/m^3 $\quad (c_p)_\sigma$ = 473. J/kg.K

3.3 Solution procedure

The finite difference techniques utilized in the solution of the problem in Section II were also employed in the solution of the present problem. In this problem, however, depending on whether phase change (condensation) takes place in the vapor phase or not,

the set of unknown variables and governing equations changes. The vapor phase continuity equation plays an important role in determining the solution format of the governing equations. The basic criterion which governs the phase change (condensation) in the working fluid is the attainment of the saturation vapor density. At any point where the vapor density reaches the saturation density corresponding to the temperature at that point, condensation will occur. The solution format of the condensation mode includes a switching from the vapor phase continuity equation to the thermodynamic relation giving the saturated vapor density for the solution of the vapor density, while the vapor continuity equation is then used for the solution of the condensation rate.

The stability of the numerical scheme was ensured by choosing a proper combination of Δx, Δy and Δt. A systematic decrease in the grid size was employed for obtaining the convergence of the numerical scheme, and the corresponding stable Δt was employed. A compromise, however, had to be made between the accuracy and the computer CPU time required for the computational runs. A 41 x 21 grid configuration (which gives a dimensionless Δx of 0.025) was found to yield qualitatively and quantitatively good results for the condensation period and very good results for the problem for the cases with insulated boundary conditions. A 41 x 41 grid configuration was employed for the cases with constant wall temperature boundaries.

3.4 Results and discussions

In this section, part of the results that will be presented for the computational runs performed will be in terms of nondimensionalized variables. Variables $< P_\gamma >^\gamma$, $< \rho_\gamma >^\gamma$ and $< u_\gamma >$ are nondimensionalized by using the corresponding reference quantities,

namely P^*, ρ^*, and v^*. P^* was chosen to be 100 kPa, ρ^* was calculated from the equation of state by using P^* and the initial temperature, T_0. The reference velocity, v^*, was computed from the vapor phase momentum equation, (3.3a), using a pressure gradient which was based on the global pressure difference applied across the packed bed and a density which was calculated from the equation of state by using T_0 and P_{av} (the average of the inlet and exit pressures). Temperatures of the solid and fluid phases are nondimensionalized in the form $\Theta = (T - T_0) / (T_{in} - T_0)$. Time, t, is kept in dimensional form for giving an insight of the actual magnitudes of the durations involved. Same thing is done for the condensation rate data and the total condensate variations as well as for the thermal charging data of the packed bed.

As in the case of the solution of the problem in Section II, two distinctly noticeable stages were observed in the solution of the problem considered. These were namely the *early stage* and the *later stage*. The *early stage* usually lasts for a very short period of time during which sharp changes in the distribution of certain field variables, such as $< P_\gamma >^\gamma$, $< \rho_\gamma >^\gamma$ and , $< u_\gamma >$, occur due to the step change boundary conditions which cause very strong transient behavior.

3.4.1 Problem with insulated wall boundary conditions

Figure 3.2 depicts the variations of the density, velocity and pressure of the vapor as well as the variation of the liquid fraction during the *early stage* at the midplane of the packed bed for insulated wall conditions for a case in which lead was used as the solid phase. It was found that, for cases with insulated boundary conditions, one-dimensional formulation would be very accurate since there was no appreciable variation of the field variables in the y-direction. Figure 3.2(a) shows that the vapor pressure distribution

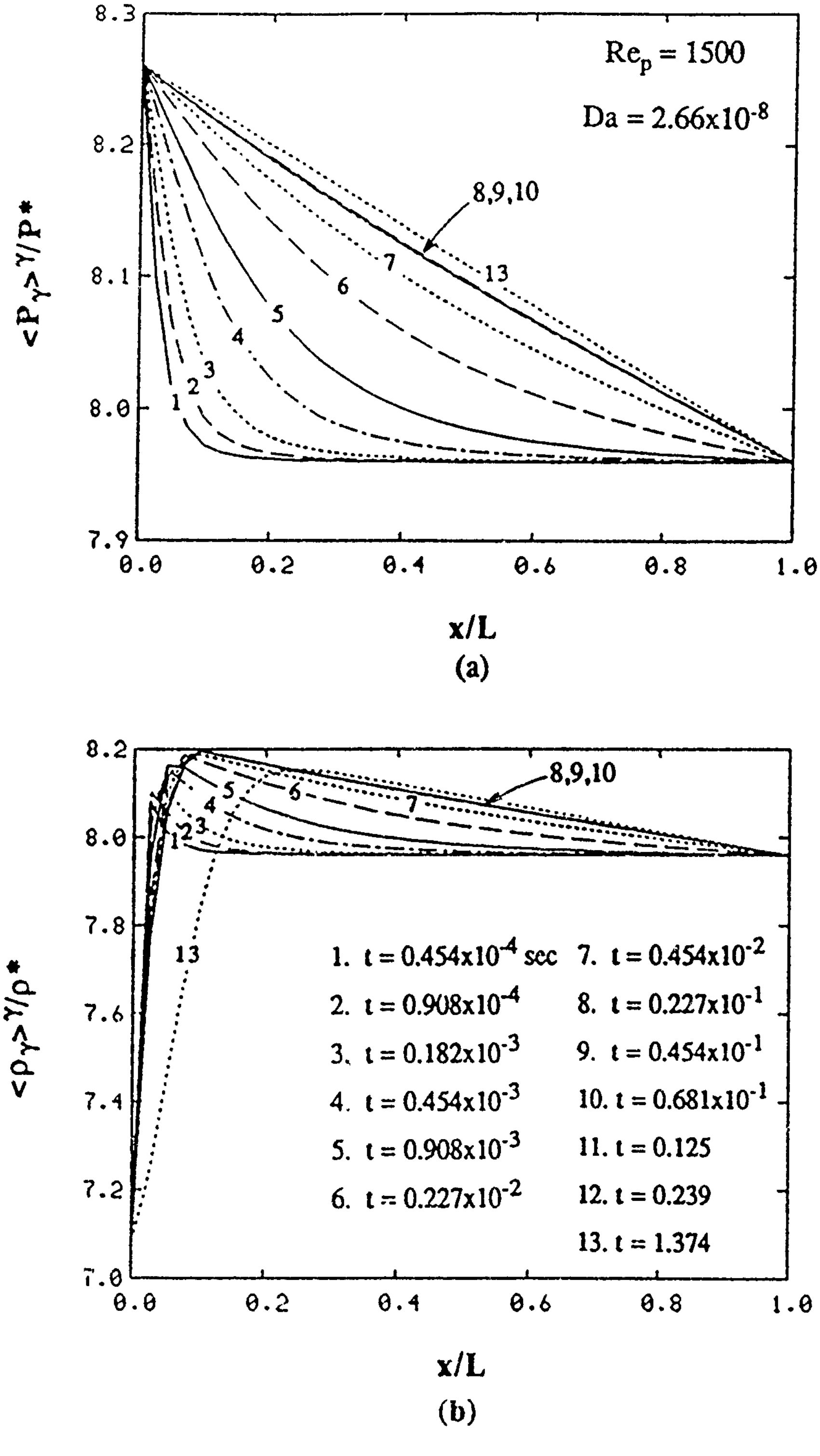

Figure 3.2: Variations of different field variable distributions during the *early stage*

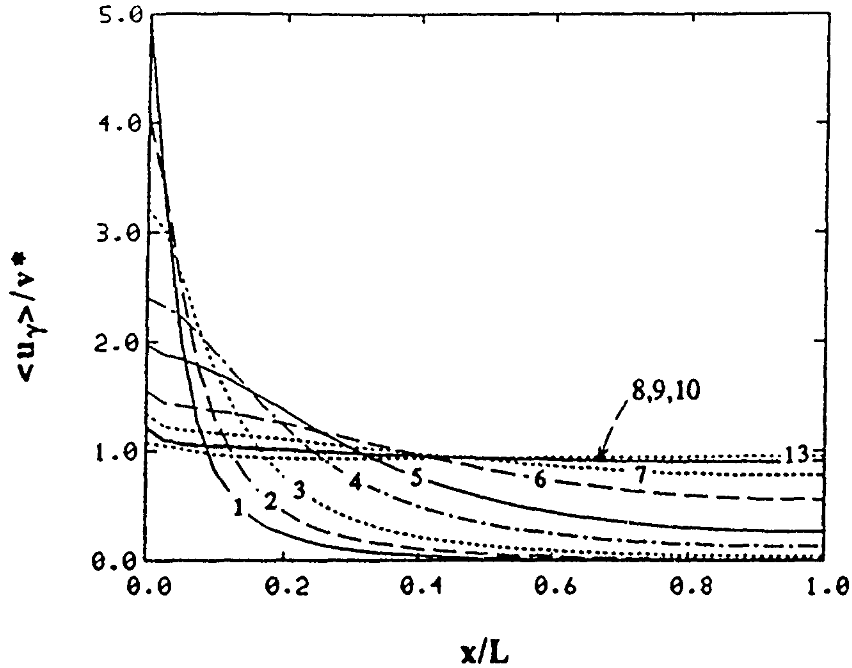

(c)

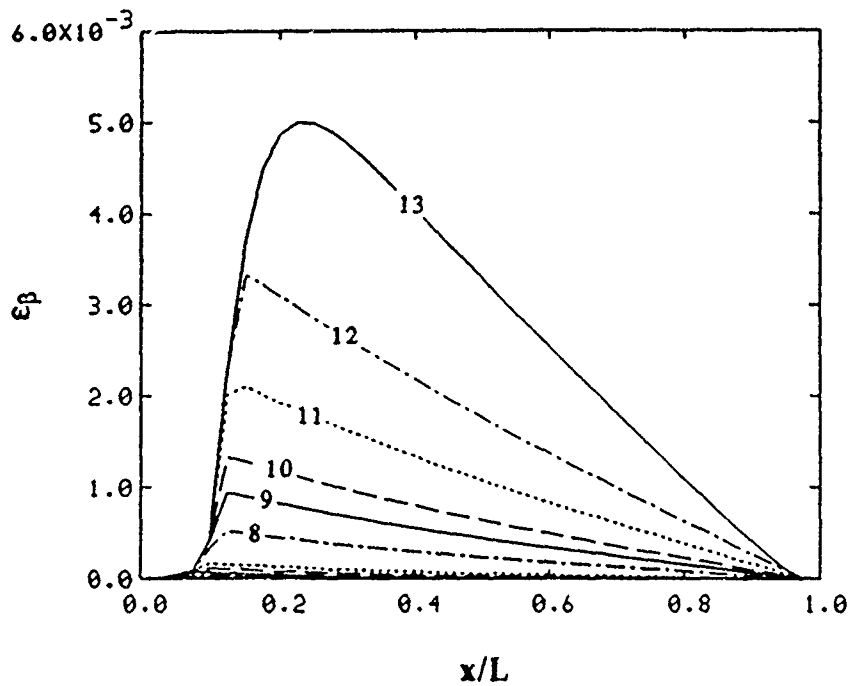

(d)

Figure 3.2 (continued)

evolves and becomes almost linear during the *early stage*. There is no appreciable thermal penetration during this period and the spatial variation of the vapor density follows the same trend as the vapor pressure as dictated by the equation of state, except at the entrance of the packed bed. The temporal increase in the density is a result of the transient effects dictated by the vapor phase continuity equation. At points where the vapor density reaches the saturation vapor density, condensation occurs and the liquid phase accumulates. Due to the physical conditions of the problem, the period of time during which the vapor phase in the packed bed maintains a high enough density for condensation to occur is relatively short compared to the total thermal charging period of the packed bed. The variation of the liquid fraction is shown in Figure 3.2(d). In Figure 3.2 the *early stage* was somewhat extended to include the time during which more than 99% of the condensation took place for this case.

Beyond the *early stage*, the changes in the field variables are mainly caused by the development of the thermal penetration depth since the pressure distribution remains almost unchanged. Distributions of the field variables of interest by time during the *later stage* are shown in Figure 3.3. In Figure 3.3(a) the solid lines depict the solid phase temperature distribution while the dotted lines depict the fluid phase temperature distribution. During the *early stage*, the effect of the transient term as well as the condensation (source) term in the vapor continuity equation die out and, therefore, during the *later stage* the vapor density variation in time becomes dependent on the convective term in this equation. The mass flow rate in the packed bed becomes constant requiring an inverse relationship between the vapor density and velocity. Figures 3.3(c,d) clearly show this behavior as a mirror image type of trend in the variations of the vapor density and vapor velocity at any instant. The spatial variation in the vapor density, on the other hand, can be explained from the equation of state. At any instant before the packed bed is fully charged, the slope of the vapor

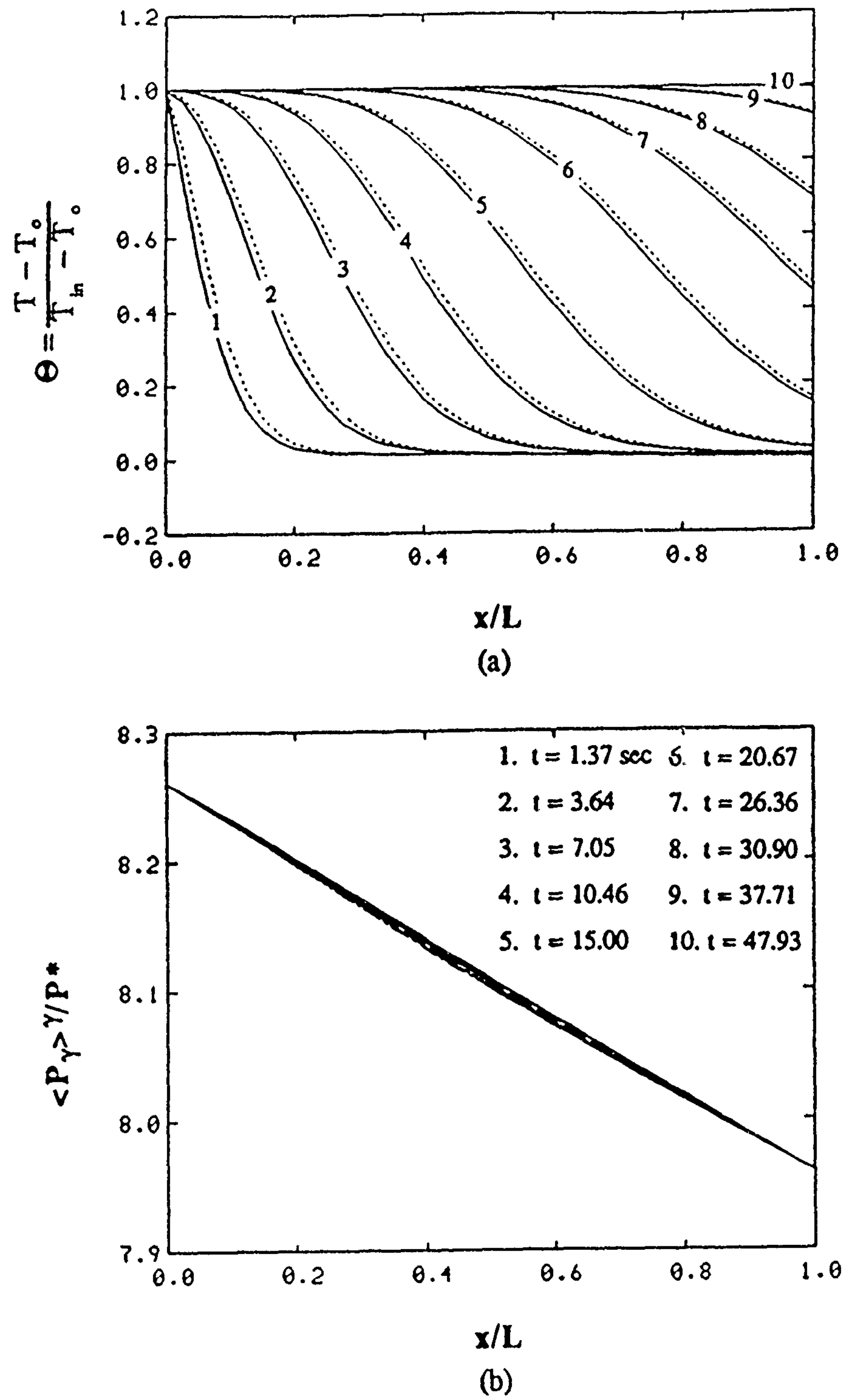

Figure 3 3: Variations of different field variable distributions during the *later stage*

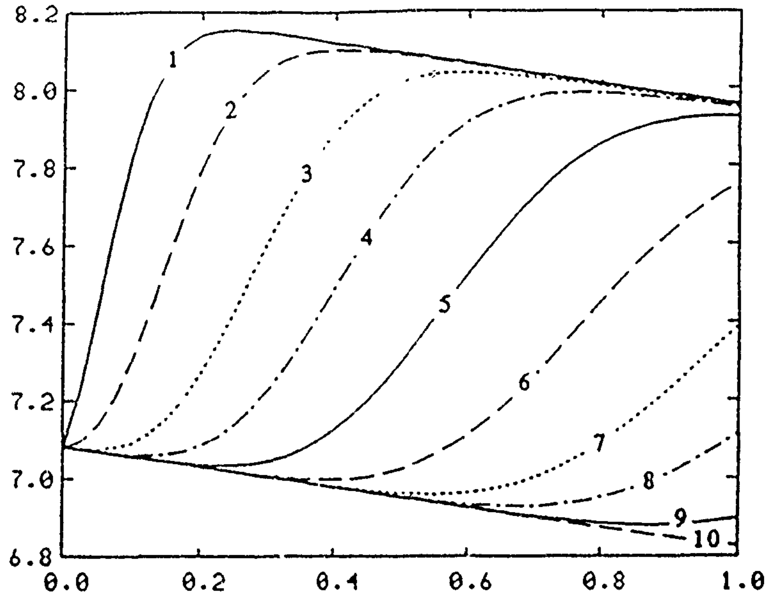

$<\rho_\gamma>^\gamma/\rho^*$

x/L

(c)

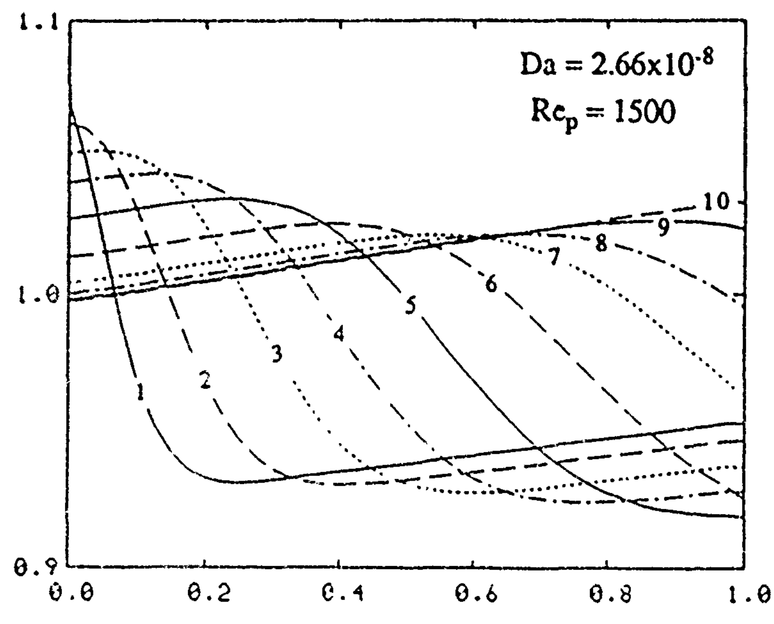

$<u_\gamma>/v^*$

x/L

(d)

Figure 3.3 (continued)

temperature profile will be larger than the slope of the vapor pressure profile for a certain length of the packed bed (meaning a sharper decrease in temperature than in pressure) causing an increase in the vapor density, where exactly the opposite behavior can be seen at the locations where the slope of the vapor temperature profile is smaller than that of the vapor pressure profile (meaning a sharper decrease in pressure than in temperature). When the packed bed becomes thermally fully charged, the vapor density variation follows exactly the same trend as that of the vapor pressure as dictated by the equation of state.

The overall condensation rate in the packed bed was computed by integrating the individual condensation rates at all the grid points over the associated volumes at each time step. The average overall condensation rate per unit width of packed bed for the case for which the *early* and *later stage* results have been presented is depicted in Figure 3.4(a). It can be seen that the overall condensation rate is higher at the beginning when the transient effects are very strong, and dies away as the sharp changes in the vapor density variation erode. The accumulative condensate in the packed bed was also computed by integrating the condensation rates at all grid points over the associated volumes at each time step and totaling with the previous sum. Figure 3.4(b) shows the variation in time of the amount of total condensate in the packed bed per unit width of the bed. As may be seen from this figure, the accumulation is fast at the start due to high condensation rate, and builds up quickly reaching an asymptotic value in a short time.

The next important analysis carried out was related to the thermal charging of the packed bed. For this, we needed to track down the variations of the relevant parameters including heat flow rates and energy storage rate. The variation in the amount of thermal energy flowing into and out of the packed bed per unit width is depicted as a function of time in Figure 3.5(a). These were computed by integrating the energy fluxes of the vapor

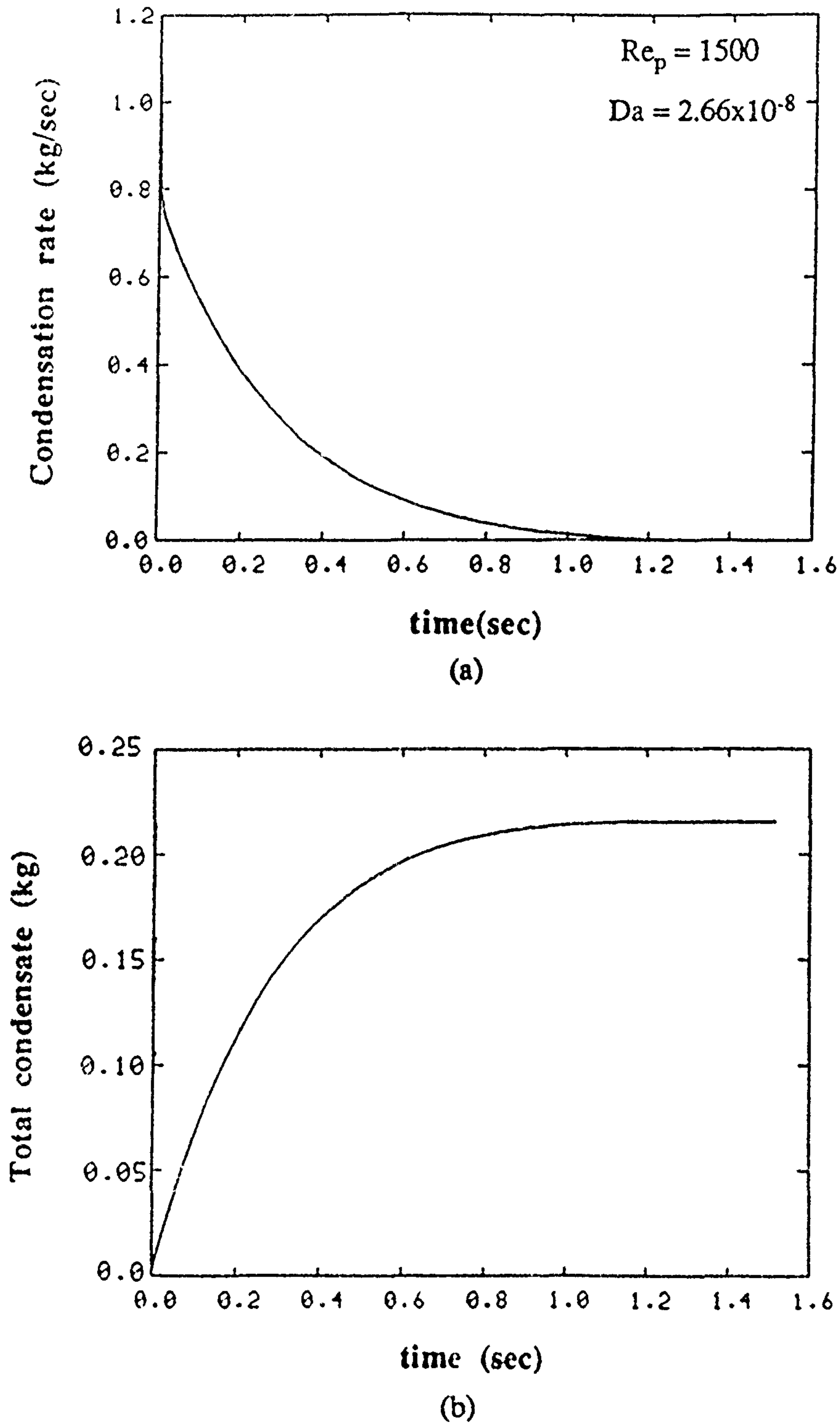

Figure 3.4: (a) Variation of average overall condensation rate in the packed bed

(b) Variation of total accumulative condensate in the packed bed

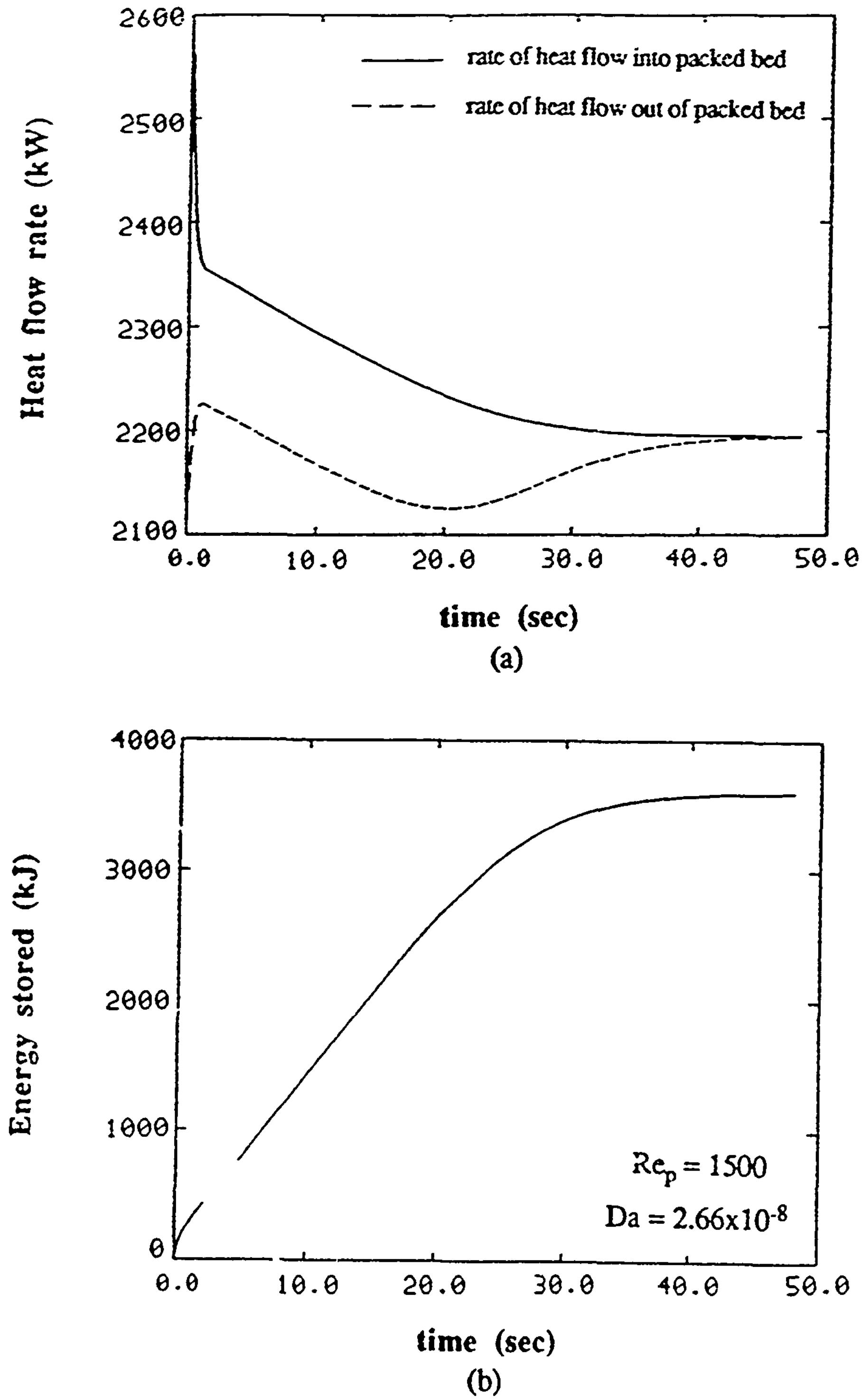

Figure 3.5: (a) Rate of heat flow into and out of the packed bed

(b) Thermal charging of the packed bed (insulated top and bottom walls)

flowing into and out of the packed bed over the inlet and the exit crosssections. A very short section of the time history of the thermal charging process at the beginning was left out in this figure in order to obtain a better scale that shows the variation of the heat flow rates clearly for the whole charging duration. During this very short time interval the rate of heat flow into the packed bed was several times larger due to the presence of large velocities at the onset of the charging process, i.e., during the *early stage*. Figure 3.5(b) shows the net energy stored per unit width of the packed bed as a function of time. This was computed in the numerical code by integrating the net heat flow rate into the packed bed over time. The value of the total net energy stored in the packed bed was also determined by a thermodynamic balance analysis between the initial and the final (fully charged) states of the packed bed. The result of the numerical computation was found to be in very good agreement with this analytical result.

3.4.2 Problem with constant temperature wall boundary conditions

The same problem was solved for constant temperature top and bottom wall boundary conditions. As expected, strong two-dimensional behavior was found in the variations of many of the field variables. Therefore, rather than presenting the results in the format of the previous section we will resort to two-dimensional contour plots for the field variable distributions. It should be noted that the solution of this problem has *early stage* and *later stage* parts just as in the case of insulated boundary conditions case. However, the distribution of three field variables at three time levels in the *later stage* will be presented here for convenience. These will be sufficient to show the two-dimensional behavior of the problem which becomes apparent during the *later stage*.

Figure 3.6 depicts the distributions of the fluid temperature, solid temperature and the vapor density in the packed bed at three different time levels. It can be seen from this figure that, although the two-dimensional behavior of the field variables is not very significant at the beginning, it becomes very much pronounced as the thermal penetration in the bed advances. In the core region of the packed bed the advancement of the thermal front follows a similar trend as in the case of insulated boundary conditions. Near the top and bottom walls, however, there is a temperature gradient in the y-direction due to heat loss. Since there is no significant variation in the vapor pressure in the y-direction, the vapor density variation in this direction is primarily determined by the fluid temperature variation. Hence, at locations closer to the top and bottom walls where the fluid temperature becomes lower the vapor density becomes higher. In the core region of the packed bed the variation of the vapor density in x-direction depends on the slopes of the temperature and pressure distributions in this direction. At points where the slope of the temperature distribution is sharper than the slope of the pressure distribution, the vapor density will be increasing and vice versa.

The average overall condensation rate per unit width of the packed bed was computed in the same manner described in the previous section. Figure 3.7(a) shows the variation of this quantity in time. Upon comparing Figure 3.7(a) with Figure 3.7(b), one can see that condensation lasts slightly longer in the case of constant wall temperature case. This is reasonable because due to the heat loss from the top and bottom, for the points next to the top and bottom boundaries near the inlet of the packed bed, it takes longer for the vapor phase to reach a temperature at which the saturation vapor density exceeds the vapor density. Hence, the duration of condensation at these points is prolonged. This also gives

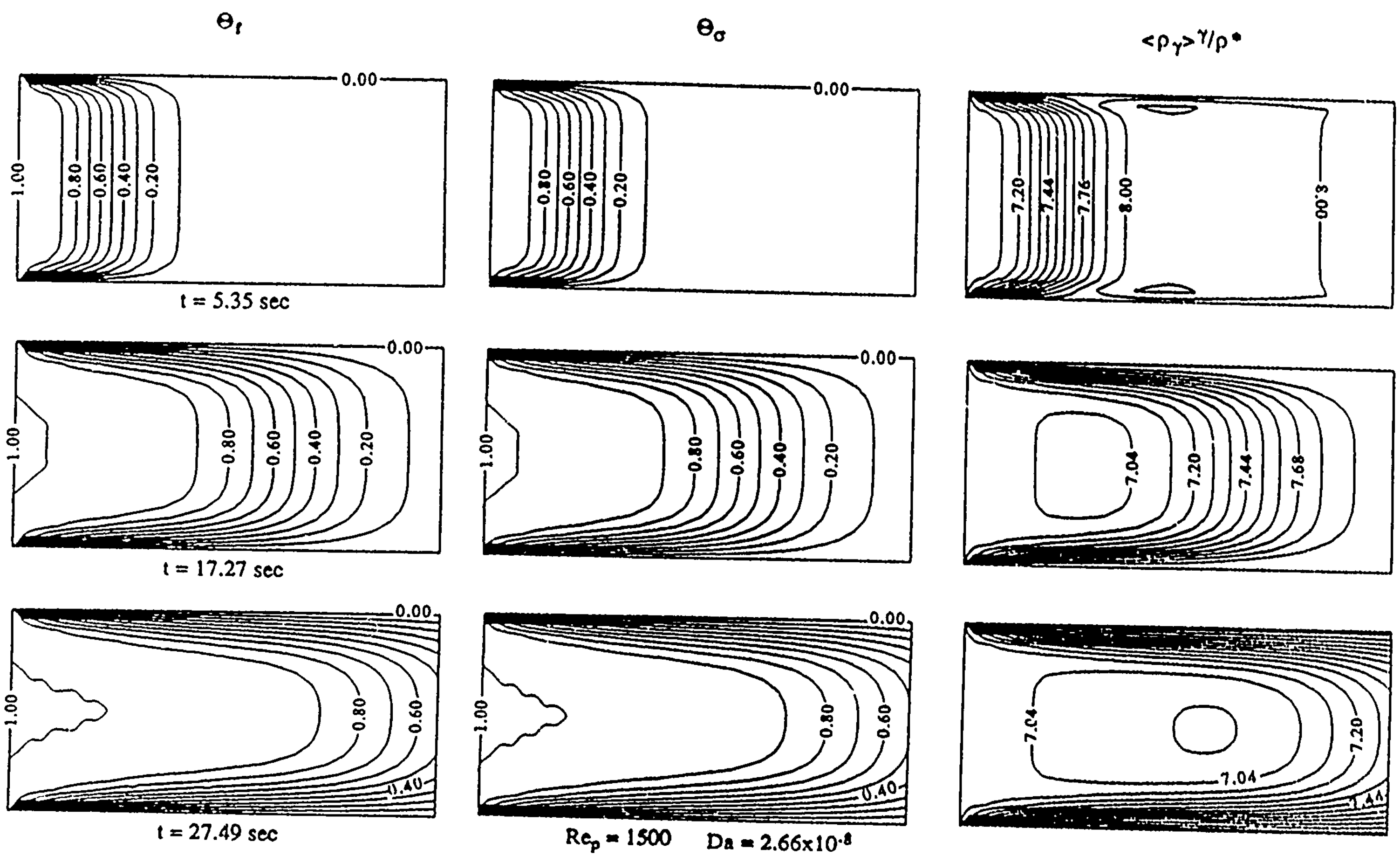

Figure 3.6: Distribution of field variables in the packed bed at different time levels during the *later stage*

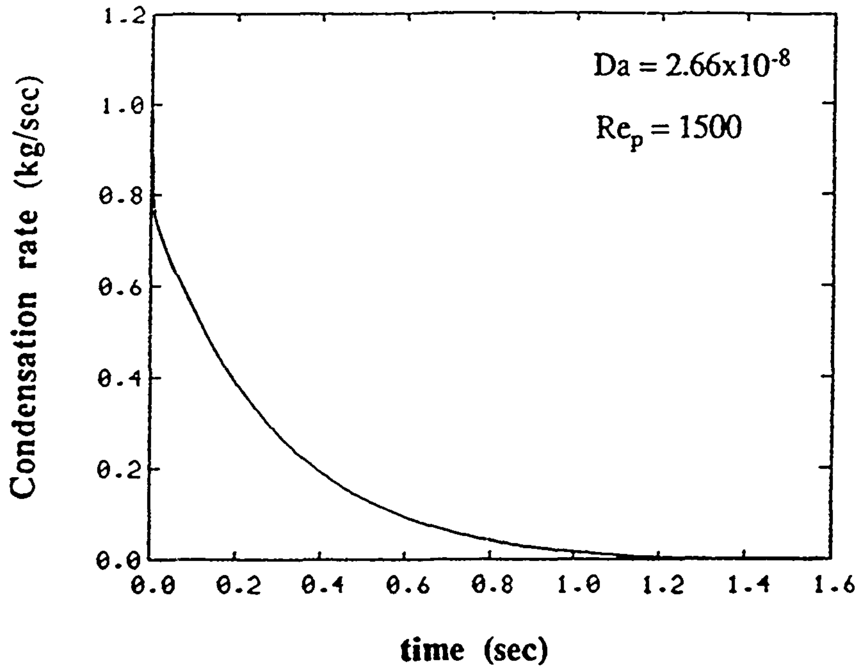

(a)

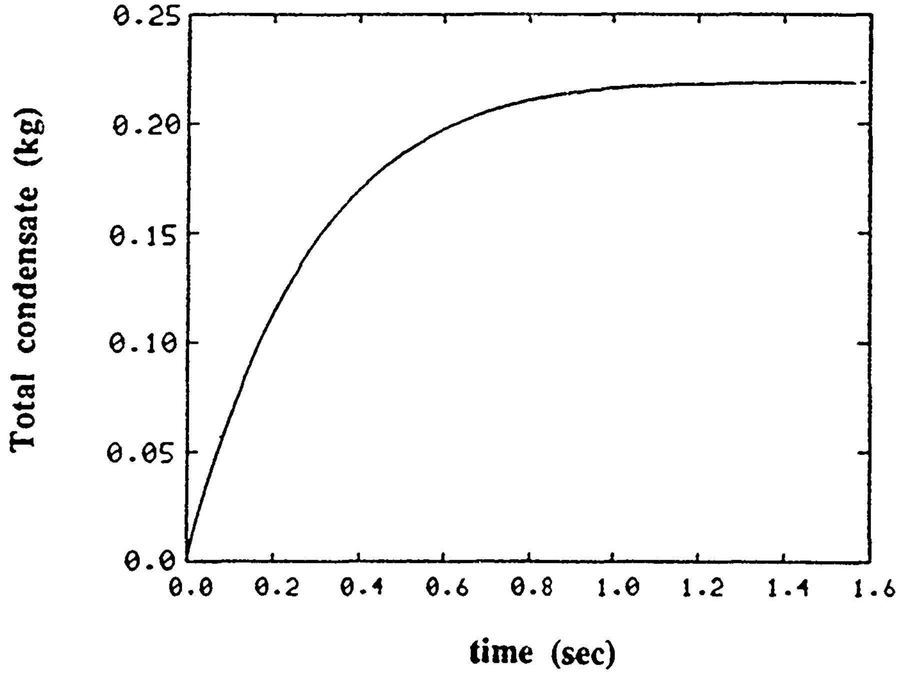

(b)

Figure 3.7: (a) Variation of average overall condensation rate in the packed bed

(b) Variation of total accumulate condensate in the packed bed

rise to a slightly larger amount of total condensate in the packed bed. This can be seen by comparing Figure 3.7(b) with Figure 3.4(b).

The variations in the amounts of heat flowing into and out of the packed bed per unit width at the inlet and exit are shown in Figure 3.8(a) as functions of time. In this case too, a small time slice at the beginning of the charging process is omitted from this figure in order to obtain a better scale in the figure. Figure 3.8(b) depicts the energy input into the packed bed, the energy that is lost from the top and bottom walls by conduction, and the net energy stored in the packed bed per unit width of the bed.

3.4.2.1 Effect of particle Reynolds number (Re_p) on condensation

The effect of Re_p on condensation was investigated by running three cases with different Re_p's while Darcy number (Da) was kept constant by keeping the particle diameter fixed. The solid phase in all these cases was lead. Different Re_p values were obtained by applying different inlet pressure boundary condition for each case. Figure 3.9(a) depicts the variation of the average overall condensation rate per unit width of the packed bed for the cases in which the nominal Re_p values were 500, 1,000 and 1,500 respectively. The corresponding variations of the total condensate in the packed bed per unit width as functions of time are shown in Figure 3.9(b). From these figures it becomes apparent that the higher the Re_p the higher will be the condensation rate and the total condensate accumulation. On the other hand, higher Re_p will cause slightly shorter duration of condensation. Higher Re_p indicates higher mass flow rates as well as higher pressure difference applied across the packed bed (larger compression forces in the vapor phase), thus, higher condensation rate. On the other hand, higher Re_p, due to higher pressure gradient applied means potential for faster propagation of the pressure, density and temperature distributions in the vapor phase and, thus, shorter condensation time.

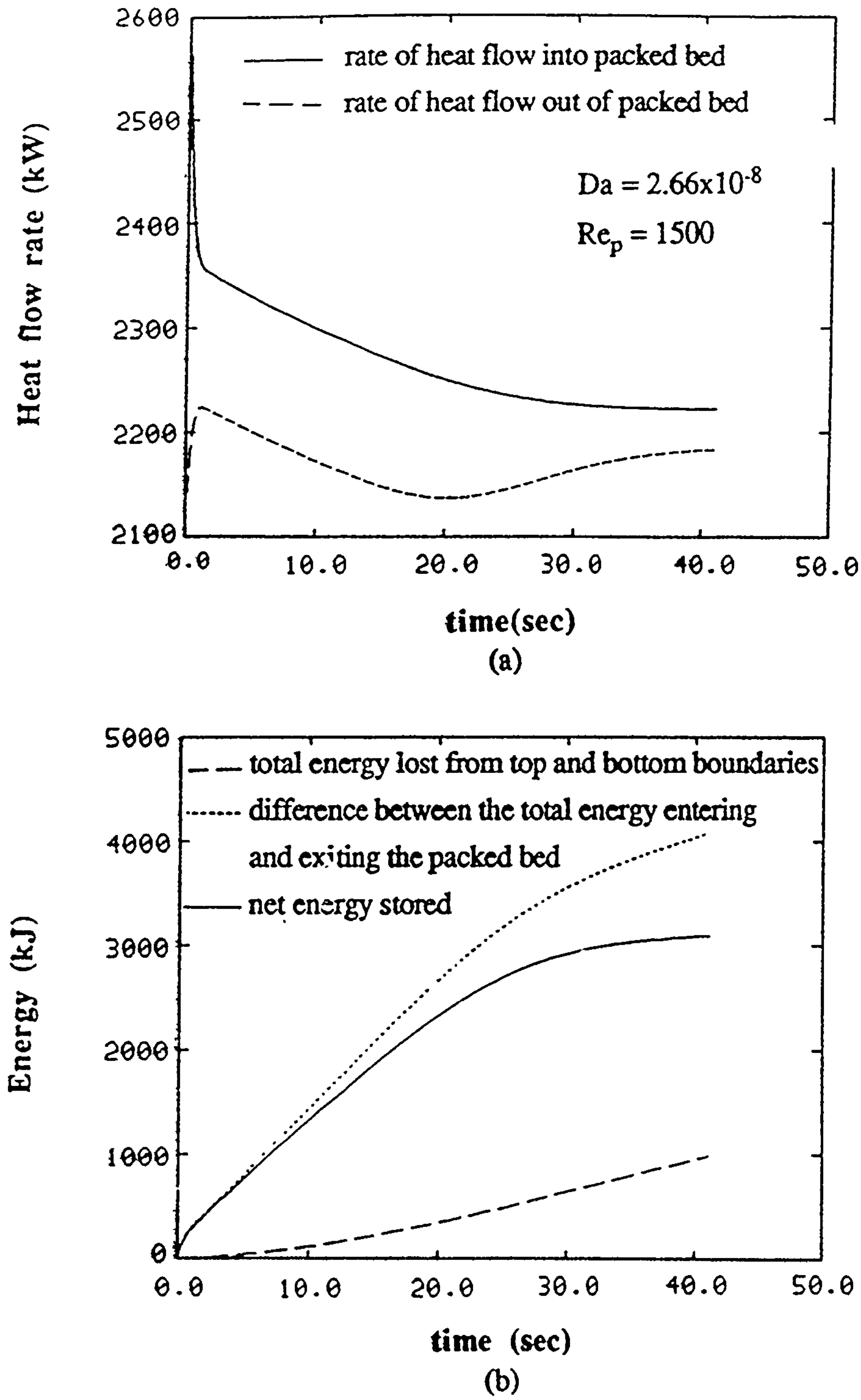

Figure 3.8: (a) Rate of heat flow at the inlet and exit of the packed bed

(b) Thermal charging of the packed bed (constant temperature walls)

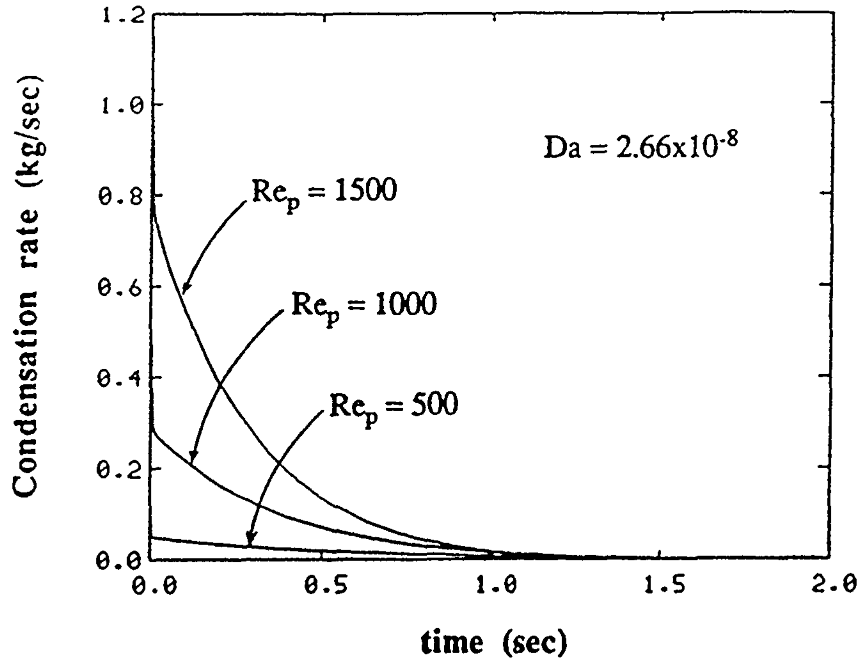

(a)

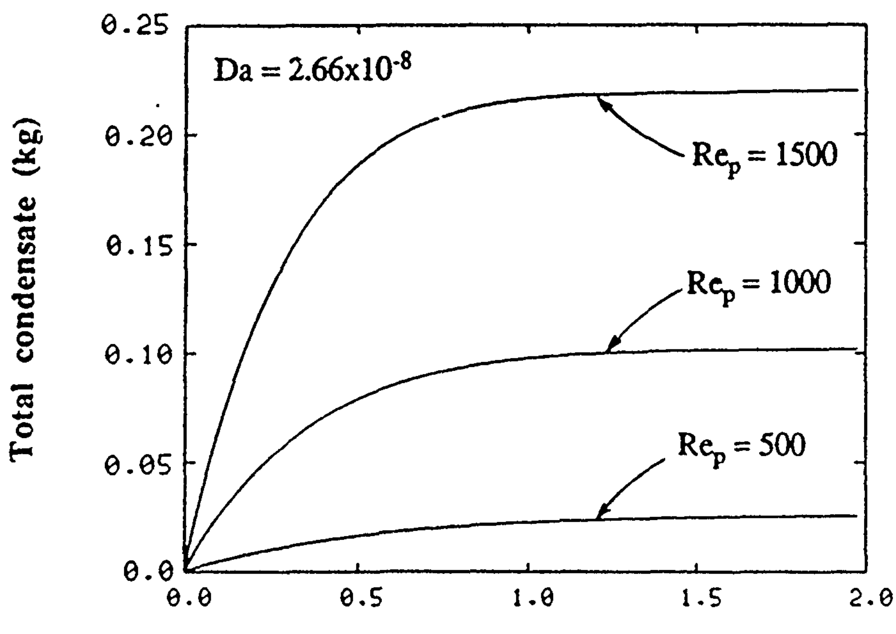

(b)

Figure 3.9: Effect of particle Reynolds number on condensation

3.4.2.2 Effect of Darcy number (Da) on condensation

The effect of Darcy number on condensation was also studied by considering three different Da values for a fixed Re_p, namely 1,500. Different Da values were obtained by changing the particle size. Figure 3.10 shows the variations of the average overall condensation rate and the total condensate accumulation in the packed bed per unit width as a function of time for Da values of 1.49×10^{-8}, 2.66×10^{-8} and 1.067×10^{-7}. The corresponding d_p values were 0.75, 1.0 and 2.0 mm, respectively. As d_p increases and, hence, Da increases, the specific surface area of the particles decreases. This causes smaller amount of heat transfer between the solid and fluid phases and a faster advancement of the thermal penetration depth of the fluid phase (faster attainment of lower densities than the saturation vapor density at the initial condensation points). Therefore, although condensation zone advances faster the condensation rate and the amount of condensate accumulation remain small. Decreasing the d_p at constant Re_p (by increasing the pressure difference applied across the packed bed) increases the vapor velocities and, hence, causes larger mass flow rates and larger condensation rates. Also as d_p is reduced the specific surface area of the particles increases. The heat transfer between the solid and fluid phases becomes more vigorous, energy is transferred at a faster rate from the fluid to the solid particles and, hence, it takes longer for the fluid phase at the initial condensation points to reach temperatures high enough at which the vapor density becomes less than the saturation vapor density and condensation stops. Hence, higher condensation rates are sustained for longer periods of time at these points, resulting in larger condensate accumulation.

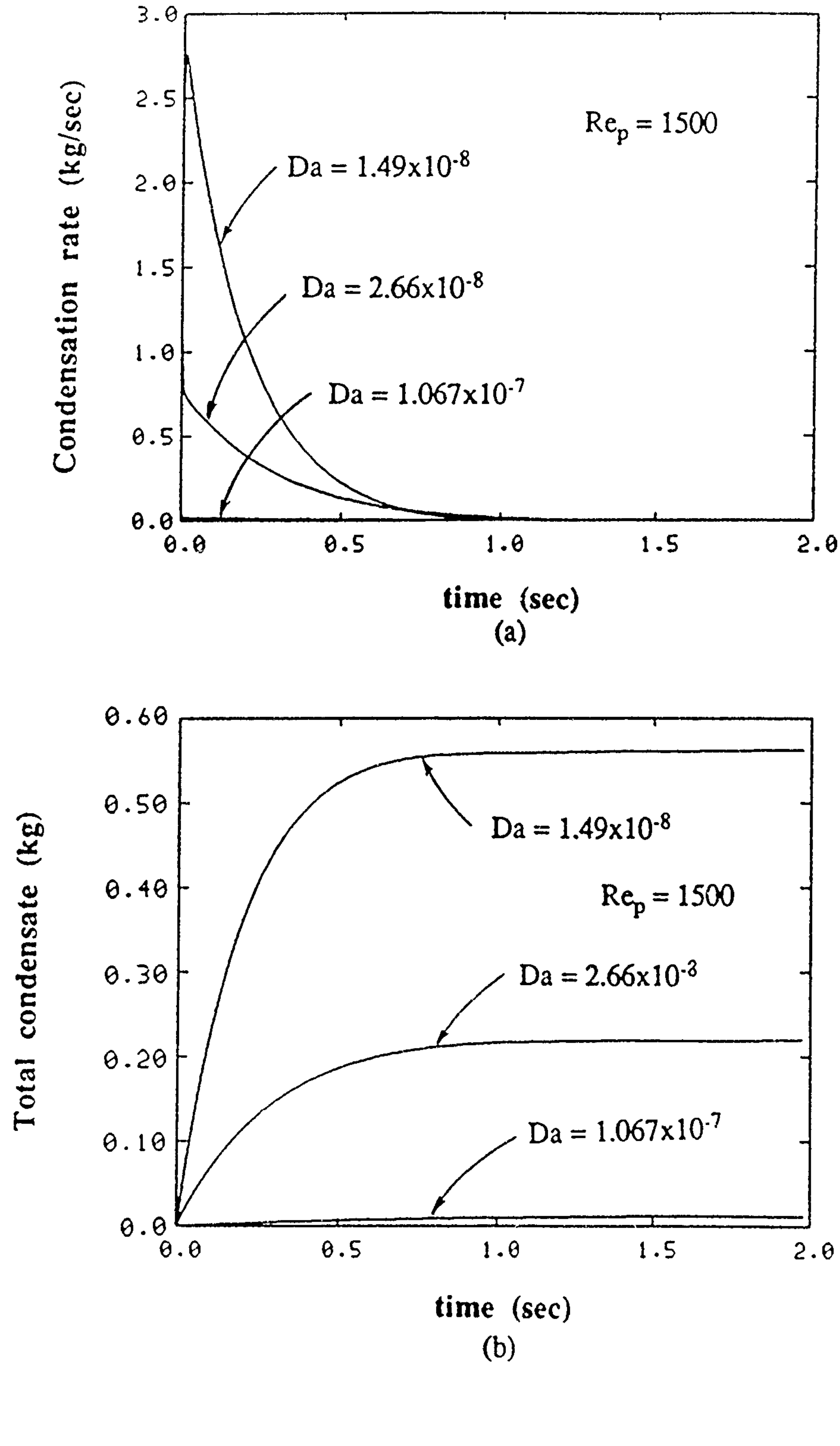

Figure 3.10: Effect of Darcy number on condensation

3.4.2.3 Effect of thermal capacity of the solid phase on condensation

In order to analyze whether the thermal capacity of the solid phase utilized had any effect on condensation, a different material, namely 1% Carbon-steel, was employed as the solid phase material for qualitative comparisons. The variations of the average overall condensation rate and the total condensate accumulation per unit width of the packed bed as functions of time are depicted in Figure 3.11, for the case of lead and steel as solid material for three different Re_p values. As may be seen from this figure, although for a fixed Re_p the condensation rate is almost the same at the beginning for both solid materials, high condensation rates are sustained for a longer period of time in the case of steel than in the case of lead. The reason for this is that the thermal capacity of steel per unit volume is approximately 2.5 times that of lead. Due to this fact along with the high heat transfer rate between the solid and fluid phases, the temperature propagation in the fluid phase will be slower in the case of steel than in the case of lead because more of the thermal energy of the fluid is transferred to the solid in the case of steel than in the case of lead. In the case of steel the vapor phase will take a longer time to reach a high enough temperature at which the vapor density will become lower than the saturation vapor density corresponding to that temperature and, therefore, the condensation durations will be longer.

3.5 Conclusions

In this section, the development of a model for analyzing condensation in a convective flow of a vapor through a packed bed was carried out. This was achieved by incorporating the basic thermodynamic fundamentals of phase change into the model.

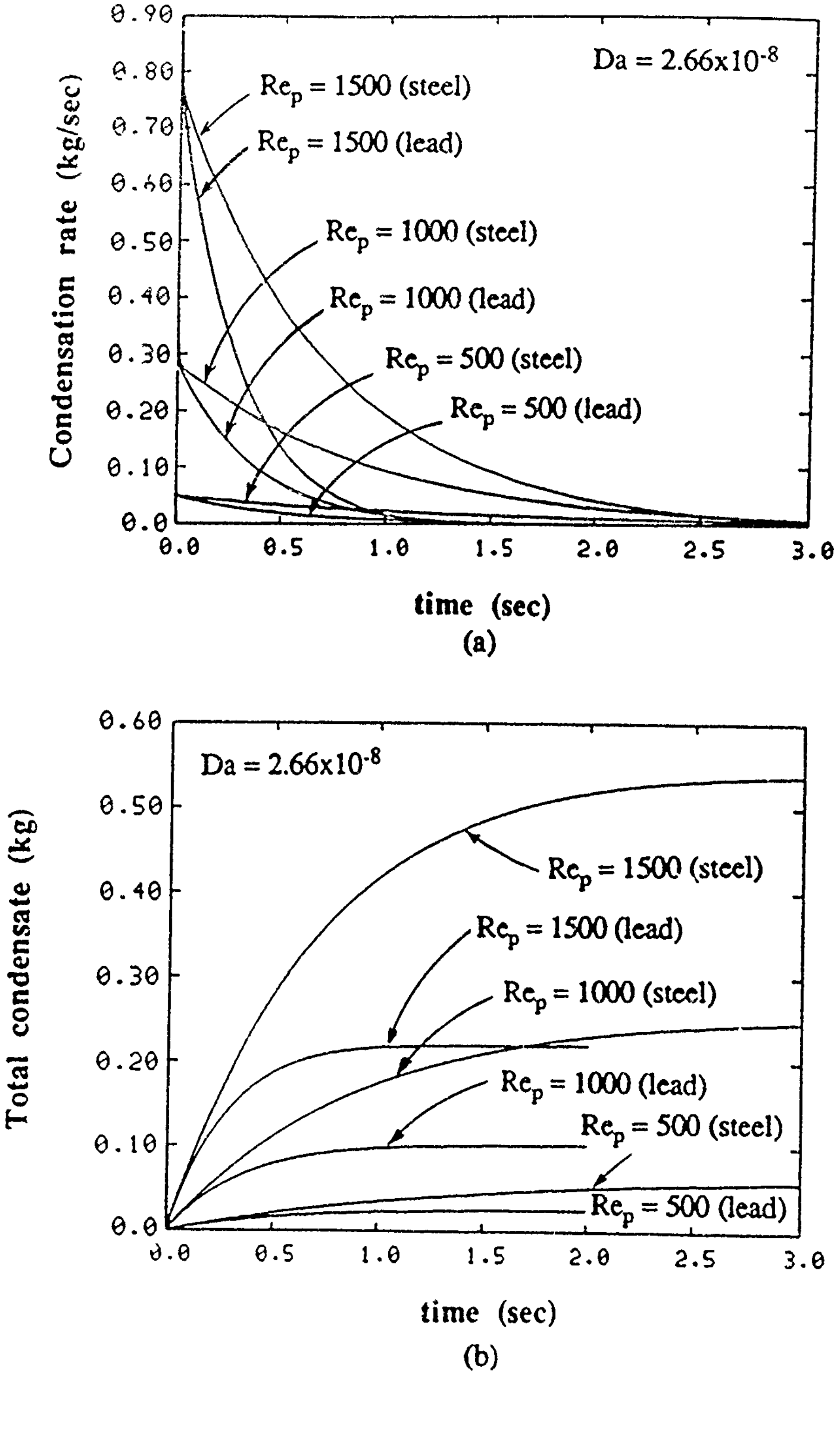

Figure 3.11: Effect of the thermal capacity of the solid phase of the packed bed on condensation

From the results of the case studies performed, it can be concluded that the amount of condensation of the working fluid is dependent on several parameters. For a fixed particle size, the higher the pressure difference applied across the packed bed, i.e., higher the nominal Re_p, larger will be the rate and total amount of condensation, and slightly shorter will be the duration of condensation in the packed bed. This is a consequence of the fact that the working fluid has larger mass flow rates and is under larger compression forces.

The amount of condensation in the packed bed was also found to be influenced by the thermophysical properties of the bed particles. This could be explained by the heat interactions between the working fluid and the solid particles which determine the time taken for the thermal penetration to travel in both the solid and the fluid phases in the packed bed. Larger thermal capacitance materials for the bed particles will result in maintaining the temperature of the vapor low and the density of the vapor high, resulting in a larger condensation rate.

Constant temperature wall conditions yielded larger amounts of condensation compared to insulated wall conditions, proving the fact that continuous heat removal from the packed bed will result in larger amounts of condensation.

Case studies in Section II also established that in the case of insulated boundary conditions with immobile liquid phase in the packed bed, the application of one-dimensional formulation is extremely accurate for the ranges of Re_p and Da considered in this study. On the other hand, for constant temperature boundary conditions two-dimensional formulation is absolutely necessary.

For the type of problem considered in this section, the amount of condensation in the packed bed is very sensitive to the variation of the fluid temperature on which the saturation

vapor density is highly dependent. Therefore, it is very crucial to formulate the problem with no local thermal equilibrium assumption between the solid and the fluid phases in order not to introduce significant inaccuracies in tracking the condensation process.

SECTION IV

ANALYSIS OF A LATENT HEAT STORAGE PACKED BED UNDERGOING A CONDENSING FLOW OF A VAPOR

In this section, the problem investigated in Section III will be extended in complexity by introducing a phase change material (PCM) to replace the sensible heat storage material of the bed particles. Therefore, in addition to phase change in the working fluid, this problem involves phase change in the bed particles. The model used in Section III is modified such that it will accommodate the phase change processes in the packed bed particles for the present problem. The numerical solution algorithm that shows some appreciable differences with that of the previous problem is discussed. This is followed by a discussion of the results of a number of case studies performed.

4.1 Statement of the problem

The problem under consideration is the thermal charging of a packed bed of regularly sized spheres of encapsulated phase change material. This form of packed bed is also known as a latent heat storage packed bed. The schematic diagram of the problem considered in the present study is shown in Figure 4.1. As in the previous section, the packed bed is initially filled with R-12 vapor at a slightly superheated state at uniform temperature and pressure. Then it is subjected to flow of superheated R-12 from a reservoir which has higher temperature and pressure than those initially prevailing in the packed bed. The physical conditions for this problem are very similar to those of the previous section. In this problem, however, the packed bed incorporates a PCM whose

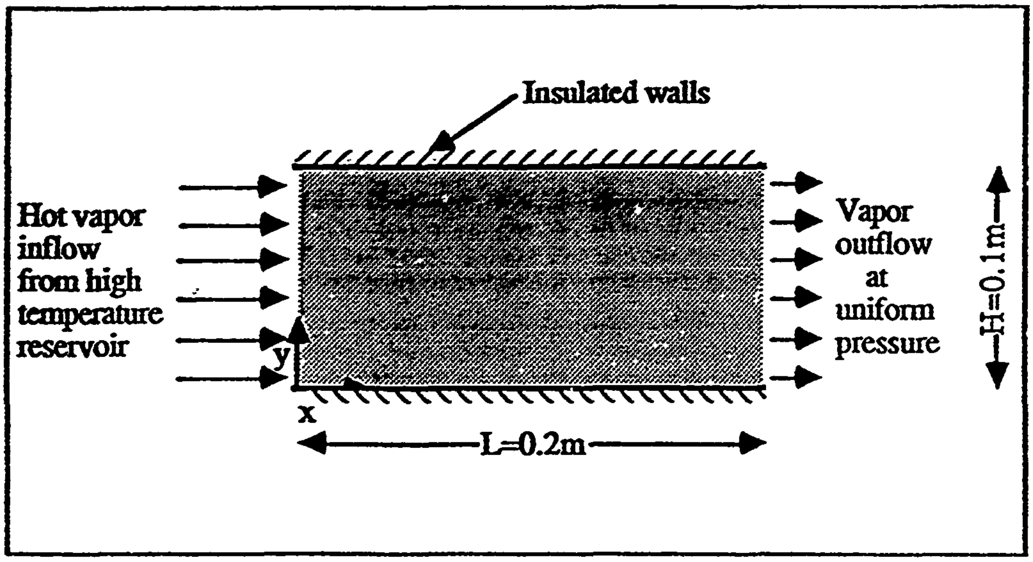

Figure 4.1: Schematic diagram of the problem

melting temperature falls within the operating temperature range. Therefore, during the course of the thermal charging process of the packed bed there will be phase change (melting) within the encapsulated PCM particles.

4.2 Mathematical model

The volume averaging technique employed previously is also utilized in the present study. All of the eight assumptions and simplifications used in Section 3.2 are assumed to be valid here too. In addition, the following assumption is also employed in the analysis of this problem: the temperature within each individual bed particle is assumed to be uniform at any instant, and the encapsulating material is assumed to have the same thermophysical properties as the PCM.

The governing equations for the present problem are similar to those of the previous problem except for the solid phase energy equation. Where a similar energy equation can be used when the PCM is not undergoing phase change, this equation becomes inapplicable when phase change is taking place in the PCM. During the process of phase change in the PCM, the PCM temperature is assumed to remain constant at a value equal to its melting temperature. The governing equations for this problem can be summarized as follows:

Vapor phase continuity equation:

$$\frac{\partial}{\partial t}\left(\varepsilon_\gamma < \rho_\gamma >^\gamma\right) + \nabla.\left(< \rho_\gamma >^\gamma < \vec{v}_\gamma >\right) = - < \dot{m} > \qquad (4.1)$$

Liquid phase continuity equation:

$$\frac{\partial \varepsilon_\beta}{\partial t} + \nabla . < \vec{v}_\beta > - \frac{< \dot{m} >}{\rho_\beta} = 0 \tag{4.2}$$

Vapor phase equation of motion:

$$\nabla < P_\gamma >^\gamma = - \frac{< \rho_\gamma >^\gamma F \varepsilon_\gamma}{K_\gamma^{1/2}} [< \vec{v}_\gamma > . < \vec{v}_\gamma >] \frac{< \vec{v}_\gamma >}{|< \vec{v}_\gamma >|} - \frac{\mu_\gamma}{K_\gamma} < \vec{v}_\gamma > \tag{4.3}$$

which takes the following one-dimensional form:

$$\frac{\partial}{\partial x} < P_\gamma >^\gamma = - \frac{< \rho_\gamma >^\gamma F \varepsilon_\gamma}{K_\gamma^{1/2}} < u_\gamma >^2 - \frac{\mu_\gamma}{K_\gamma} < u_\gamma > \tag{4.3a}$$

Liquid phase equation of motion:

$$< \vec{v}_\beta > = - \frac{k_{r\beta} K}{\mu_\beta} \left\{ k_\varepsilon \nabla \varepsilon_\beta + k_{<T>} \nabla < T_f >^f + (\rho_\beta - < \rho_\gamma >^\gamma) \vec{g} \right\} \tag{4.4}$$

Fluid phase energy equation :

$$\left[\varepsilon_\beta \rho_\beta (c_p)_\beta + \varepsilon_\gamma < \rho_\gamma >^\gamma (c_p)_\gamma \right] \frac{\partial < T_f >^f}{\partial t} - < \dot{m} > \Delta h_{vap}$$

$$+ \left[\rho_\beta (c_p)_\beta < \vec{v}_\beta > + < \rho_\gamma >^\gamma (c_p)_\gamma < \vec{v}_\gamma > \right] . \nabla < T_f >^f = \nabla . \left[k_{feff} \nabla < T_f >^f \right]$$

$$+ h_{\sigma\beta} a_{\sigma\beta} \left[< T_\sigma >^\sigma - < T_f >^f \right] + h_{\sigma\gamma} a_{\sigma\gamma} \left[< T_\sigma >^\sigma - < T_f >^f \right] \tag{4.5}$$

Solid phase (PCM) energy equation:

When there is no phase change in the PCM we have:

$$\varepsilon_\sigma \rho_\sigma (c_p)_\sigma \frac{\partial < T_\sigma >^\sigma}{\partial t} = \nabla . \left[k_{\sigma eff} \nabla < T_\sigma >^\sigma \right]$$

$$- h_{\sigma\beta} a_{\sigma\beta} \left[< T_\sigma >^\sigma - < T_f >^f \right] - h_{\sigma\gamma} a_{\sigma\gamma} \left[< T_\sigma >^\sigma - < T_f >^f \right] \tag{4.6a}$$

and when the PCM is undergoing phase change we have:

$$< T_\sigma >^\sigma = T_{melt} \tag{4.6b}$$

Volume constraint relation:

$$\varepsilon_\sigma + \varepsilon_\gamma(t) + \varepsilon_\beta(t) = 1 \tag{4.7}$$

Equation of state for vapor phase:

$$< P_\gamma >^\gamma = < \rho_\gamma >^\gamma R_\gamma < T_f >^f \tag{4.8}$$

Thermodynamic relation for the saturation density of vapor:

$$\rho_{\gamma, s} = \frac{\exp\left(A - \frac{B}{T_f} \right)}{R_\gamma T_f} \tag{4.9}$$

where A, and B are known constants, T_f is in degrees Kelvin and $\rho_{\gamma, s}$ is in kg/m^3.

The modeling of the other parameters including the effective thermal conductivities of the solid (PCM) and the fluid phases, k_{seff} and k_{feff}, the permeability of the packed bed, K, the permeability for the vapor phase, K_γ, the geometric factor, F, the relative permeability of the liquid phase, $k_{r\beta}$, the empirical correlations for the fluid-to particle heat transfer coefficient, $h_{\sigma j}$, and the specific surface area of the packed bed for the vapor phase and for

the liquid phase, $a_{\sigma\gamma}$ and $a_{\sigma\beta}$, is carried out exactly in the same way as was done in Section III in equations (3.10) through (3.18).

4.2.1 Initial and boundary conditions

Following the arguments in Section 3.2.1, the initial conditions for the present problem are mathematically given as:

$$
\begin{aligned}
&T_f(x,y,t=0) = T_s(x,y,t=0) = T_o \\
&P_\gamma(x,y,t=0) = P_o \qquad\qquad (4.10) \\
&u_\gamma(x,y,t=0) = 0
\end{aligned}
$$

There is a continuous flow of high temperature vapor into the packed bed from a reservoir while the pressure at the exit of the packed bed is maintained at the initial bed pressure. The following mathematical forms express these boundary conditions:

$$
\begin{aligned}
&T_f(x=0,y,t) = T_{in} \\
&P_\gamma(x=0,y,t) = P_{in} \qquad \text{at } t > 0^+ \qquad\qquad (4.11) \\
&P_\gamma(x=L,y,t) = P_{out} = P_o
\end{aligned}
$$

where:

$T_o = 300\,K \quad P_o = 796kPa \quad T_{in} = 350\,K \quad P_{out} = 796kPa \quad$ and $\quad P_{in} = 811.2kPa$

Since we were primarily interested in the energy storage characteristics of the packed beds, insulated wall boundary conditions which were the most appropriate ones have been used in this section. These are given as:

$$
k_{\sigma eff} \left.\frac{\partial T_\sigma}{\partial y}\right|_{y=0,\, y=H} = k_{feff} \left.\frac{\partial T_f}{\partial y}\right|_{y=0,\, y=H} = 0 \qquad\qquad (4.12)
$$

4.2.2 Physical conditions for the numerical runs

In the present problem two different phase change materials (latent heat storage materials) and a sensible heat storage material were considered for qualitative comparisons in the thermal charging behavior of the packed bed. The PCMs selected for this study were myristic acid which has a melting temperature equal to 331 K, and lithium-nitrate-trihydrate which has a melting temperature of 303 K. We will refer to these materials as PCM1 and PCM2, respectively. The sensible heat storage material chosen was 1% Carbon steel.

The physical property values of the materials which were used in the numerical computations are as follows:

R-12:

$k_\gamma = 0.0097 W/m.K$ $(c_p)_\gamma = 710 J/kg.K$ $\mu_\gamma = 12.6x10^{-6} kg/m.s$ $R_\gamma = 0.0687588 J/kg.K$
$\Delta h_{vap} = 111300 J/kg$ $(c_p)_\beta = 1115 J/kg.K$ $\mu_\beta = 179.2x10^{-6} kg/m.s$ $\rho_\beta = 1190.35 kg/m^3$
$k_\beta = 0.0545$ W/m.K

Myristic acid (PCM1):

$c_p = 1590 J/kg.K$ $k = 0.1$ W/m.K $\rho = 860 kg/m^3$ for solid phase
$c_p = 2260 J/kg.K$ $k = 0.1$ W/m.K $\rho = 860 kg/m^3$ for liquid phase

Lithium-nitrate-trihydrate (PCM2):

$c_p = 2090 J/kg.K$ $k = 0.5$ W/m.K $\rho = 1550 kg/m^3$ for solid as well as liquid phase

1% Carbon-steel:

$c_p = 473 J/kg.K \quad k = 43\ W/m.K \quad \rho = 7800 kg/m^3$

4.3 Solution procedure

The numerical scheme used for the previous problem is used here with some modifications that accommodate the phase change processes in the PCM. These include some flags in the numerical code that perform the checks for differentiating which one of equations (4.6a) and (4.6b) will be used for computing the PCM temperature.

In the solution of this problem, depending on whether phase change is occurring in either the working fluid or the PCM at a given location and instant in the packed bed, the governing equations and the solution format take different forms. It is assumed that the condensation occurs when the density of the vapor becomes equal to the saturation vapor density.

When there is no phase change in either the working fluid or the bed particles, the field variables $<\rho_\gamma>^\gamma$, ε_β, $<u_\gamma>$, $<\vec{v}_\beta>$, $<T_f>^f$, $<T_\sigma>^\sigma$, ε_β, and $<P_\gamma>^\gamma$ are determined from equations (4.1) to (4.8), respectively. At the same time $\rho_{\gamma,s}$ is determined from equation (4.9). This is necessary for determining when to switch to the special solution format used for situations in which condensation takes place in the working fluid. It is carried out in order to determine when to switch from noncondensing mode to condensing mode solution format.

The phase change process in the PCM also needs special consideration. The following physical characteristics of the PCM are built into the numerical code. Once the PCM at a certain location and time reaches its melting temperature during the thermal

charging of the packed bed, its temperature remains constant until phase change (melting) is complete in the capsules at that location. During this period, the solid phase (or PCM) energy equation should not be used for determining the PCM temperature. However, the amount of heat that is transferred to the PCM while it is undergoing melting is integrated in time in order to determine when the phase change is completed. Once the phase change is completed in the PCM at a certain location, the procedure of determining the PCM temperature is switched back to solution from the regular PCM energy equation, i.e., equation (4.6a), with appropriate liquid PCM properties incorporated into the numerical code.

At each time step, after the PCM temperature reaches the melting temperature, the convective heat transfer rate from the working fluid to the PCM and conduction heat transfer rates to and from the PCM are summed up for each node and taken into account. Furthermore, during a given time step both the net energy input to the PCM and the net total energy accumulated in the PCM up to the end of that time step are computed on a unit volume basis for each node where the PCM is undergoing phase change. This process is carried out until the net total energy accumulated in the PCM becomes equal to the latent heat of fusion of the PCM. During this period the solid temperature is taken to be equal to T_{melt} as given by equation (4.6b). After this period $< T_\sigma >^\sigma$ is again computed from equation (4.6a).

Implementation of the stability of the numerical scheme and the accuracy of the solutions were carried out as explained in the previous sections. A 41 x 21 grid configuration (which corresponds to a dimensionless Dx or Dy of 0.025) was found to yield accurate enough solutions.

4.4 Results and discussions

It was again found convenient to nondimensionalize some of the field variables in presenting the numerical solutions, and keep others in dimensional form to have a better understanding of the variations of the important parameters. Variables $<P_\gamma>^\gamma$, $<\rho_\gamma>^\gamma$, and $<u_\gamma>$ are nondimensionalized with respect to the corresponding reference quantities P^*, ρ^* and v^*. However, the pertinent parameters of the thermal charging of the packed bed and the condensation of the working fluid are presented in dimensional form per unit width of the packed bed as a function of the dimensional time. The value chosen for P^* was 100 kPa, while ρ^* was then computed from the equation of state using P^* and the initial temperature, T_0. The calculation of the reference velocity, v^*, was based on the vapor phase momentum equation by incorporating the global pressure difference applied across the packed bed and the vapor density as calculated from the equation of state by using the mean value of the inlet and exit pressures.

Due to the physical conditions considered in the present study, the maximum local liquid fraction of the working fluid did not exceed the critical value above which the liquid becomes mobile, i.e., the liquid phase was always in pendular state. This, combined with the fact that only insulated boundary conditions were considered in the present study, made the problem essentially one-dimensional. It was checked through numerical experimentation that the solution of the one-dimensional form of the governing equations did not have any appreciable difference from the solution to the two-dimensional form. Therefore, the results of the one-dimensional solution will be presented for convenience.

Two distinct stages that were observed in the previous two problems can be easily identified in the solution of the present problem too. The *early stage* with very strong transient effects, i.e., drastic spatial and temporal changes in the field variables, lasts for a

very short time. During the *early stage* the pressure distribution across the packed bed evolves and assumes an almost linear form which is maintained afterwards during the rest of the charging process which will again be referred to as the *later stage.*

The first PCM employed for the encapsulated bed particles is myristic acid (or PCM1), which has a melting temperature of 331 K. The results for the case in which this material is used will be presented in detail. Once the high pressure, high temperature vapor is applied at the inlet of the packed bed, the vapor moving through the packed bed becomes compressed. Since it gives most of its excess internal energy to the colder PCM particles, its density reaches the saturation vapor density at certain locations and condensation takes place. Most of this condensation occurs in the *early stage* while the pressure distribution linearizes and the density of the vapor adjusts itself accordingly. Afterwards, the vapor reaches superheated conditions at all locations and no more condensation takes place.

The *early stage* variations of the density, velocity and the pressure of the working fluid, and the liquid fraction are shown in Figure 4.2. The *early stage* is somewhat extended such that it includes the period during which more than 99% of the condensation in the working fluid is completed. The consequence of the step change boundary conditions can easily be seen from the high velocities at the inlet of the packed bed. These high velocities die out as the pressure distribution becomes linear. Except for a short thermal entry region, during the *early stage* the changes in the field variables are mostly pressure dependent because there is no appreciable thermal penetration. It should be noted that since the liquid fraction never reaches the critical value for becoming mobile, the e_b distribution remains the same throughout the *later stage*. The early stage results for this problem are qualitatively similar to the ones of the problem in Section III.

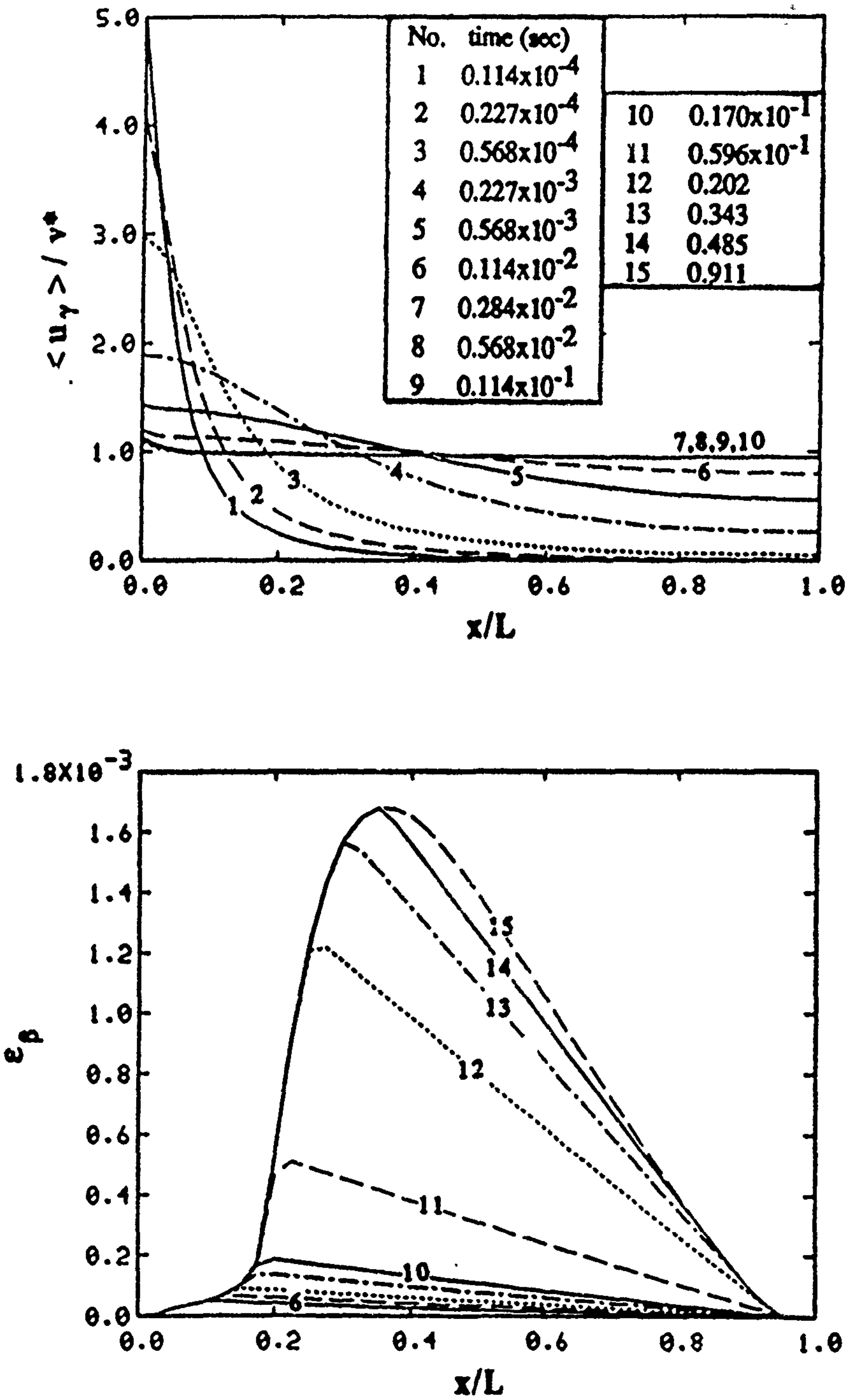

Figure 4.2: Variations of different field variable distributions during the *early stage*

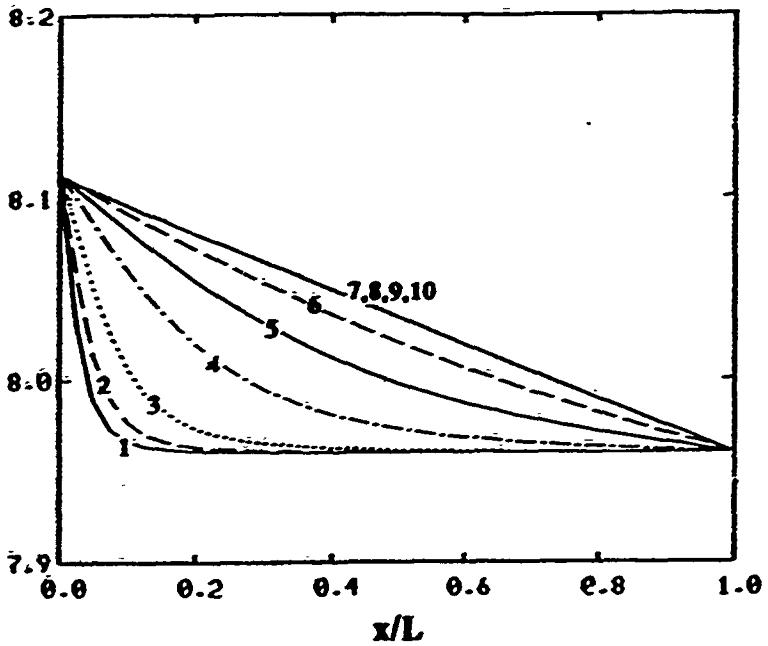

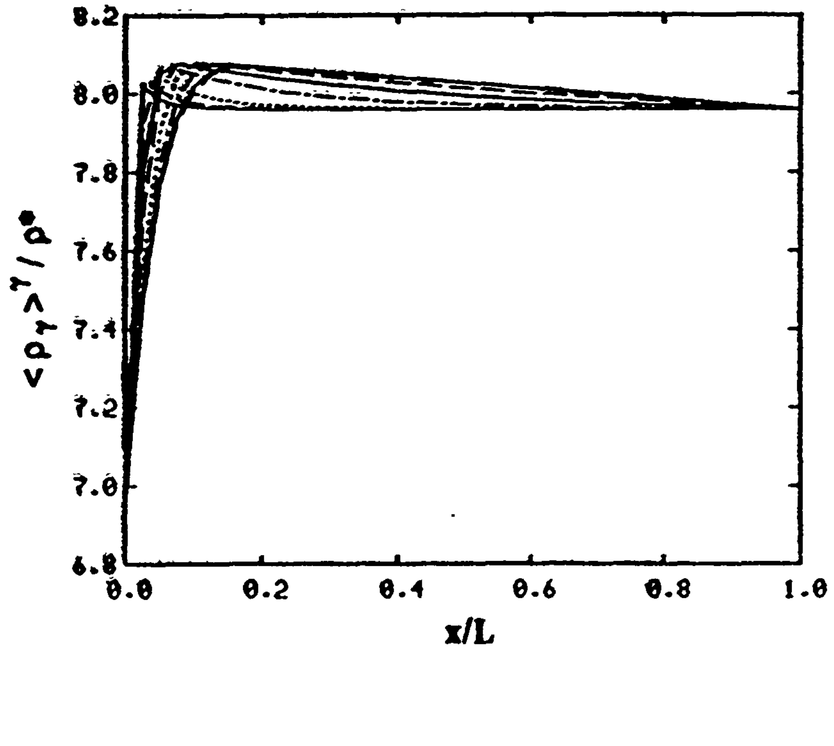

Figure 4.2 (continued)

The changes in the field variables during the *later stage* can be attributed to the development of the thermal penetration depth. As may be seen from Figure 4.3, the pressure distribution remains linear. The variations of the temperatures of the working fluid and the PCM are very smooth until the PCM reaches its melting temperature. After the onset of melting in the PCM, a distinct discontinuity can be observed in the smoothness of the PCM temperature distribution. This is because for a certain length of the packed bed there is no change in the PCM temperature while the PCM is undergoing melting. In this region the working fluid also adjusts itself accordingly. This can be observed in the temperature profiles for time levels 2 through 8 in Figure 4.3(a). This kind of qualitative behavior can also be seen in the vapor velocity and density variations along the packed bed at the corresponding time levels. This is a consequence of the fact that the vapor density variation is precisely related to the pressure and temperature variations. It can also be noticed that there is an inverse relationship between the vapor density and vapor velocity. This is due to the fact that the transient term in the vapor continuity equation loses its dominance and the convective term dominates during the later stage. Once the packed bed becomes thermally charged, then the vapor density distribution becomes linear similar to the pressure distribution as can be explained by the equation of state.

The variation of the average overall condensation rate and the accumulative condensate per unit width of the packed bed are shown in Figure 4.4. The overall condensation rate was computed by integrating the condensation rates at the individual grid points over the associated volumes. Integration of this over time yielded the accumulative condensate per unit width of the packed bed. Again the qualitative behavior in these figures is very similar to the ones in the previous section.

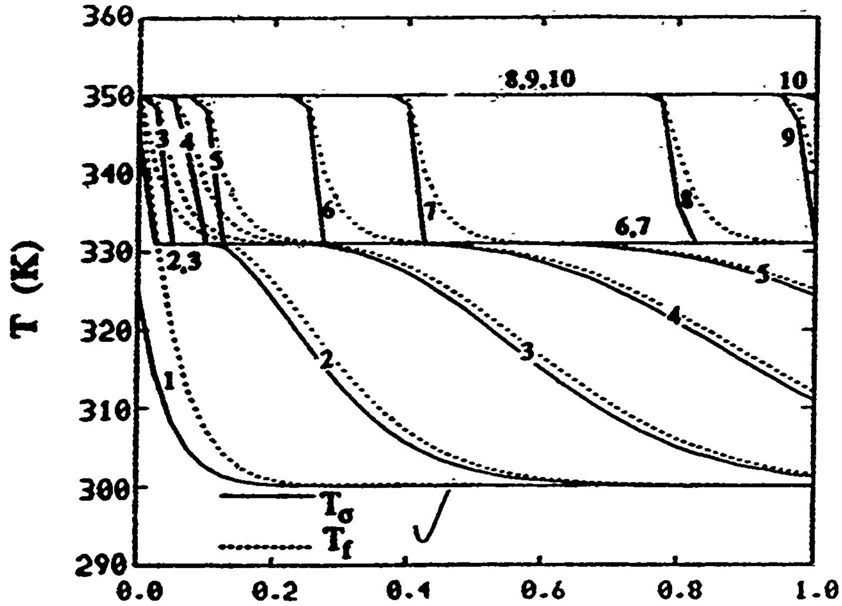

(a)

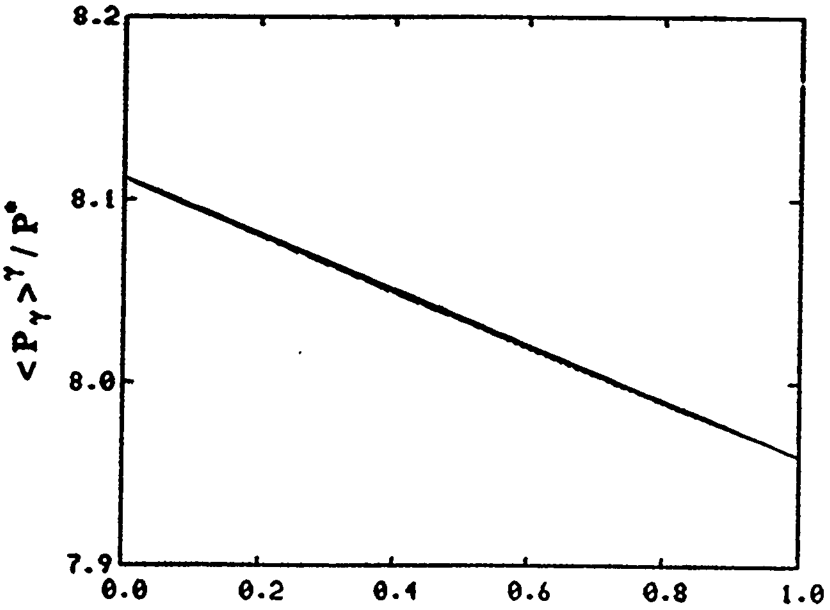

(b)

Figure 4.3: Variations of different field variable distributions during the *later stage*

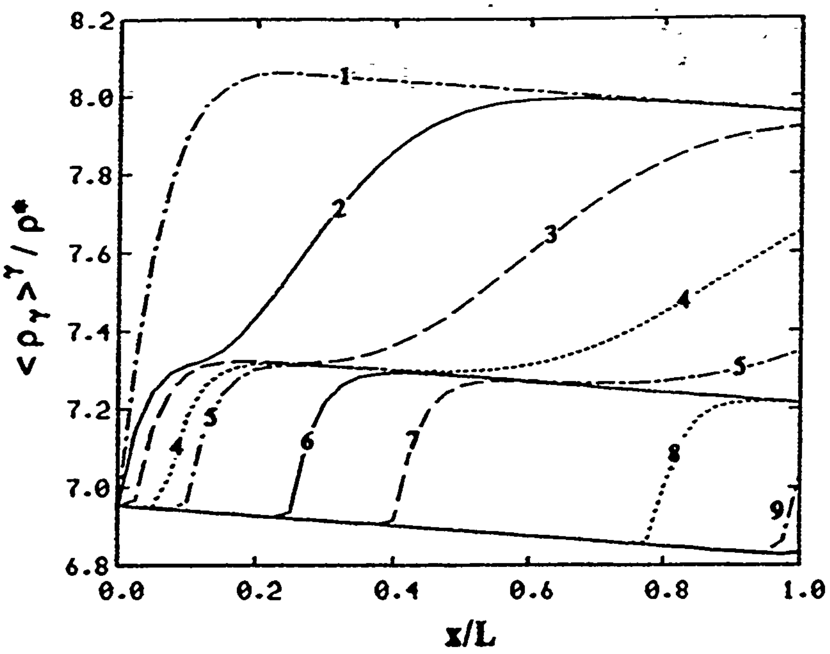

(c)

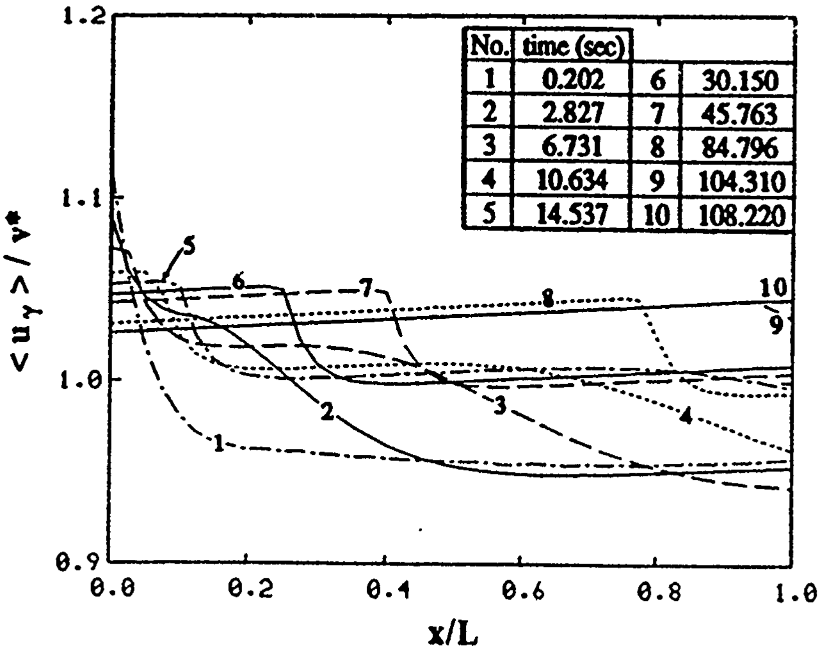

(d)

Figure 4.3 (continued)

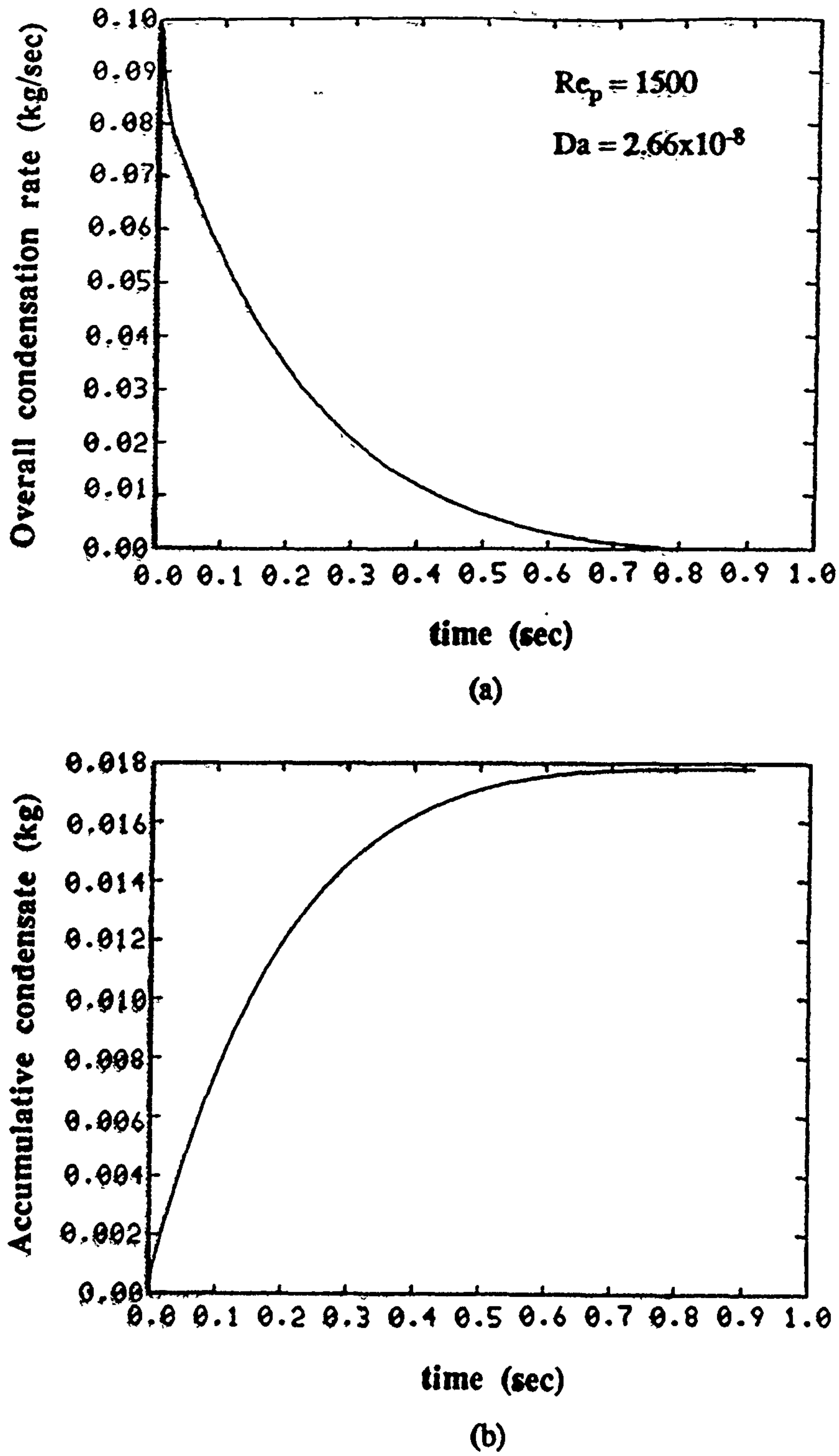

Figure 4.4: (a) Variation of average overall condensation rate in the packed bed

(b) Variation of total accumulate condensate in the packed bed

Of interest to the thermal charging of the packed bed are the rates of heat flowing into and out of the packed bed as a function of time. These were also computed for the given crosssection of the packed bed with a unit width. The variations of these quantities are depicted in Figure 4.5(a) except for a very short time section at the beginning of the charging process, which was left out for obtaining a better scale on the figure. The variation of the net energy stored per unit width of the packed bed as a function of time is also depicted in Figure 4.5(b). At the beginning of the charging process, the vapor flowing out of the packed bed leaves at a low temperature close to the initial temperature and, thus, there is a large difference between the heat flow rates at the inlet and at the exit of the packed bed. Hence, the rate of energy storage is large. Afterwards, for a major portion of the charging process there is a uniform difference between the rates of heat flowing into and out of the packed bed causing a linear increase in the amount of energy stored. Once the phase change is complete in all particles of the packed bed, both the working fluid temperature and the PCM temperature at the exit of the bed rise rapidly causing a rapid decrease in the gap between the heat flow rates at the inlet and the exit. When the packed bed becomes completely charged thermally, there remains no difference between the amount of heat flowing into and out of the packed bed.

4.4.1 Qualitative comparison of condensation in the working fluid

Besides myristic acid (PCM1), two more materials were considered for the particles of the packed bed. These were lithium-nitrate-trihydrate, or PCM2, and 1% Carbon-steel. Computational runs were made for these cases with the same initial and boundary conditions as in the case of PCM1. Figure 4.6 depicts the overall average condensation rate and condensate accumulation histories for all three cases. Since condensation in the

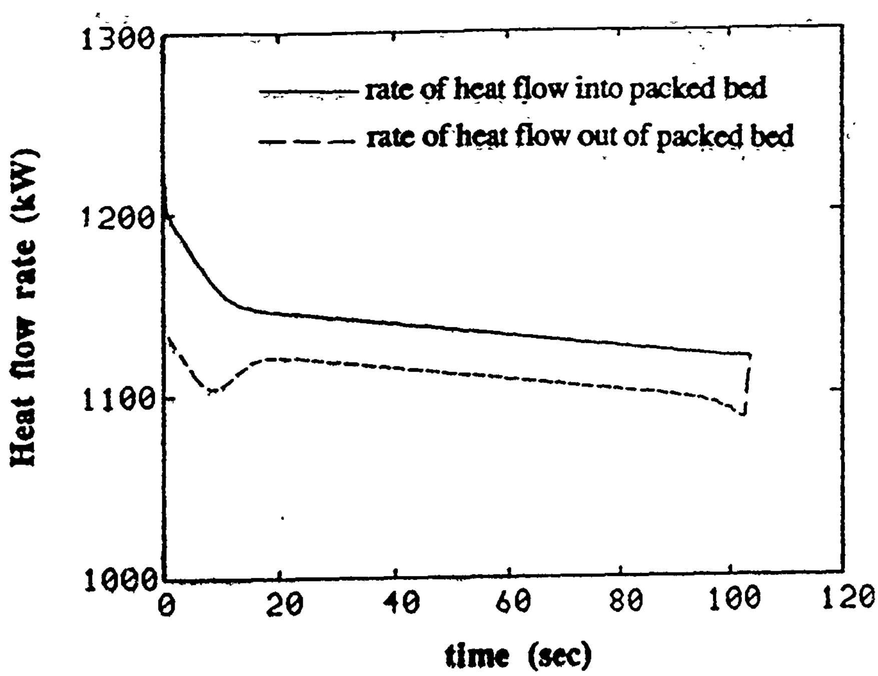

(a)

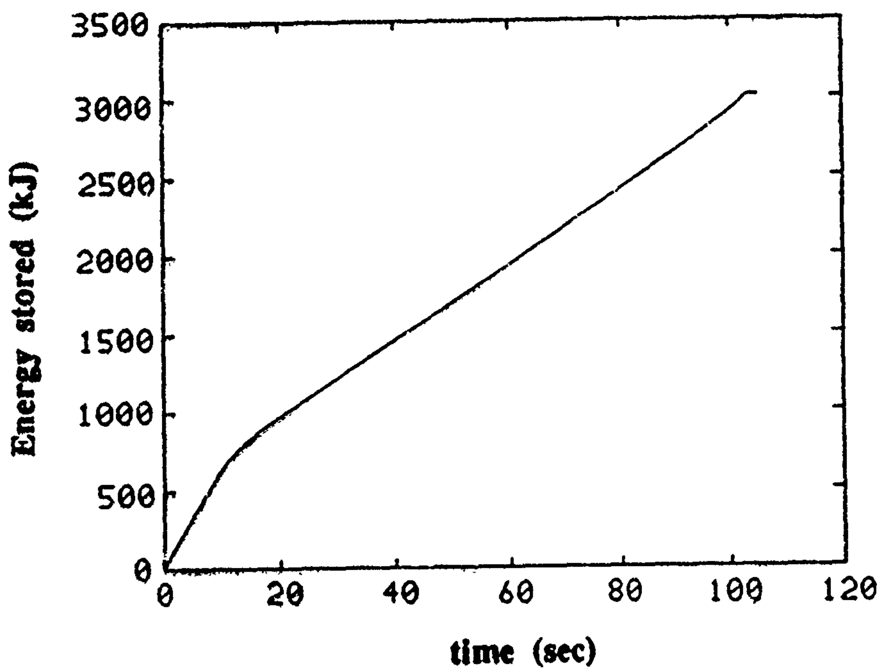

(b)

Figure 4.5: (a) Rate of heat flow into and out of the packed bed

(b) Thermal charging of the packed bed (insulated top and bottom walls)

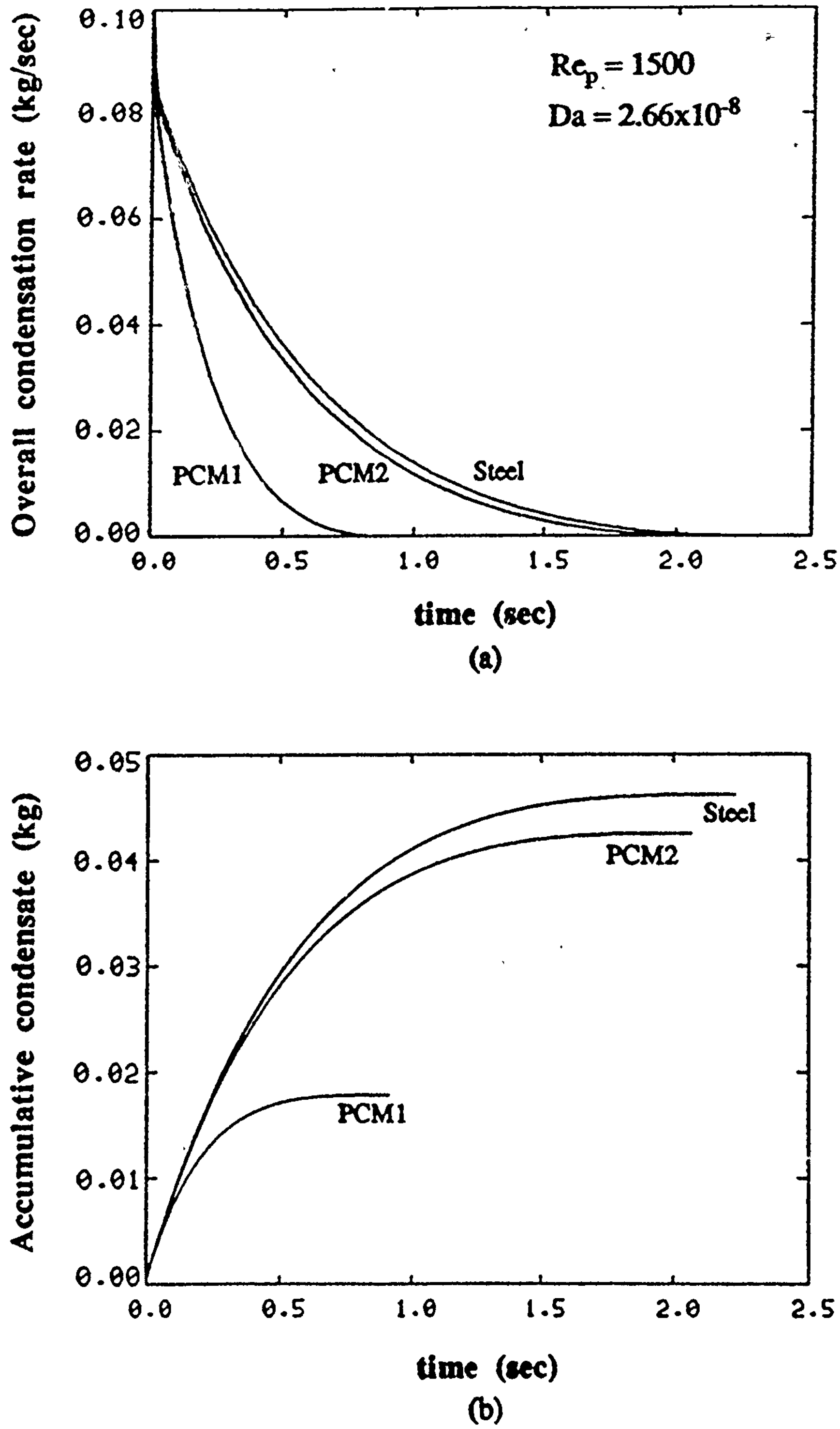

Figure 4.6: Comparison of condensation for cases with different bed particle materials

working fluid takes place in a very short span of time at the beginning, with no significant thermal penetration in the packed bed, the difference in the results for the three materials considered can be attributed mainly to their physical properties. An analysis shows that the thermal capacitance per unit volume of PCM2 is only approximately 12% different from that of steel, where the thermal capacitance per unit volume of PCM1 is almost 3 times smaller than that of steel. Due to this fact and the high heat transfer rate from the working fluid to the solid phase, the temperature propagation in both the solid phase as well as the working fluid is slower in the cases with steel and PCM2 than in the case with PCM1. Thus, for the former two cases it takes longer time for condensation to end. This is as a result of the longer time needed for the vapor to reach at a high enough temperature at which the vapor density becomes lower than the saturation vapor density. Consequently, higher condensation rates are sustained for longer periods and larger condensate accumulation takes place in the case of steel and PCM2.

4.4.2 Qualitative comparison of the thermal charging process

The three materials considered for bed particles in this section are the same as those of the previous section. Time histories of the rates of heat flow into and out of the packed bed for the three cases are shown in Figure 4.7, while that of the net energy stored in the packed bed per unit width is shown in Figure 4.8. It can be seen that, although at the beginning of the charging process the energy storage is almost the same for all three cases, it shows a different variation during later times. While that of the case with steel looks like a conventional charging curve which decays exponentially with time, the cases with the PCMs have a linear variation for a major portion of the charging period. These linear portions correspond to the time spans during which the temperature of the working fluid at the exit of the packed bed is fairly constant and approximately equal to the melting

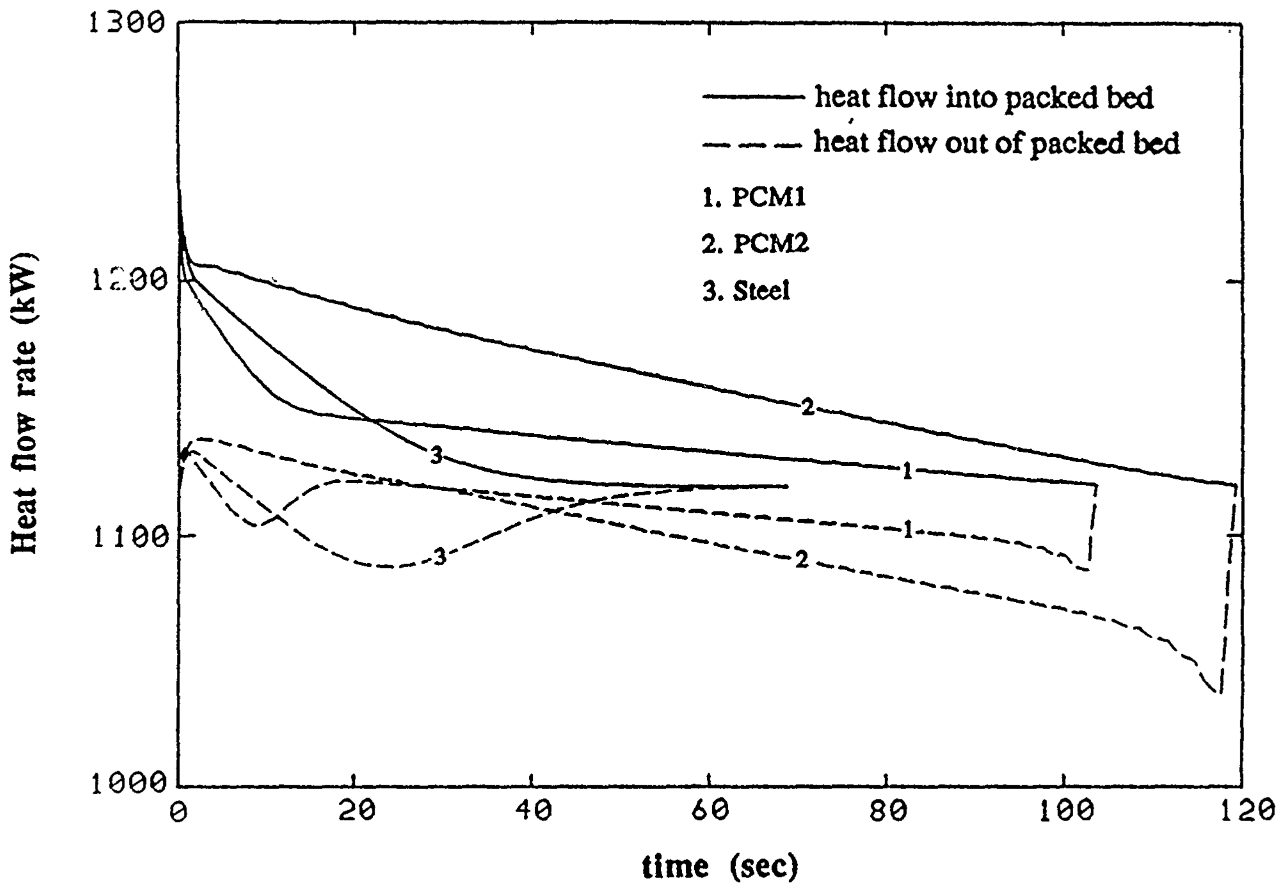

Figure 4.7: Heat flow rate into and out of the packed bed for cases with different bed particle materials

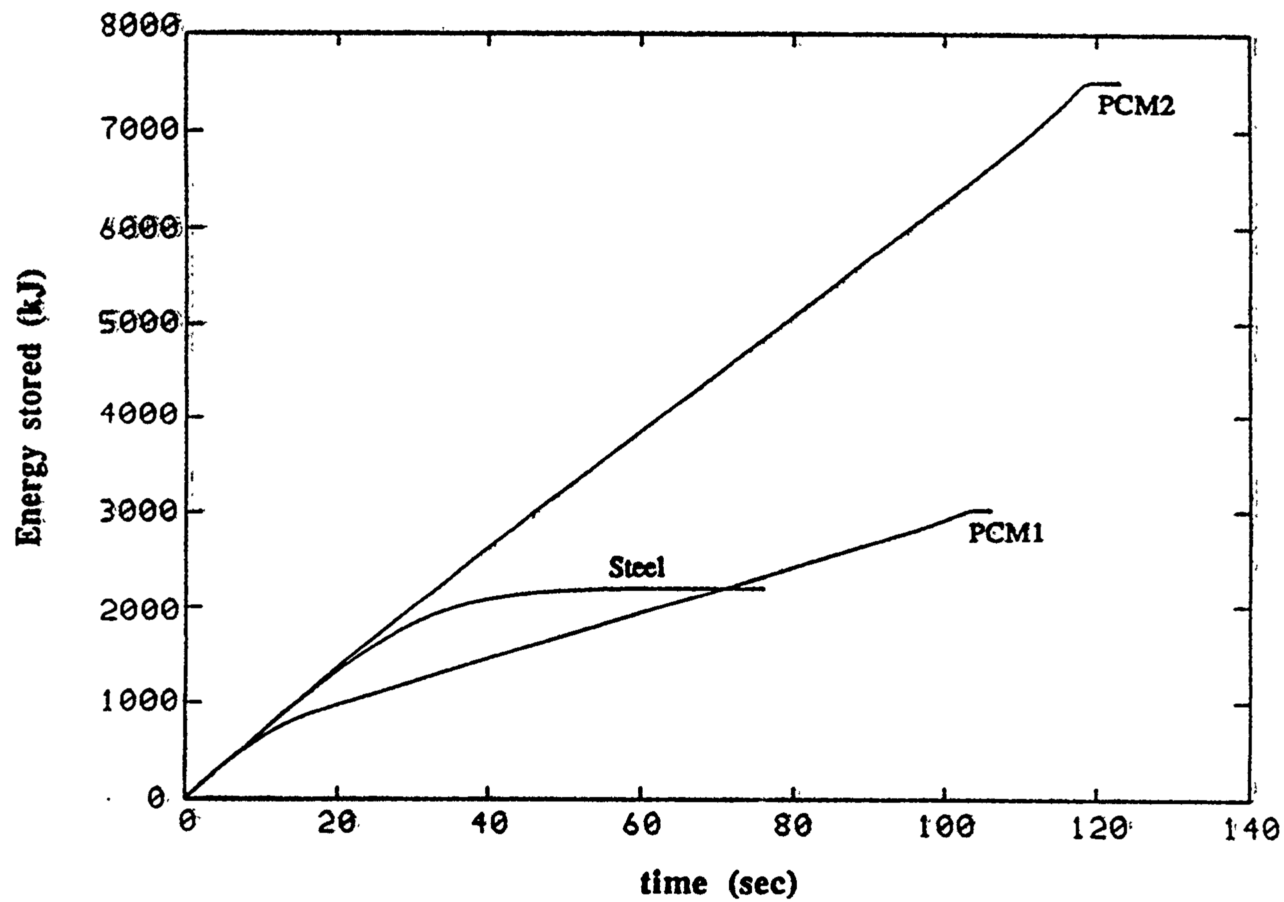

Figure 4.8: Thermal charging of the packed bed for cases with different bed particle materials

temperature of the PCM, since once the PCM reaches it melting temperature its temperature remains constant until phase change is complete in the PCM. During this period the vapor temperature cannot drop below the melting temperature of the PCM and, thus, we have a fairly constant vapor exit temperature. In order to illustrate this more clearly, the time history of the vapor exit temperature is presented in Figure 4.9 for the three cases. As may be seen from this figure, the vapor exits the packed bed at a lower temperature for a longer period of time in the case of PCM2 than in the case of PCM1. This is partly due to the lower melting temperature of PCM2 and partly due to its larger thermal capacitance. Therefore, the difference between the rates of heat flowing into and out of the bed is larger and lasts longer in this case, thus, giving a larger amount of net energy stored.

Figure 4.8 also shows that using a PCM with a certain melting temperature may not always be a better choice over a sensible heat storage material. For instance, for the boundary conditions and the size considered in the present work, steel seems to perform better than PCM1 if we are interested in the energy storage range of up to 2200 kJ per unit depth over approximately 50 seconds with no limitation on the weight of the packed bed.

4.5 Conclusions

In this section, in which the emphasis was given to the study of the behavior of energy storage packed beds, it was shown that the characteristics of the thermal charging of the latent heat storage packed beds differed appreciably from those of the sensible heat storage packed beds. While the thermal charging curve of a sensible heat storage packed bed looks very much like the conventional charging curve of a capacitor, that of a latent heat storage packed bed shows different behavior in that its variation is linear in time during

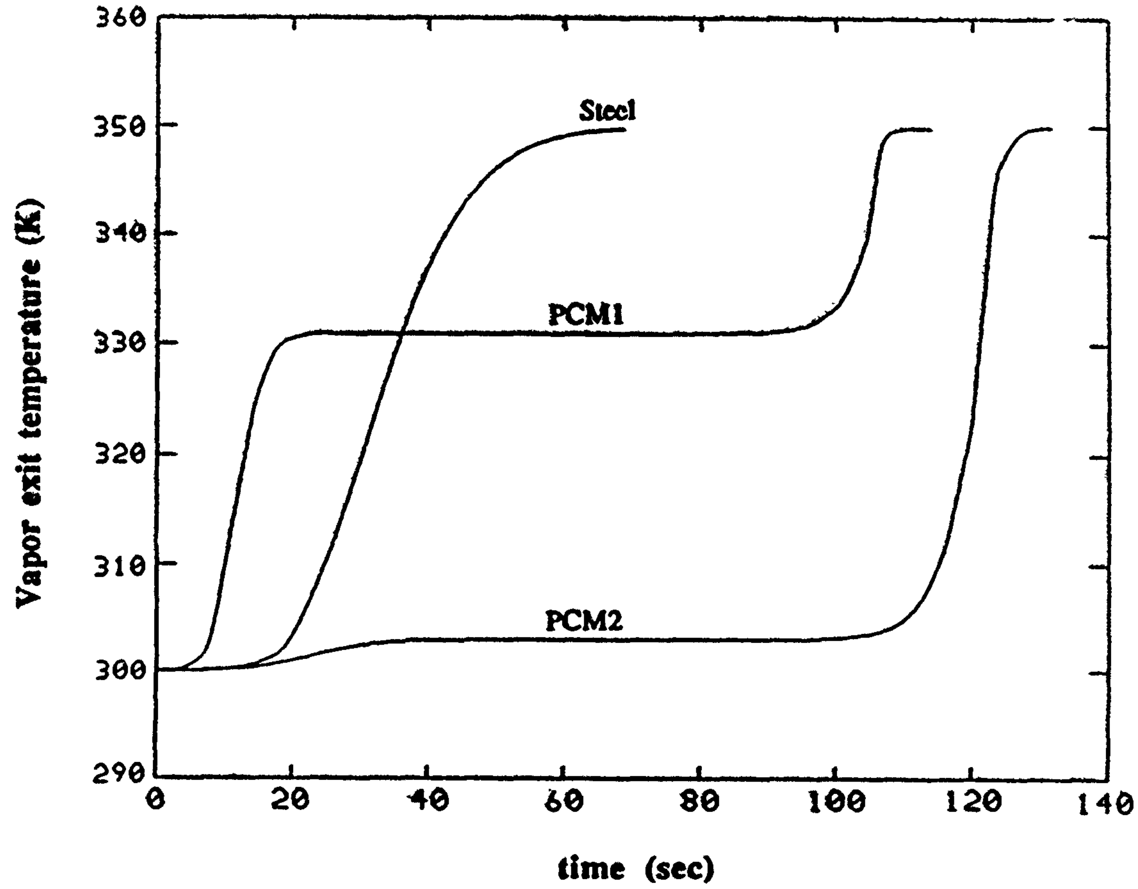

Figure 4.9: Time history of vapor exit temperature for cases with different bed particle materials

a major part of the charging process. This behavior, which is the consequence of a fairly constant vapor exit temperature during the part of the charging process in which phase change takes place in the PCM, was found to be dependent on the melting temperature of the PCM. Case studies performed showed that energy storage in a packed bed employing a PCM would be more efficient if the melting temperature of the PCM is close to the lower end of the operating range of the packed bed. Because this way optimum use of the storage capacity would be realized, i.e., the least amount of energy would be able to escape from being stored in the bed particles.

In the investigations in Section IV the differences between the solid and fluid temperatures became even more apparent than in the previous cases in Sections II and III, confirming the necessity of modeling such problems with no local thermal equilibrium assumption.

SECTION V

ANALYSIS OF THERMAL CHARGING AND DISCHARGING OF SENSIBLE HEAT AND LATENT HEAT STORAGE PACKED BEDS

5.1 Introduction

The operation of the packed bed which employs encapsulated PCM as energy storage medium is of interest for the operation during thermal charging and discharging modes. It is important to analyze the transient response of the packed bed during these modes of operation in order to determine the duration for energy storage or removal, or for determining the size of the packed bed required for a given operating range. In this section, thermal charging and discharging of sensible heat and latent heat storage packed beds are modeled and simulated. The results of this investigation show that the energy storage characteristics of a latent heat storage packed bed are quite different than those of a sensible heat storage packed bed, and that they are very much dependent on the melting/freezing temperature of the phase change material utilized for energy storage.

5.2 Problem statement and formulation

The physical system considered consists of a horizontal channel filled with randomly packed fixed particles of regularly sized and shaped spheres, forming a packed bed as shown in Figure 5.1. The depth of the packed bed is assumed to be large enough in order to avoid three-dimensionality of the problem. Initially the void volume of the packed bed is filled with quiescent working fluid which is at uniform temperature and pressure and in thermal equilibrium with the bed particles. Vapor from a reservoir at a higher

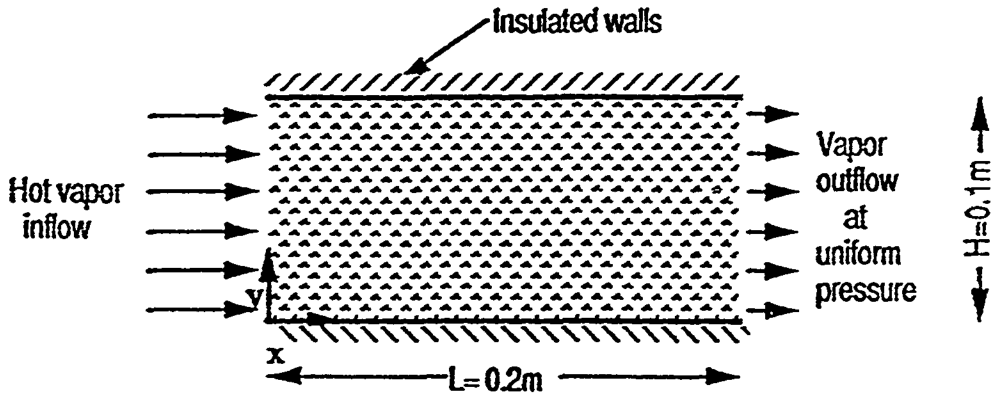

Figure 5.1: Schematic diagram of the problem.

temperature and pressure is allowed to flow through the packed bed in the thermal charging mode. In the thermal discharging mode, vapor at a lower temperature is considered to flow through the packed bed. Relatively high particle Reynolds number flows are considered in this work, assuring that the flow of the Refrigerant-12 vapor is forced convective flow in nature.

The governing equations for the present problem were developed by use of the well known "local volume averaging" technique and they follow from the previous work of Vafai and Sozen (1990). It should be emphasized that in modeling the physical phenomena, the thermophysical properties of the encapsulation material were assumed to be essentially the same as those of the PCM in the case of latent heat storage packed bed. Due to the insulated boundary conditions employed in this investigation, the problem essentially reduces to be one-dimensional. The governing equations are given as follows:

Vapor phase continuity equation:

$$\frac{\partial}{\partial t}\left(\varepsilon < \rho_v >^v\right) + \frac{\partial}{\partial x}\left(< \rho_v >^v < u_v >\right) = 0 \tag{5.1}$$

Vapor phase momentum equation:

$$\frac{\partial < P_v >^v}{\partial x} = -\frac{< \rho_v >^v F \varepsilon}{K_v^{1/2}} < u_v >^2 - \frac{\mu_v}{K_v} < u_v > \tag{5.2}$$

Vapor phase energy equation:

$$\varepsilon < \rho_v >^v c_{p_v} \frac{\partial < T_v >^v}{\partial t} + c_{p_v} < \rho_v >^v < u_v > \frac{\partial < T_v >^v}{\partial x}$$
$$= \frac{\partial}{\partial x}\left\{k_{veff} \frac{\partial < T_v >^v}{\partial t}\right\} + h_{sv}\, a_{sv}\left\{< T_s >^s - < T_v >^v\right\} \tag{5.3}$$

Solid phase (or PCM) energy equation:

$$(1-\varepsilon)\rho_s c_{p_s} \frac{\partial < T_s >^s}{\partial t} = \frac{\partial}{\partial x}\left\{k_{seff} \frac{\partial < T_s >^s}{\partial x}\right\} - h_{sv} a_{sv} \left\{< T_s >^s - < T_v >^v\right\} \quad (5.4)$$

Vapor phase equation of state:

$$< P_v >^v = < \rho_v >^v R < T_v >^v \quad (5.5)$$

where subscript or superscript "s" denotes the solid phase in the case of sensible heat storage packed bed or the PCM in the case of latent heat storage packed bed.

The above set of equations forms a system of five equations in five unknowns, namely, $< \rho_v >^v$, $< u_v >$, $< T_v >^v$, $< T_s >^s$, and $< P_v >^v$.

The initial conditions of the problem were as follows:

$$\begin{aligned} &P_v(x, t=0) = P_0 \\ &T_v(x, t=0) = T_s(x, t=0) = T_0 \\ &u_v(x, t=0) = 0 \end{aligned} \quad (5.6)$$

and the corresponding initial values of ρ_v are calculated from eqn. (5).

The boundary conditions of the problem were as follows:

$$\begin{aligned} &P_v(x=0, t) = P_{in} \\ &P_v(x=L, t) = P_0 \\ &T_v(x=0, t) = T_{vin} \end{aligned} \quad (5.7)$$

where $P_0 = 100\,\text{kPa}$, $P_{in} = 106.83\,\text{kPa}$, $T_0 = 300\,\text{K}$ and $T_{vin} = 350\,\text{K}$ for thermal charging mode, and $T_{vin} = 300\,\text{K}$ for thermal discharging mode. The nominal particle Reynolds number, Re_p, for these boundary conditions was taken as 1,000.

Modeling of the permeability of the packed bed, K_v, and geometric function F in the vapor phase momentum equation, the specific interfacial surface area of the packed bed, the fluid-to-particle heat transfer coefficient and the effective thermal conductivities of the two phases were carried out exactly in the same way as in Section II. Also, an average value of 0.39 was used for the porosity of the packed bed based on the findings of Benanati and Brosilow (1962). The diameter of the bed particles was taken to be 2 mm.

The thermophysical properties used in the present investigation were as follows:

Refrigerant-12	1% Carbon-steel	Myristic acid (PCM)
$c_p = 710\,J\,kg^{-1}\,K^{-1}$	$c_p = 473\,J\,kg^{-1}\,K^{-1}$	$c_p = 1590\,J\,kg^{-1}\,K^{-1}$ (solid)
$k = 0.0097\,W\,m^{-1}\,K^{-1}$	$k = 43\,W\,m^{-1}\,K^{-1}$	$c_p = 2260\,J\,kg^{-1}\,K^{-1}$ (liquid)
$\mu = 12.6x10^{-6}\,kg\,m^{-1}\,s^{-1}$	$\rho = 7800\,kg\,m^{-3}$	$k = 0.1\,W\,m^{-1}\,K^{-1}$
$R = 68.7588\,J\,kg^{-1}\,K^{-1}$		$\rho = 860\,kg\,m^{-3}$
		$h_{sf} = 200.5x10^3\,J\,kg^{-1}$

5.3 Solution Procedure

It should be noted that for the solution of the problem for latent heat storage packed bed (LHSPB), the solution algorithm is the same as in the case of sensible heat storage packed bed presented in Section 2.3 except that during the thermal charging process, once the temperature of the PCM reaches its melting temperature it remains constant until melting of the PCM is complete. This condition has been incorporated into the numerical algorithm such that at a given point once the melting temperature is reached, the PCM temperature is kept constant while the net rate of heat flowing into the associated volume is continuously monitored and integrated over time to give the energy that is used to melt the PCM until it

becomes equal to the amount required for melting. After this stage the PCM temperature is again computed from eqn. (5.4), this time with the liquid properties of the PCM incorporated in eqn. (5.4). Similar provisions are made for the thermal discharging process of the LHSPB which involves freezing of the PCM.

5.4 Results and discussions

The two problems considered in the present work were the complete thermal charging and thermal discharging of two types of packed beds, one with sensible heat storage material, chosen to be 1 % Carbon-steel, and the other one with latent heat storage material, chosen to be myristic acid (a PCM with a melting point of 331 K). Thermal charging or discharging was assumed to be complete when the difference between the incoming and exiting vapor temperatures were less than 0.01 K.

In the solution of the thermal charging problem it was found that two distinct stages were present; namely, the *early stage* and the *later stage.* These have been discussed in detail in the previous sections. In this work, emphasis is given to the thermal charging and discharging characteristics of the two types of packed beds using a compressible working fluid.

Figure 5.2 depicts the variation in the temperature distribution of the vapor and solid phases during the thermal charging processes for the case of sensible heat storage material, while Figure 5.3 shows the corresponding variations in the case of the latent heat storage material (PCM). The results presented in Figures 5.2 and 5.3 were obtained under identical operating conditions (which were given after eqn. (5.7)). From Figure 5.3 it can be easily seen how the thermal charging of the packed bed starts with sensible heating of

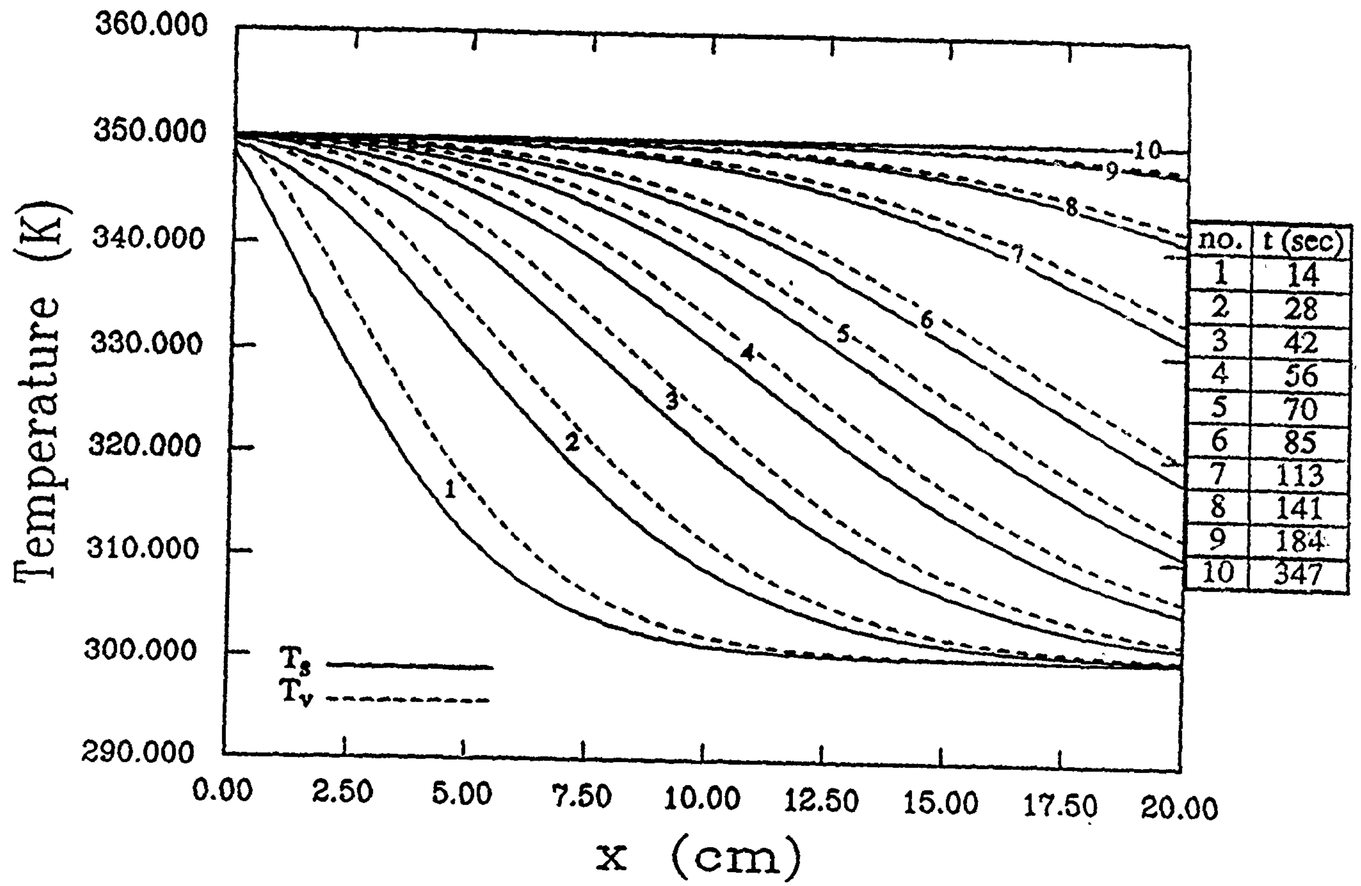

Figure 5.2: Temperature distribution in the sensible heat storage packed bed during thermal charging.

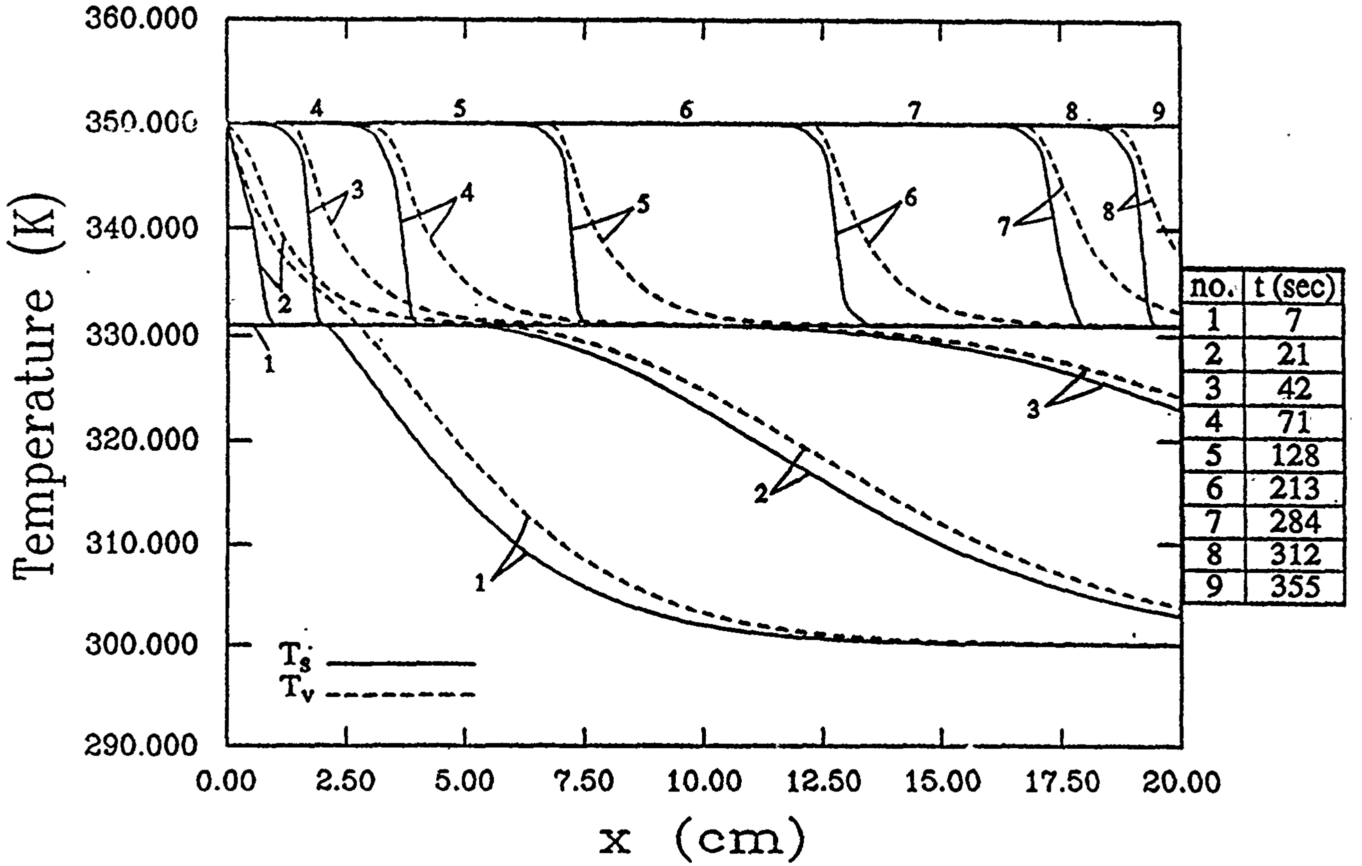

Figure 5.3: Temperature distribution in the latent heat storage packed bed during thermal charging.

the PCM particles (as can be seen from the first three time levels presented) and once the melting temperature, 331 K, of the PCM is attained, the PCM temperature remains constant until phase change is complete at that location and afterwards sensible heating takes place again. Figures 5.4 and 5.5 depict the variation of the corresponding temperature distributions for the thermal discharging modes of the two packed beds considered. From these figures it can be seen that in the case of sensible heating or cooling of the packed bed, the temperature distribution is quite smooth. This is seen both in Figures 5.2 and 5.4 as well as in certain portions of Figures 5.3 and 5.5. In Figure 5.3, sensible heating of a major portion of the packed bed occurs during the earlier stages of the thermal charging as discussed. Similarly, it can be seen from Figure 5.5 that the major portion of the sensible cooling is again at the early stages of the thermal discharging (time levels 1 through 5), during which the temperature drops to the freezing point of the PCM.

The rate of heat flow (enthalpy flux) into and out of the packed bed per unit width of the packed bed is shown in Figure 5.6 for the thermal charging of the sensible heat storage packed bed (SHSPB). The decrease in the heat flux into the SHSPB is due to a decrease in the mass flow rate of the working fluid, R-12. This was an interesting finding for the compressible flow with inertia effects, and this behavior differed completely from an incompressible flow modeled by Darcy's law. The corresponding decrease in the mass flow rate at the exit of the SHSPB also results in a decrease in the rate of heat flow out of the bed at the beginning. However, as the temperature of the bed particles and, hence, that of the working fluid at the exit of the bed start increasing, i.e., less of the energy of the working fluid is being dumped into the bed particles, the heat flux out of the SHSPB starts increasing until the inlet and exit vapor temperatures become equal and the heat fluxes into and out of the bed level off. It should be noted that the heat flux at the inlet of the SHSPB starts at a value of zero at time equal to zero and sharply increases as the flow of hot vapor

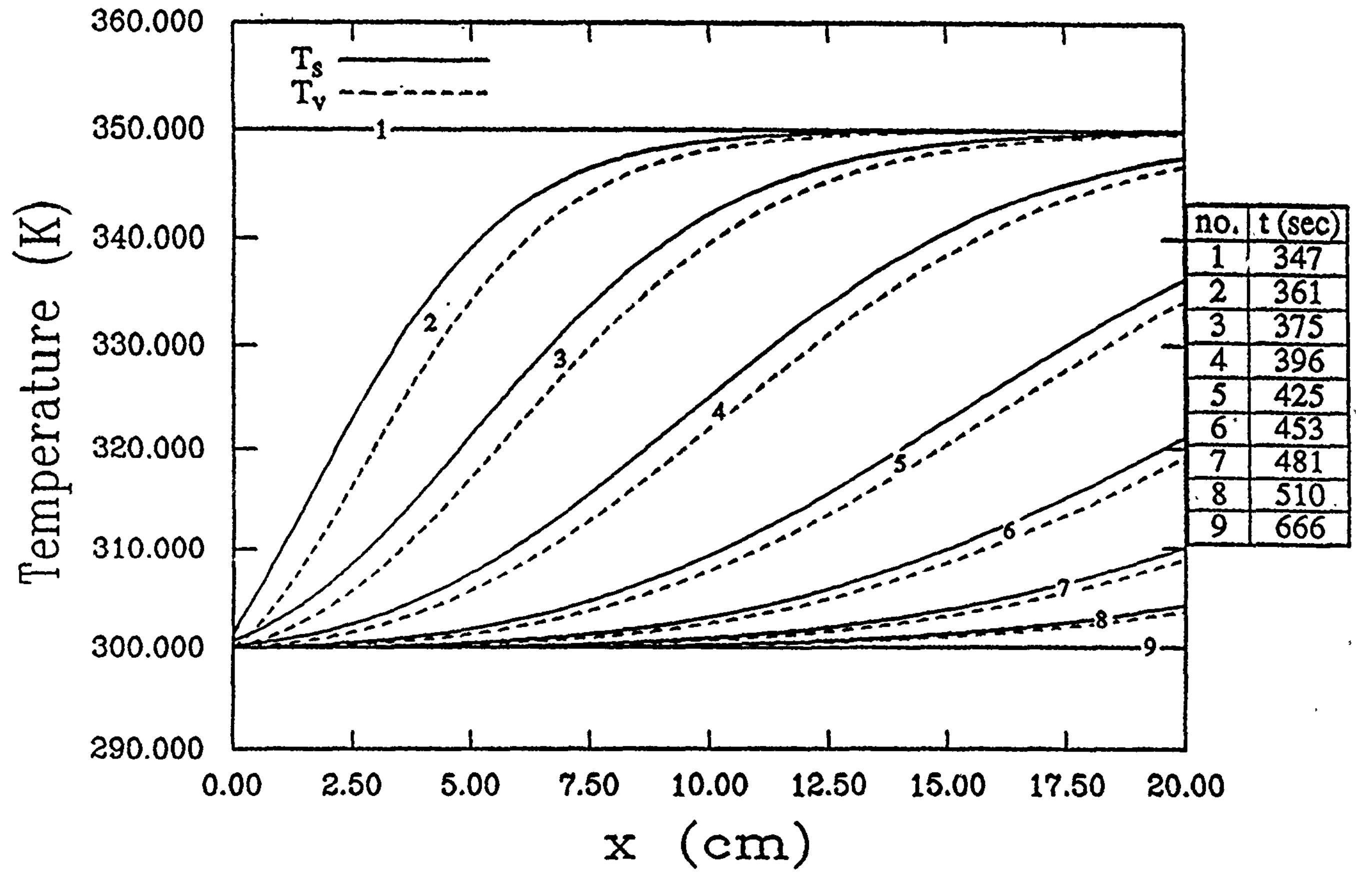

Figure 5.4: Temperature distribution in the sensible heat storage packed bed during thermal discharging.

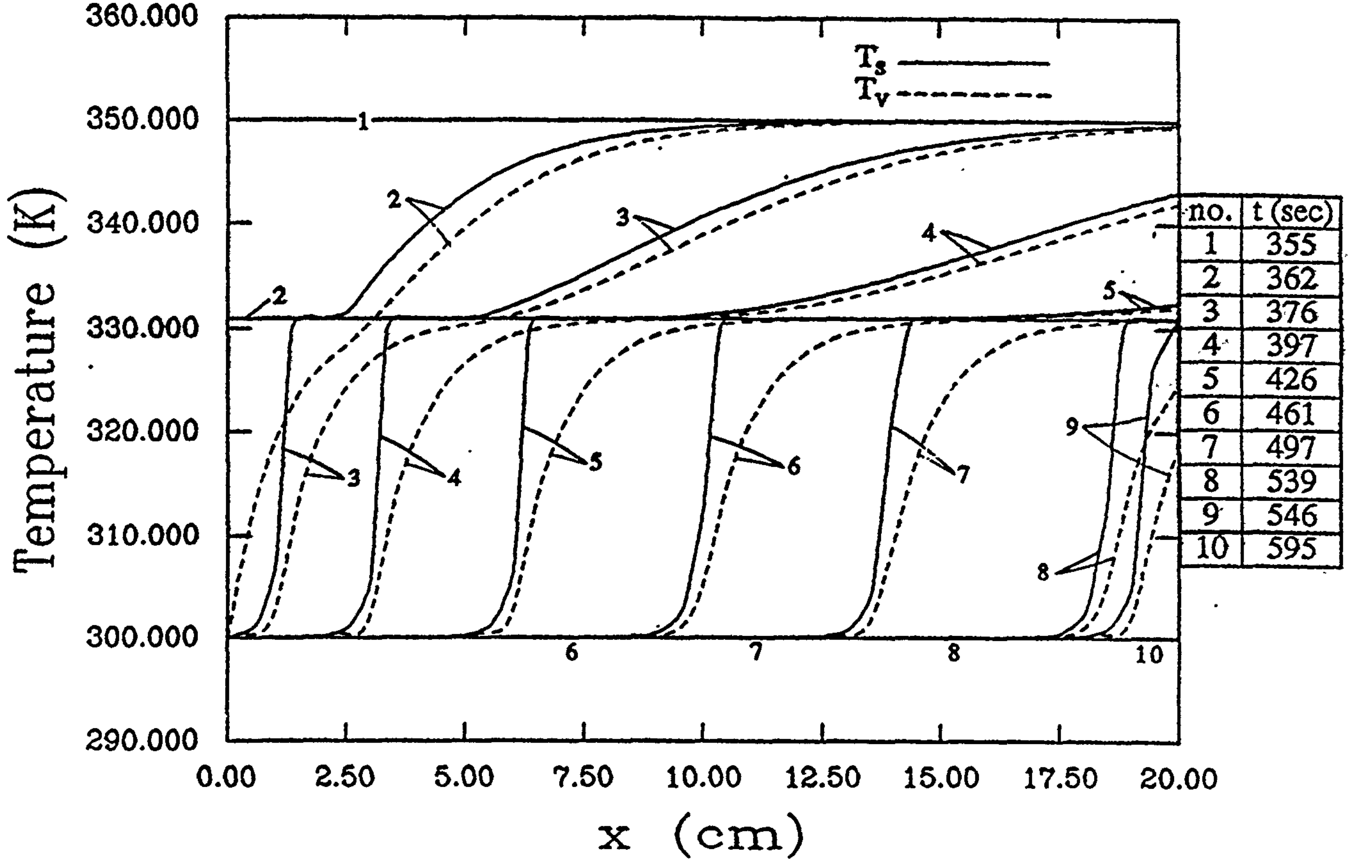

no.	t (sec)
1	355
2	362
3	376
4	397
5	426
6	461
7	497
8	539
9	546
10	595

Figure 5.5: Temperature distribution in the latent heat storage packed bed during thermal discharging.

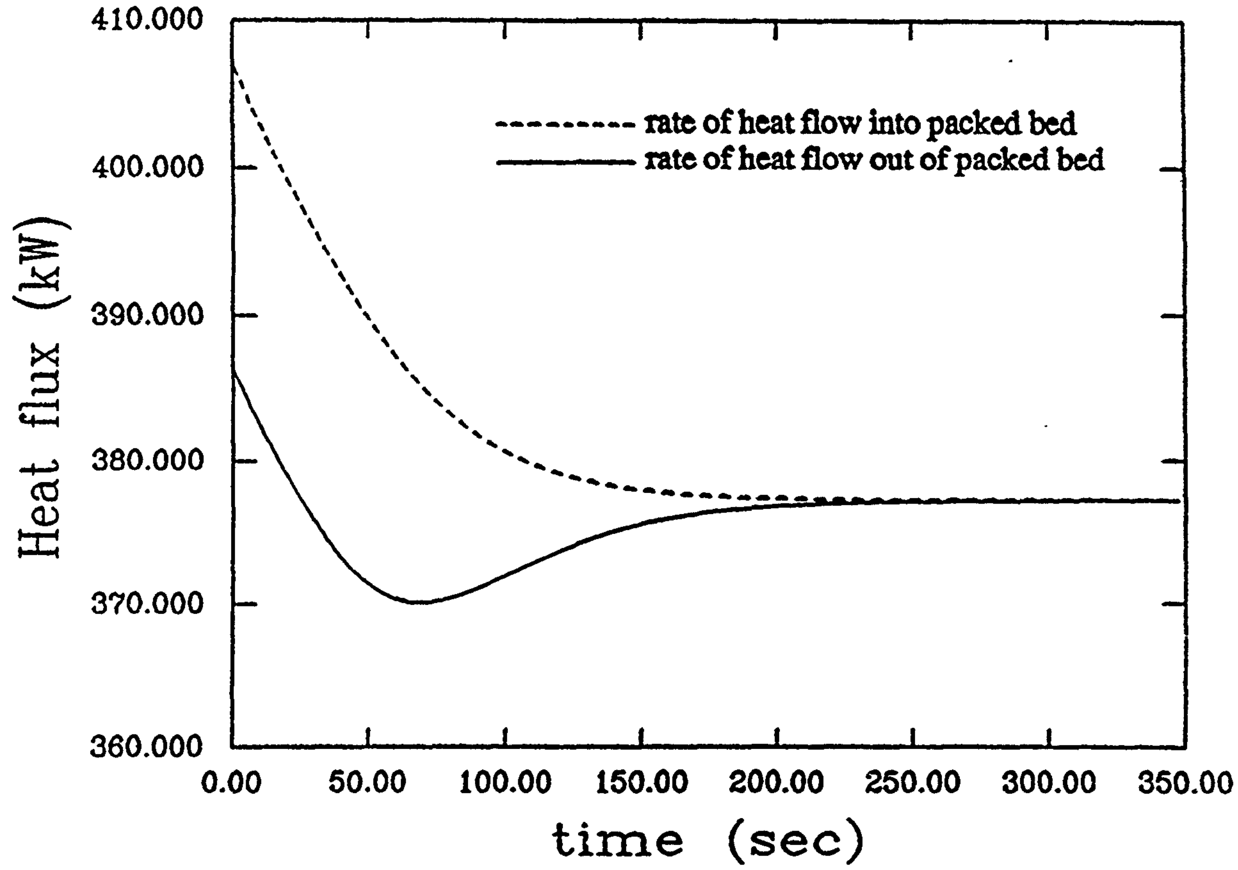

Figure 5.6: Heat flow rate into and out of the SHSPB during thermal charging.

into the bed starts. This very short portion of the charging history was omitted from Figure 5.6 in order to obtain a better scale for the figure. Figure 5.7 shows the variation of heat fluxes into and out of the SHSPB during the thermal discharging mode. As may be seen, due to the decrease in the vapor inlet temperature (300 K) there is a sharp decrease in the heat flux into the bed at the beginning. Later increase in the heat flux into the bed is due to an increase in the mass flow rate of the vapor contrasting to the decrease during the charging process. Earlier increase in the heat flux out of the bed is due to the same reason, where later decrease and leveling off with the heat flux into the bed can be explained due to the fact that the exit temperature of the vapor phase starts decreasing and gradually less amount of thermal energy is being removed from the SHSPB. The time history of the thermal charging and discharging of the SHSPB is shown in Figure 5.8. This figure depicts the variation of the net energy stored per unit width of the SHSPB. In this case the thermal charging and discharging times of the bed are practically equal.

Figure 5.9 depicts the variation of the heat flux in continuous form for the complete thermal charging followed by the complete discharging of the SHSPB. The corresponding variations for the latent heat storage packed bed (LHSPB) are depicted in Figure 5.10. A few interesting points can be observed in the thermal charging and discharging of the LHSPB. Both during the charging and the discharging modes there is a major portion of each process during which there is quite a uniform difference between the heat fluxes into and out of the LHSPB which is not seen in the case of the SHSPB. The reason for this kind of behavior is the fact that during these portions of the charging or the discharging, the temperature of the PCM in the particles downstream of the packed bed remains constant at the melting/freezing temperature. Hence, for these portions of the charging or discharging processes, the vapor exit temperature is practically equal to the melting/freezing temperature of the PCM and, therefore, the difference between the inlet and exit temperatures for the

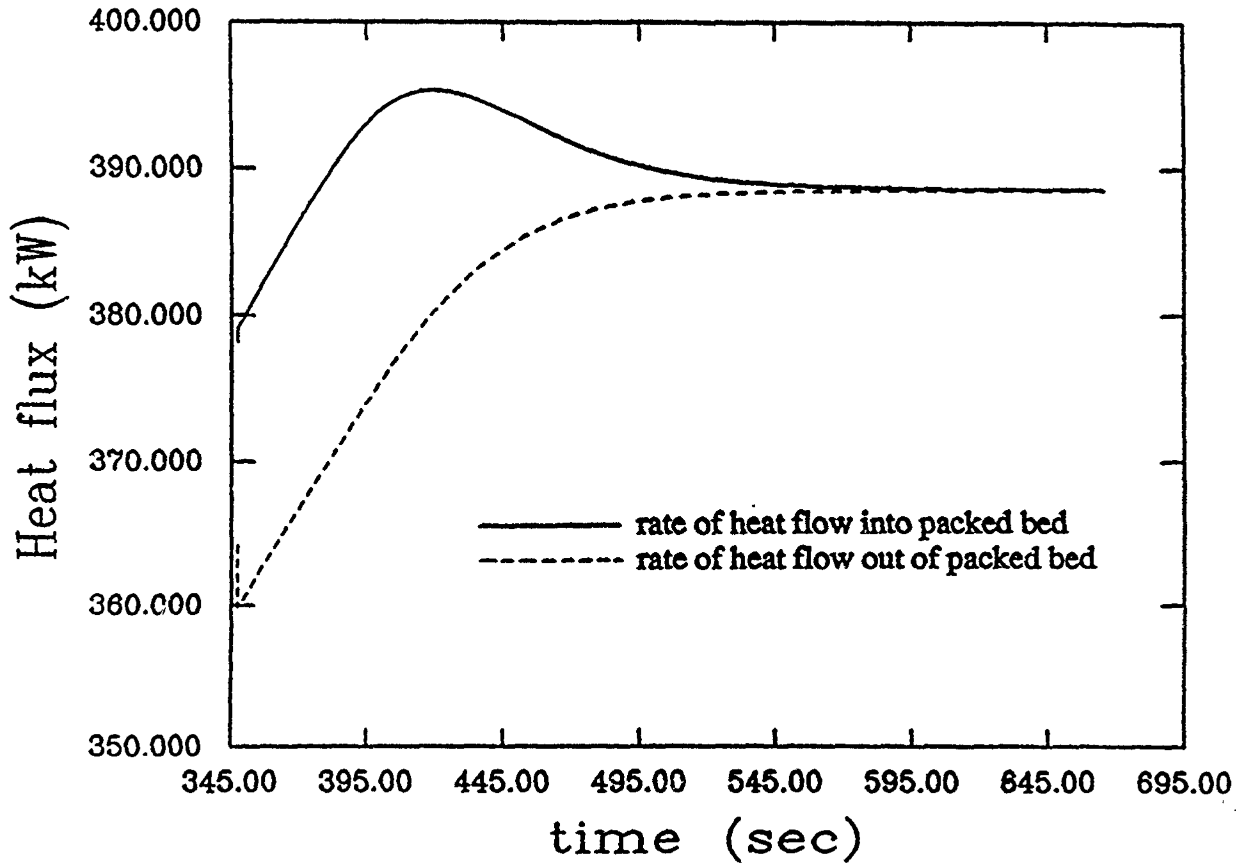

Figure 5.7: Heat flow rate into and out of the SHSPB during thermal discharging.

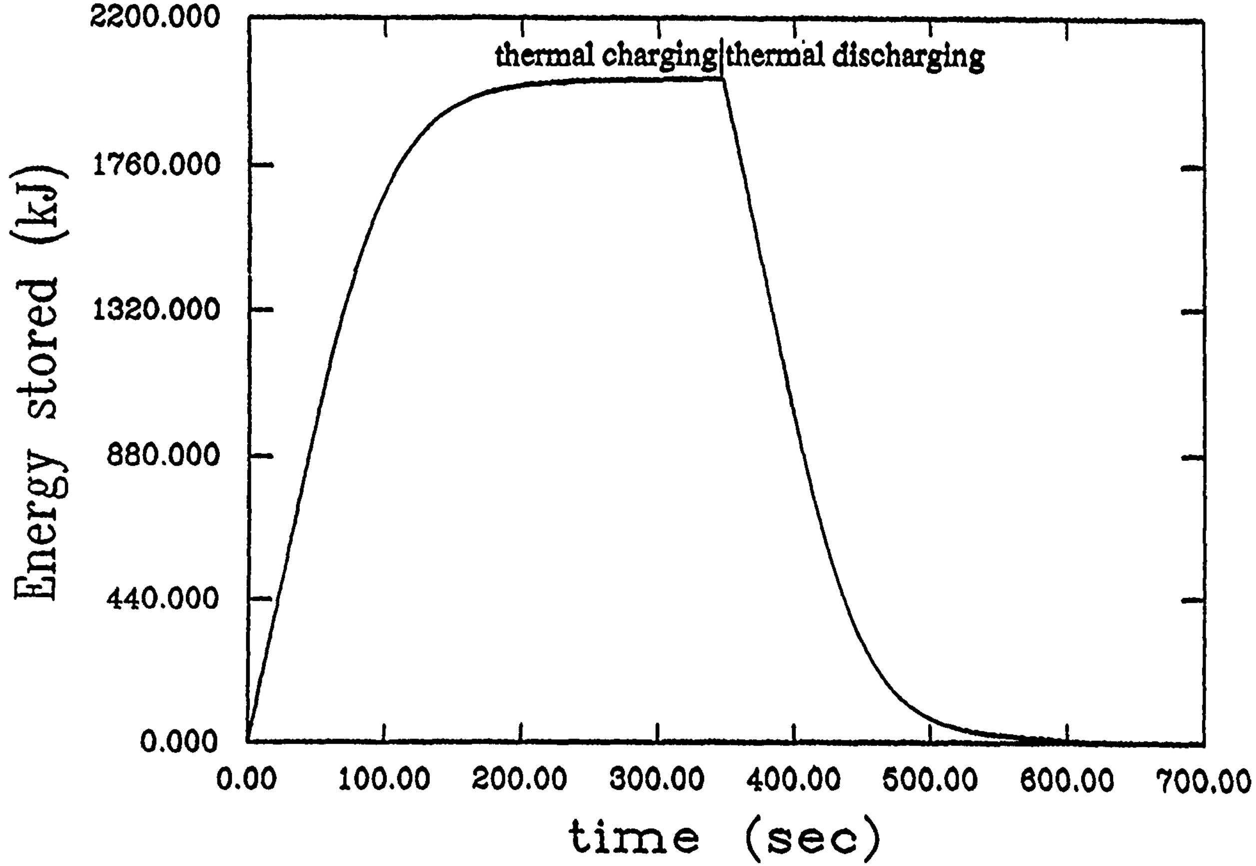

Figure 5.8: Thermal charging and discharging of the SHSPB.

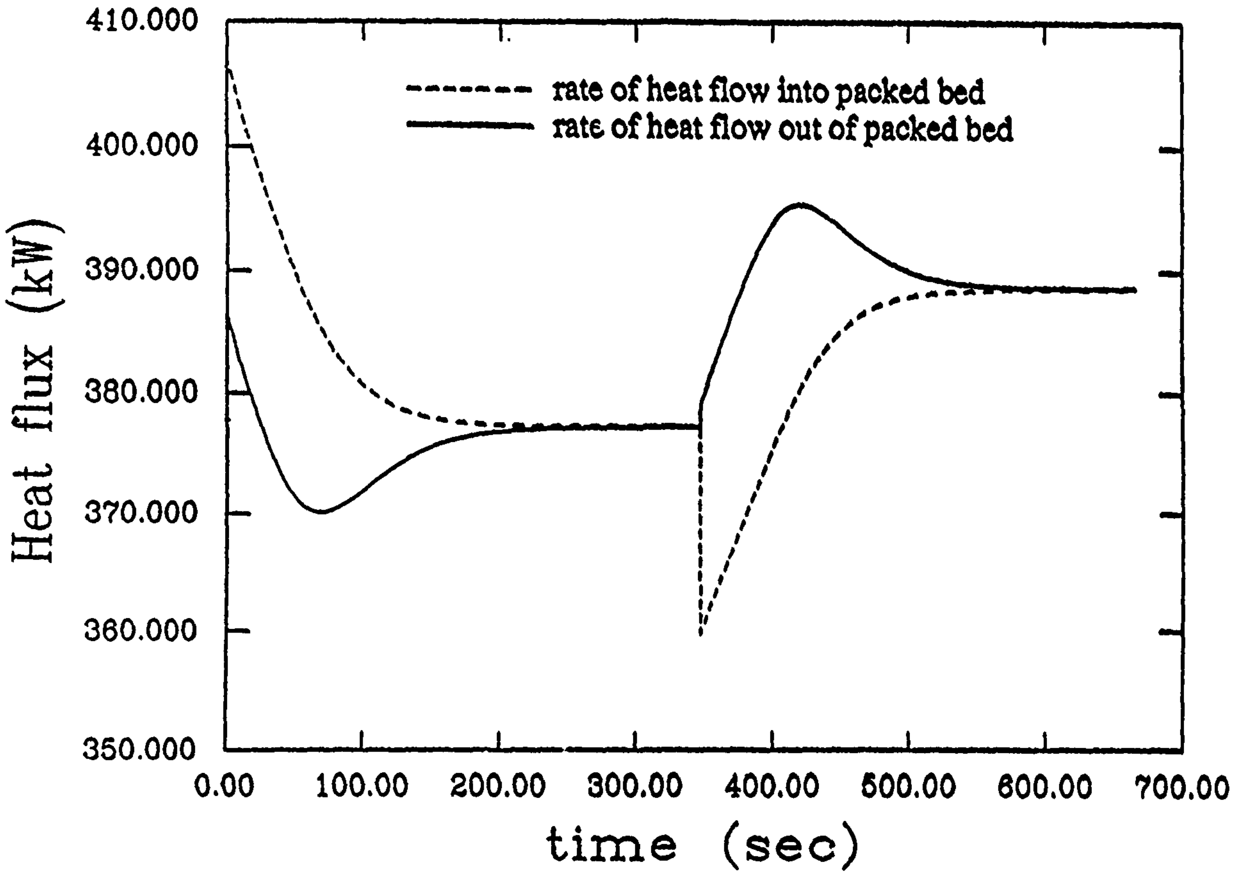

Figure 5.9: Heat flow rate into and out of the SHSPB during complete thermal charging followed by complete discharging.

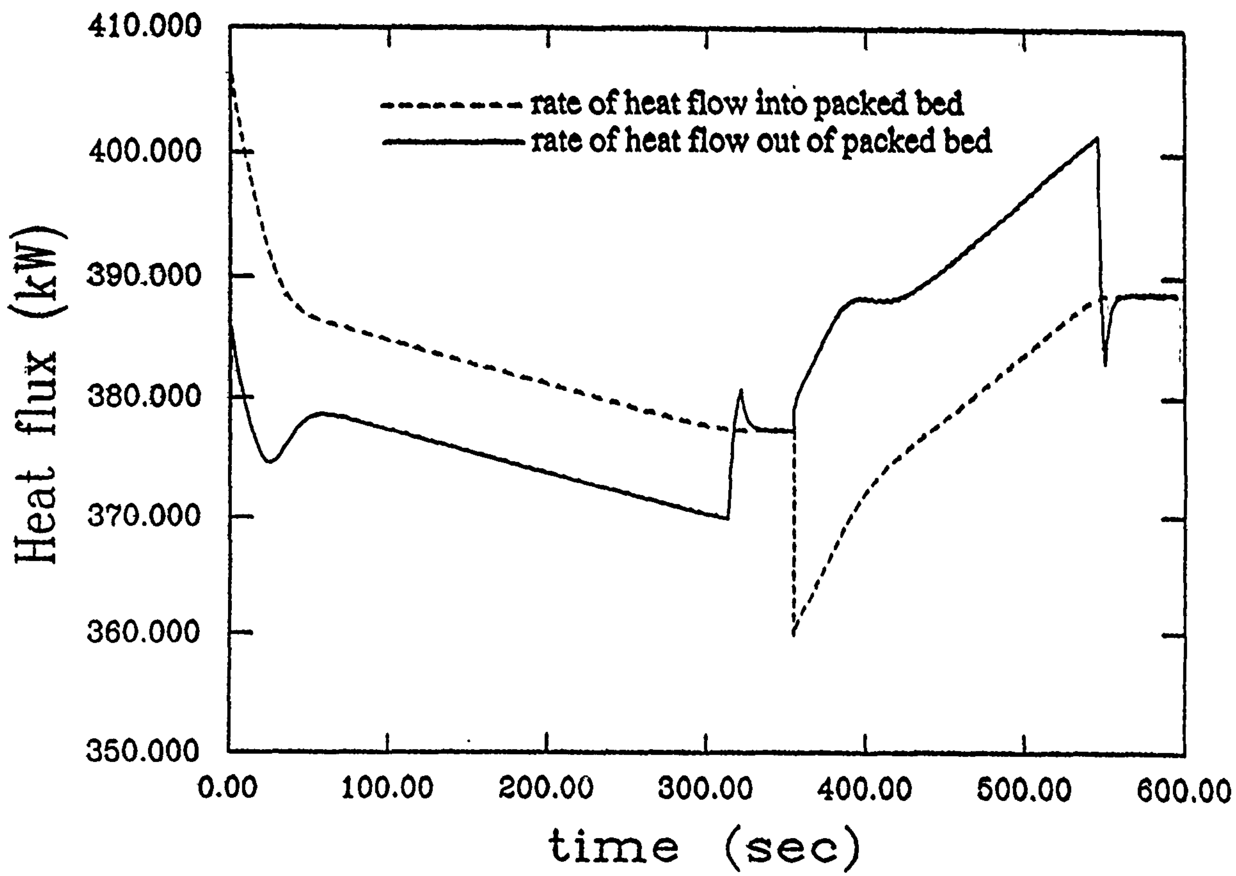

Figure 5.10: Heat flow rate into and out of the LHSPB during complete thermal charging followed by complete discharging.

vapor phase remains practically unchanged. This can be easily seen from Figure 5.11 which depicts the time history of the vapor exit temperature for the complete thermal charging and discharging of both the SHSPB and the LHSPB. Another interesting observation can be made with respect to the charging and discharging times of the LHSPB. From both Figures 5.10 and 5.11 it can be easily observed that the thermal discharging of the LHSPB lasts considerably shorter than the thermal charging. The reason for this can be seen from these figures again. For the major portion of the discharging process during which the temperature of the PCM downstream of the LHSPB remains at the melting/freezing point, there is a constant temperature difference between the vapor inlet and and vapor exit temperatures. This difference is larger than the corresponding difference in the charging process, i.e., the difference between the vapor inlet temperature and the melting point of the PCM during the charging process is only 19 K where during the discharging process the difference between the vapor inlet temperature and the freezing point of the PCM is 31 K, and, hence, energy is stored at a lower rate in the charging process than energy is removed during the discharging process for the portions of these processes under discussion.

Figure 5.12 depicts the time histories of the net energy stored in the packed bed during the charging and the discharging modes of the SHSPB and the LHSPB respectively. While the rate of energy storage and removal follows a similar trend in the case of the SHSPB, i.e., very fast at the beginning and decaying afterwards, this was not the behavior in the case of the LHSPB. Again, this was due to the fact that a major portion of the packed bed remains at constant temperature (melting/freezing point) during the thermal charging/discharging of the LHSPB.

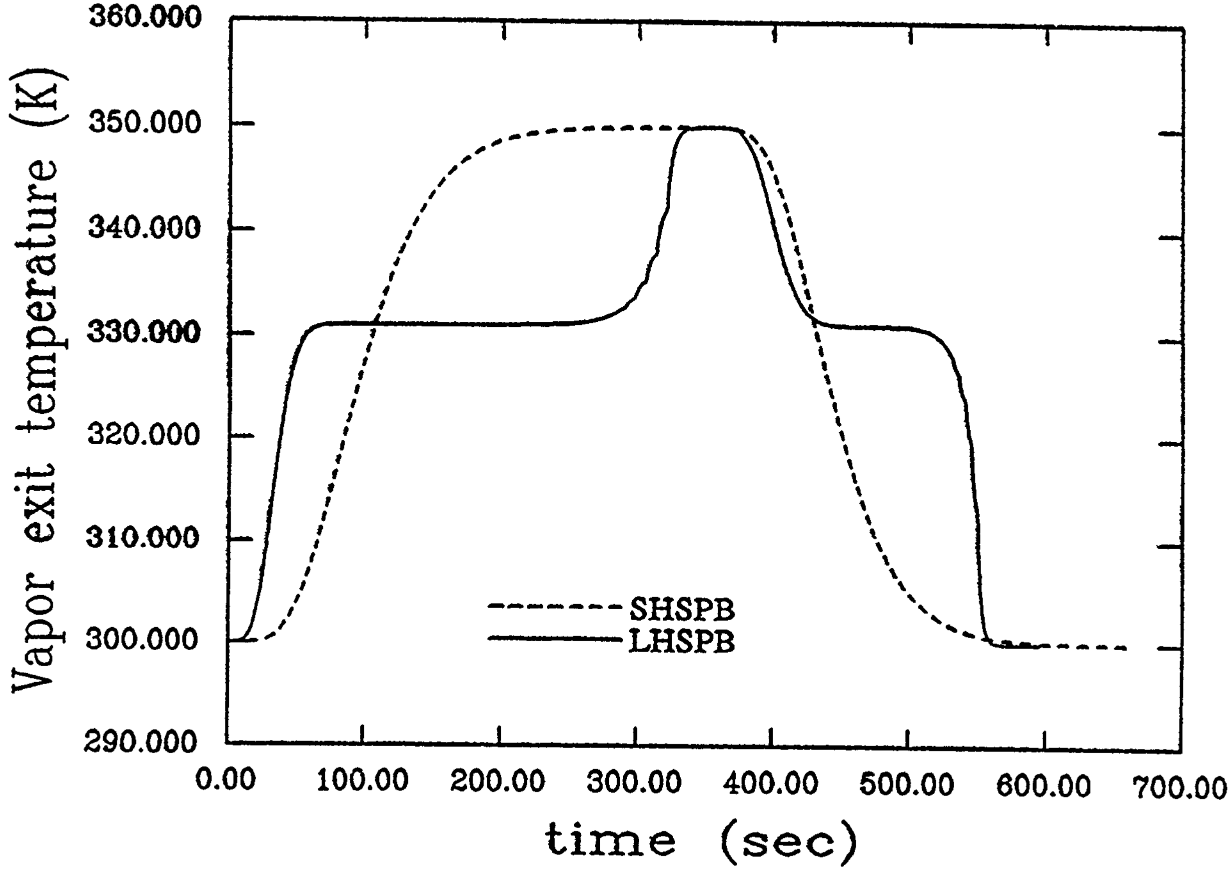

Figure 5.11: Time history of vapor exit temperature for complete charging followed by complete discharging of the packed beds.

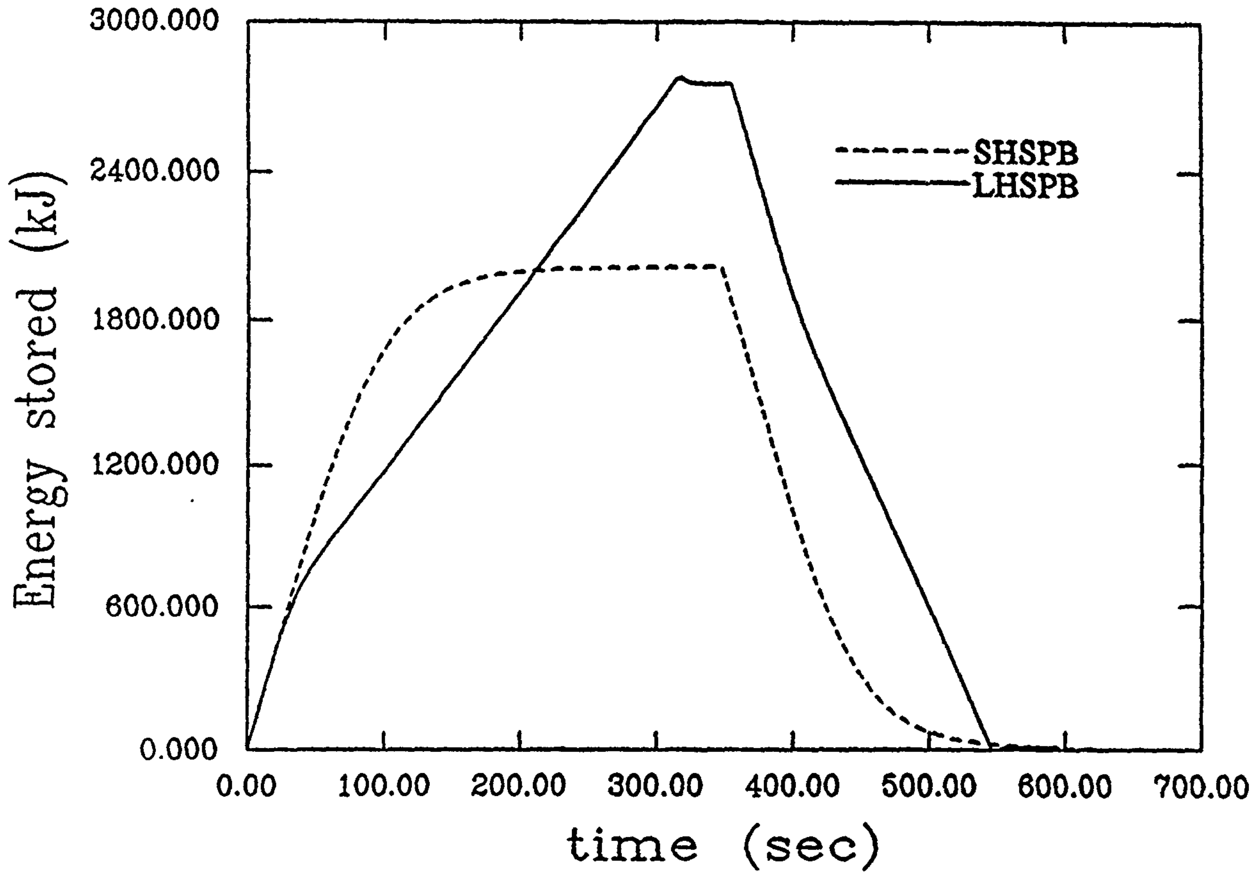

Figure 5.12: Thermal charging and discharging of the SHSPB and the LHSPB.

5.5 Conclusions

The transient processes of thermal charging and discharging of an SHSPB and an LHSPB with a compressible working fluid were simulated. The investigations showed distinctly different energy storage characteristics for these two kinds of packed beds. The high energy storage density of the LHSPB was clearly observed from the studies carried out. For the two energy storage materials considered, although the density of the sensible heat storage material (1% Carbon steel) was approximately 9 times larger than that of the PCM (myristic acid), the total energy storage capacity of the LHSPB was higher.

Use of a compressible working fluid and accounting for the inertia effects in the vapor phase momentum equation resulted in a time-dependent mass-flow rate through the packed bed. Utilization of non-local-thermal-equilibrium analysis was found to be crucial especially in the case of LHSPB.

Also, in the case of the LHSPB it was observed that the thermal charging and discharging times differed considerably. The main reason for this difference is that for a major portion of the charging or discharging process the PCM temperature downstream of the packed bed remains constant at the melting/freezing temperature of the PCM. An important conclusion which was obtained from our results is that closer the PCM melting/freezing temperature to the charging temperature (vapor inlet temperature during thermal charging mode) longer will be the time taken for charging and shorter will be the time taken for discharging of the packed bed. Likewise, closer the PCM melting/freezing temperature to the discharging temperature (vapor inlet temperature during thermal discharging mode) longer will be the time taken for discharging and shorter will be the time taken for charging of the packed bed.

SECTION VI

ANALYSIS OF OSCILLATING COMPRESSIBLE FLOW THROUGH A PACKED BED

6.1 Introduction

In storage of thermal energy in packed beds, the dynamic behavior of the packed bed system is an important consideration. Ideal conditions of constant temperature and pressure inlet conditions are quite difficult to maintain. Therefore, examining those conditions more closely approximating the real-life situations, such as variable pressure or variable temperature inlet conditions, provides better insight to such problems.

Rigorous models have been developed by Vafai and Sozen (1990), and Sozen and Vafai (1990) for the forced convective flow of a superheated ideal gas and forced convective condensing flow of a vapor through a packed bed as presented in Sections II and III. The former of these studies concentrated on the parameters influencing the LTE and two-dimensionality of the transport phenomena while the latter one concentrates on the condensing flows through a packed bed. The LTE assumption has not been used in any of these studies, and inertia effects have been accounted for by the use of the Ergun-Forchheimer relation rather than Darcy flow formulation.

In the present section, compressible flow of an ideal gas through a packed bed is investigated for oscillating inlet pressure and oscillating inlet temperature boundary conditions in order to represent more closely the real-life conditions for certain situations. For example, in real applications, more often than not, some form of oscillation prevails in the inlet pressure or temperature. It is then crucial to know the qualitative and quantitative effects of the oscillations on the thermal charging characteristics and the net energy storage capabilities of the packed bed. Our aim is to analyze the behavior of the transport processes

and energy storage characteristics in these oscillating boundary condition flows through porous media with specific attention on packed beds.

6.2 Problem statement and formulation

A rectangular packed bed is assumed to be formed by regularly shaped and sized spheres packed between two horizontal walls. The schematic diagram of the physical system under consideration is depicted in Figure 6.1. Relatively high-speed flows are considered in the present study and, therefore, the flow is essentially forced convective in nature. In the present study the top and bottom walls are assumed to be insulated, and the depth to be infinitely long, thus, rendering the problem essentially one-dimensional. The working fluid was taken to be superheated Refrigerant-12 which was modeled as an ideal gas, while the material of the packed bed particles was chosen to be 1% carbon-steel. The governing equations following the previous section are given as follows:

$$\frac{\partial}{\partial t}\left(\varepsilon < \rho_v >^v\right) + \frac{\partial}{\partial x}\left(< \rho_v >^v < u_v >\right) = 0 \tag{6.1}$$

$$\frac{\partial < P_v >^v}{\partial x} = -\frac{< \rho_v >^v F \varepsilon}{K_v^{1/2}} < u_v >^2 - \frac{\mu_v}{K_v} < u_v > \tag{6.2}$$

$$\begin{aligned} \varepsilon < \rho_v >^v c_{p_v} \frac{\partial < T_v >^v}{\partial t} + c_{p_v} < \rho_v >^v < u_v > \frac{\partial < T_v >^v}{\partial x} \\ = \frac{\partial}{\partial x}\left\{k_{veff} \frac{\partial < T_v >^v}{\partial x}\right\} + h_{sv} a_{sv} \left\{< T_s >^s - < T_v >^v\right\} \end{aligned} \tag{6.3}$$

$$(1-\varepsilon)\rho_s c_{p_s} \frac{\partial < T_s >^s}{\partial t} = \frac{\partial}{\partial x}\left\{k_{seff} \frac{\partial < T_s >^s}{\partial x}\right\} - h_{sv} a_{sv} \left\{< T_s >^s - < T_v >^v\right\} \tag{6.4}$$

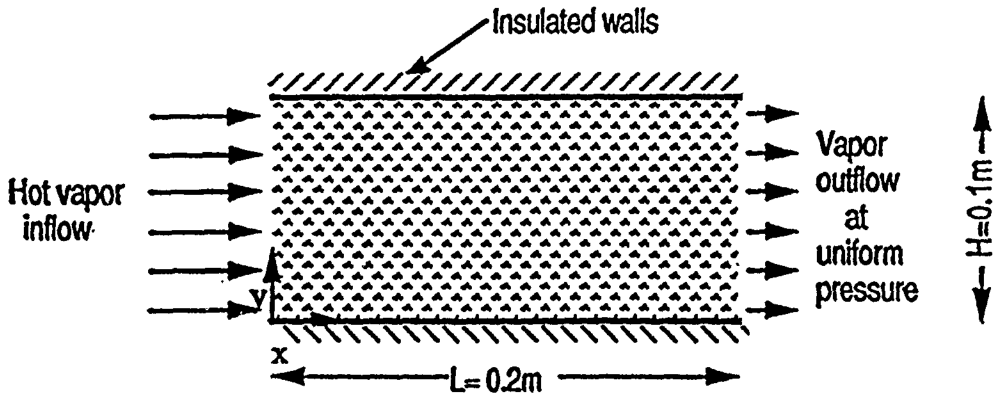

Figure 6.1: Schematic diagram of the problem.

$$< P_v >^v = < \rho_v >^v R < T_v >^v \tag{6.5}$$

These equations represent the gas phase continuity equation, gas phase momentum equation, gas phase energy equation, solid phase energy equation and the equation of state for the working fluid, respectively, where the unknown variables solved from these equations are, respectively, $< \rho_v >^v$, $< u_v >$, $< T_v >^v$, $< T_s >^s$, and $< P_v >^v$.

Modeling of the permeability of the packed bed, K_v, and the geometric function F appearing in the gas phase momentum equation, the effective thermal conductivities, the fluid-to-particle heat transfer coefficient and the specific interfacial surface area of the packed bed was performed as in Section II.

6.3 Initial and boundary conditions

The initial conditions employed in the solution of the problem were:

$$\begin{aligned} &P_v(x, t=0) = P_0 \\ &T_v(x, t=0) = T_s(x, t=0) = T_0 \\ &u_v(x, t=0) = 0 \end{aligned} \tag{6.6}$$

corresponding values of ρ_v being computed from equation (5).

The boundary conditions used for the case with oscillating inlet gas pressure can be mathematically expressed as:

$$\begin{aligned} &P_v(x=0, t) = P_{av} + A\,\mathrm{Cos}(2\pi f t) \\ &P_v(x=L, t) = P_0 \\ &T_v(x=0, t) = T_{vav} \end{aligned} \tag{6.7}$$

where f is the frequency and A is the amplitude of the cosinusoidal variation of the inlet pressure, and again the corresponding ρ_v values are computed from equation (5).

The boundary conditions employed for the case with oscillating gas phase inlet temperature condition can similarly be expressed as:

$$
\begin{aligned}
&P_v(x=0,t)=P_{av}\\
&P_v(x=L,t)=P_0\\
&T_v(x=0,t)=T_{vav}+B\,\mathrm{Cos}(2\pi f t)
\end{aligned}
\tag{6.8}
$$

where f is the frequency and B is the amplitude of the variation of the inlet gas temperature. ρ_v is computed as in the previous case. The boundary conditions for the case with constant temperature and constant pressure at the inlet are similar to those in equation (12) with A being equal to zero.

In the case studies performed, the following values have been used for the variables:

$$P_0 = 100\ \text{kPa} \qquad P_{av} = 104\ \text{kPa} \qquad T_0 = 300\ \text{K} \qquad T_{vav} = 350\ \text{K}.$$

The nominal particle Reynolds number for the average inlet pressure and temperature was 745.

6.4 Results and discussions

The solution procedure was exactly similar to those of the problems in the previous sections. In order to explore any differences in the transport phenomena and energy storage characteristics of the packed bed with oscillating flow boundary conditions from those of constant boundary conditions, we considered these cases for different ranges by using different values for parameters A, f, and B in equations (6.7) and (6.8) in different runs.

In previous sections we have observed that for constant temperature and pressure boundary conditions at the inlet, the solution of the problem had two distinct stages. Namely, the *early stage* during which the pressure evolution in the packed bed takes place very rapidly causing drastic variation in the other field variables, and the *later stage* in which the changes in the field variables are mostly temperature dependent. The

distributions of different field variables along the packed bed during the early stage are depicted in Figure 6.2 for the case with constant inlet temperature and pressure. In this figure the gas phase density was nondimensionalized with respect to an average density value calculated from the equation of state using average values of gas phase pressure and temperature, i.e., average of the initial and inlet conditions. Likewise, the nominal value of the velocity used for nondimensionalizing the gas phase velocity was computed from equation (6.2) based on the average density and the average pressure gradient along the packed bed. These characteristics have been discussed in detail in Sections II and III. Similar characteristics were observed in the present work with the exception that in the case of oscillating inlet pressure condition the pressure distribution within the packed bed was not very close linearly as it was in the other cases. Rather, it showed an oscillating behavior along the packed bed.

First, temperature variation of the solid and fluid phases within the packed bed with respect to time was considered. Figure 6.3 depicts this variation for the case with constant temperature and constant pressure inlet boundary conditions. For convenience this case will be called Case I. Figure 6.4 shows the temperature variations for constant temperature, and oscillating pressure at the inlet of the packed bed. This case will be called Case II. For Case II, the chosen parameters were $A = 2\,\mathrm{kPa}$ and $f = 0.05\mathrm{Hz}$. For Case III, which is for constant pressure but oscillating temperature inlet boundary condition, the temperature variations are shown in Figure 6.5. For this case we had $B = 25\mathrm{K}$ and $f = 0.05\mathrm{Hz}$. Qualitatively Figures 6.3 and 6.4 depict similar behavior for the solid and fluid phase temperature variations with larger temperature difference between the two phases at the beginning, and narrowing difference as the thermal front moves within the packed bed. This behavior is also valid for Case III in the downstream section of the packed bed but not at the entrance region because of the oscillating temperature inlet

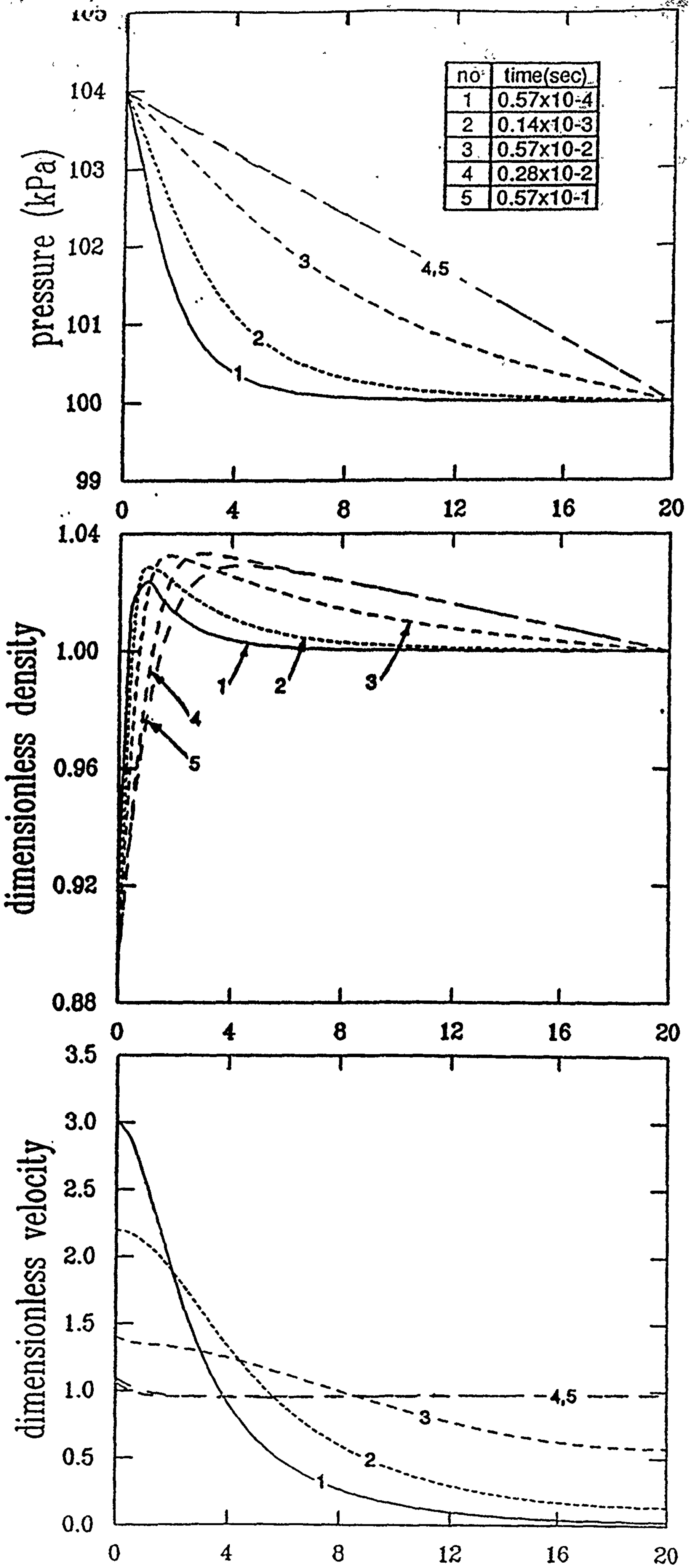

Figure 6.2: Variation of different field variables during *early stage*.

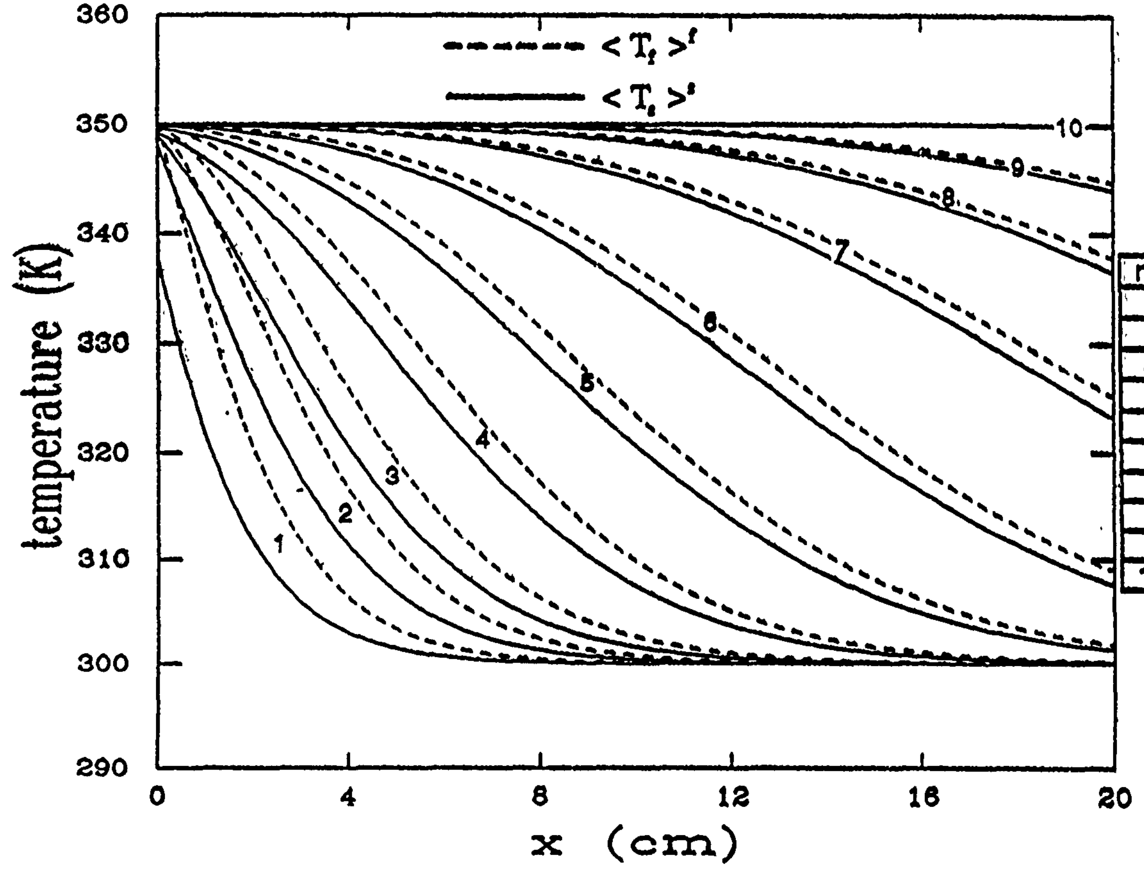

no	time(sec)
1	5.8
2	12.9
3	20.0
4	34.2
5	55.5
6	83.9
7	126.5
8	169.1
9	211.6
10	382.0

Figure 6.3: Temperature distribution in the packed bed, A = 0, B = 0.

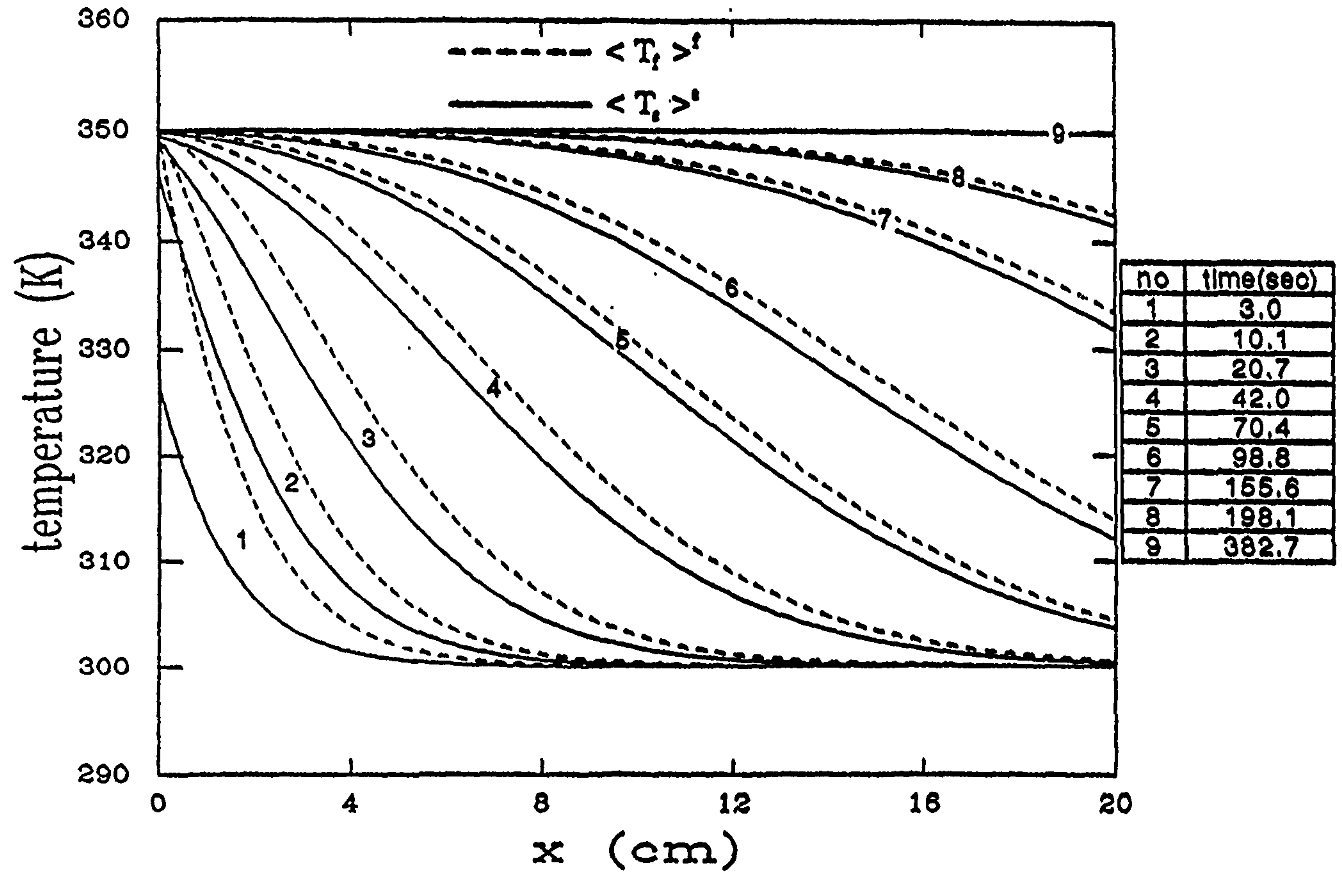

Figure 6.4: Temperature distribution in the packed bed, A = 2 kPa, f = 0.05 Hz.

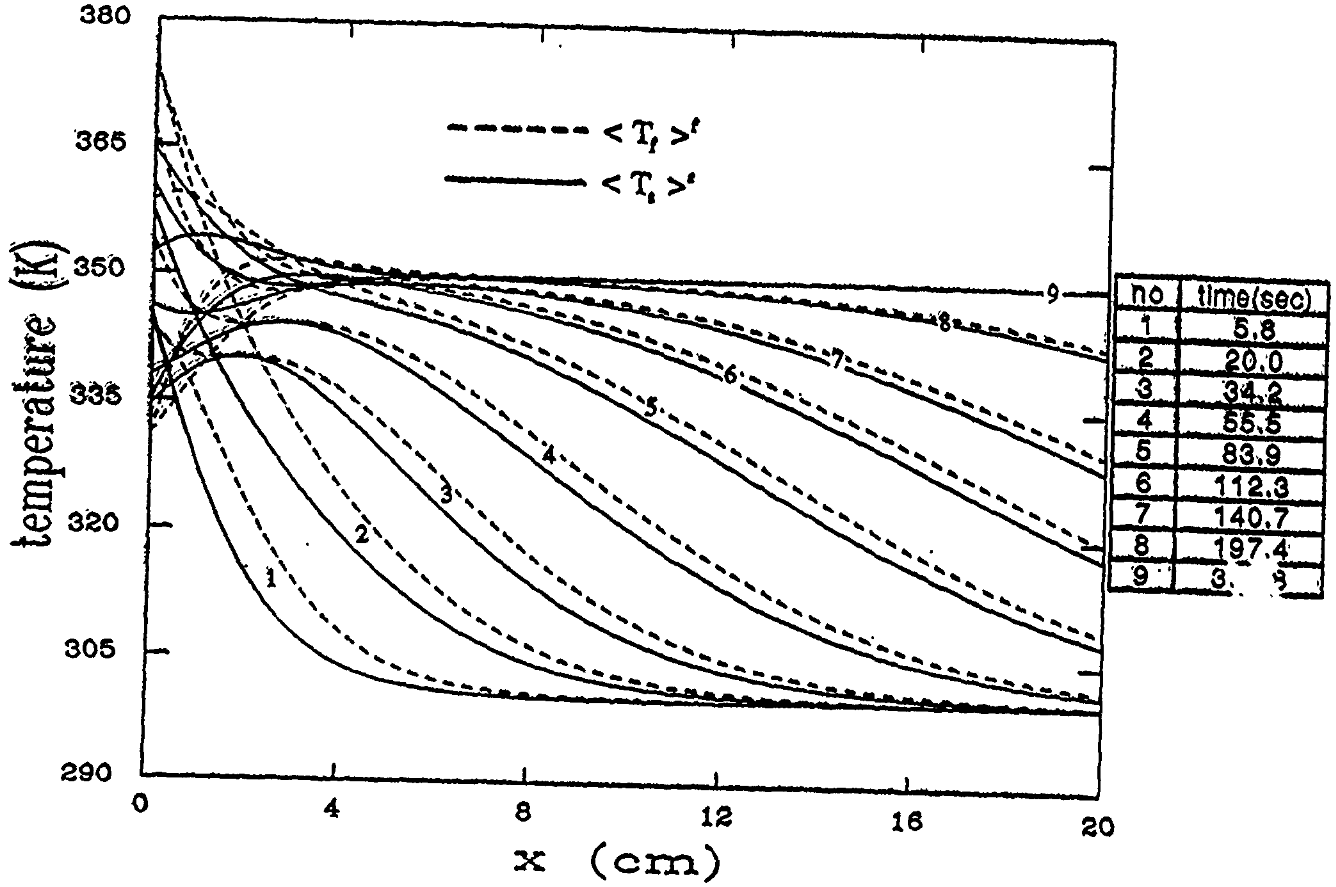

Figure 6.5: Temperature distribution in the packed bed, B = 25 K, $f = 0.05$ Hz.

condition. At the entrance region the temperature difference between the solid and fluid phases can increase or decrease due to the oscillating inlet fluid temperature and due to the fact that there will be a lag time for the response of the solid phase temperature to this oscillation.

Figure 6.6 depicts the variation of the gas phase density, pressure and velocity at four different time levels for three different cases for Case II during one complete cycle of the pressure oscillation. These three cases involved different values for parameters A and f as shown in Figure 6.6. Cases in Figures 6.6(a) and 6.6(b) have the same amplitude but different frequency of inlet pressure oscillation, where cases in Figures 6.6(b) and 6.6(c) have the same frequency but different amplitudes of inlet pressure oscillation. In each case the four time levels depicted were chosen so that they would span over one complete cycle of oscillation (the very first cycle in the process). Although the pressure distribution is nearly linear along the packed bed during the first three time levels, a careful examination of the figures at the fourth time level reveals that the pressure distribution in the packed bed picks up from the oscillating inlet condition and shows an oscillating behavior along the packed bed too, i.e., spatial oscillation in addition to temporal oscillation. Also as can be expected, the range of variation of the gas phase velocity is higher in the case with larger amplitude in the inlet pressure oscillation. The comparison of the range of velocity variation in Figure 6.6(c) compared to those in Figures 6.6(a) and 6.6(b) reveals this clearly. The variation in the gas phase density can be explained by the use of the equation of state and the variation of the pressure and temperature along the packed bed. At the entrance region the sharp decrease in the temperature at the beginning of the charging process requires an increase in the gas phase density since the rate of decrease in gas phase pressure is less pronounced than that in temperature.

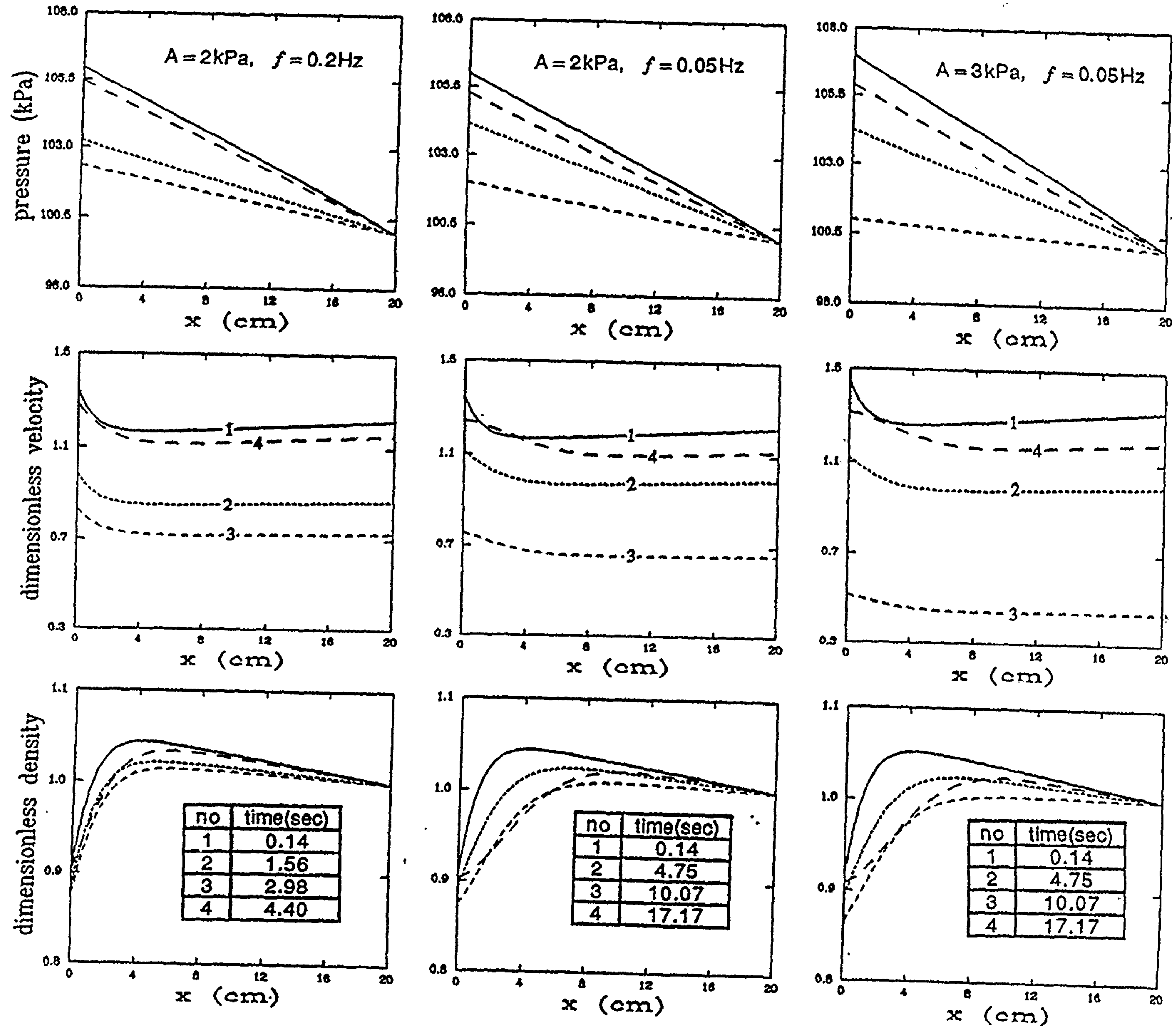

Figure 6.6: Variation of field variables during the first complete pressure cycle.

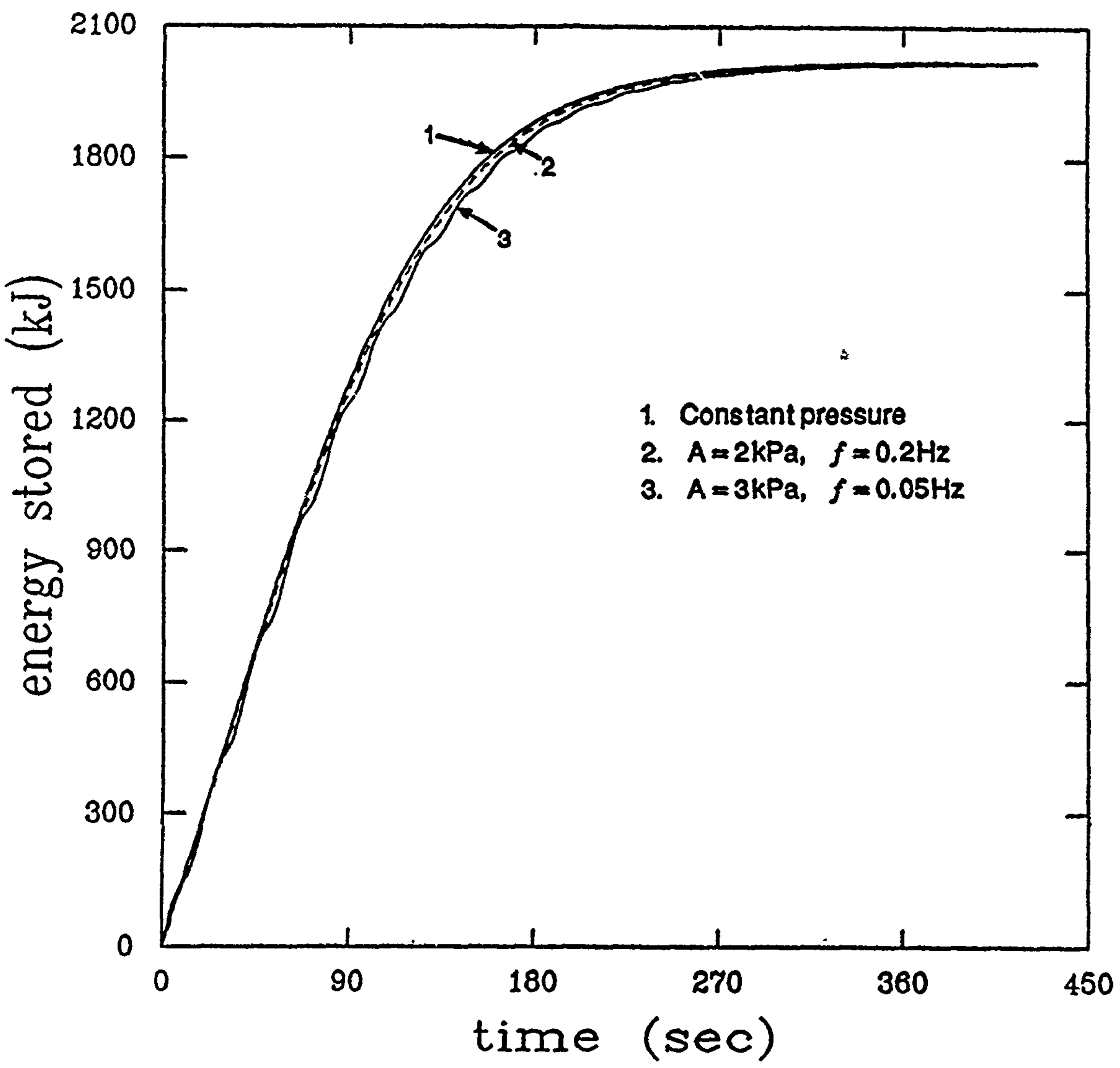

Figure 6.7: Time history of energy storage in the packed bed.

Figure 6.7 depicts the time history of the net energy storage per unit width of the packed bed for Case I and two cases of Case II. As expected, the asymptotic value of the total net energy stored in each case is the same. As the amplitude of the oscillations in the inlet pressure increases, the oscillations in the net energy stored become more pronounced since the oscillations in effect result in oscillations in the mass flow rate of the gas phase through the packed bed. Larger frequencies, on the other hand, tend to smooth the variation in the net energy storage.

The variations in the rate of heat flow into and out of the packed bed for Case I and Case II with $A = 2\,kPa$ and $f = 0.05Hz$ are depicted in Figure 6.8. The oscillating behavior in this figure is that of Case II and the smooth variation is that of Case I. Although the heat flow rates into and out of the packed bed oscillate in Case II due to the oscillation in the inlet pressure and, hence, the mass flow rate, the average variation of each of these quantities is qualitatively very similar to those of Case I, i.e., the variation of the difference between the heat flowing into and out of the packed bed has the same trend in both cases.

The comparison of the rate of heat flow into and out of the packed bed for Cases I and III is shown in Figure 6.9. For Case III in this figure, $B = 25K$ and $f = 0.05Hz$. Again, due to the oscillating inlet temperature, the density and velocity of the gas and, hence, the mass flow rate into the packed bed oscillates. However, this oscillation in temperature has a less pronounced effect on the heat flow rates into and out of the packed bed than the oscillation in the inlet pressure has as shown in Figure 6.8. The difference between the scales of Figures 6.8 and 6.9 should be noted. Part of the reason for this behavior may be attributed to the fact that, in calculating the gas phase velocity, the pressure gradient term in the gas phase momentum equation is much more dominant than the inertia term which involves the gas phase density, which in turn varies proportional to

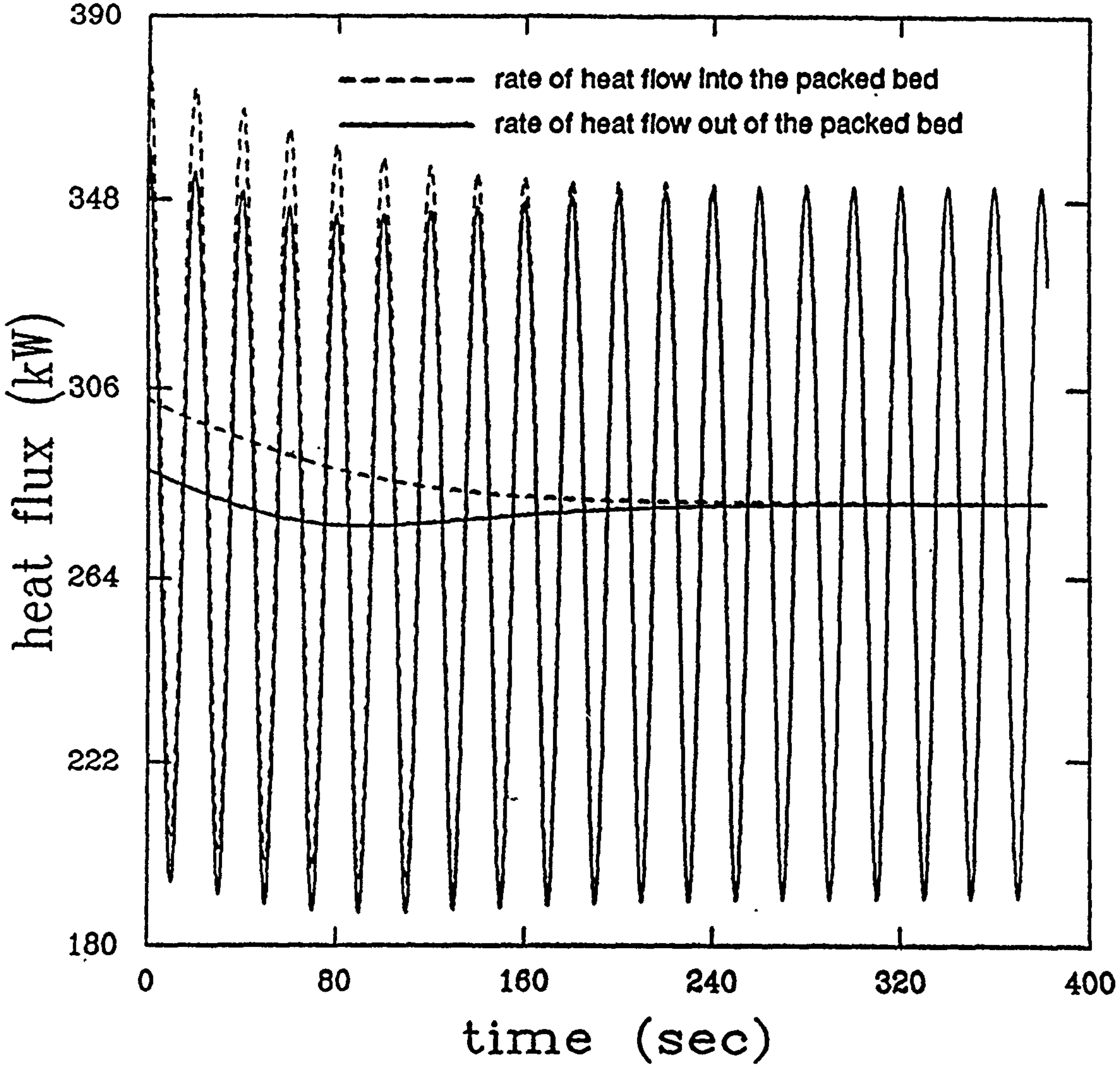

Figure 6.8: Time history of heat flow rates into and out of the packed bed.

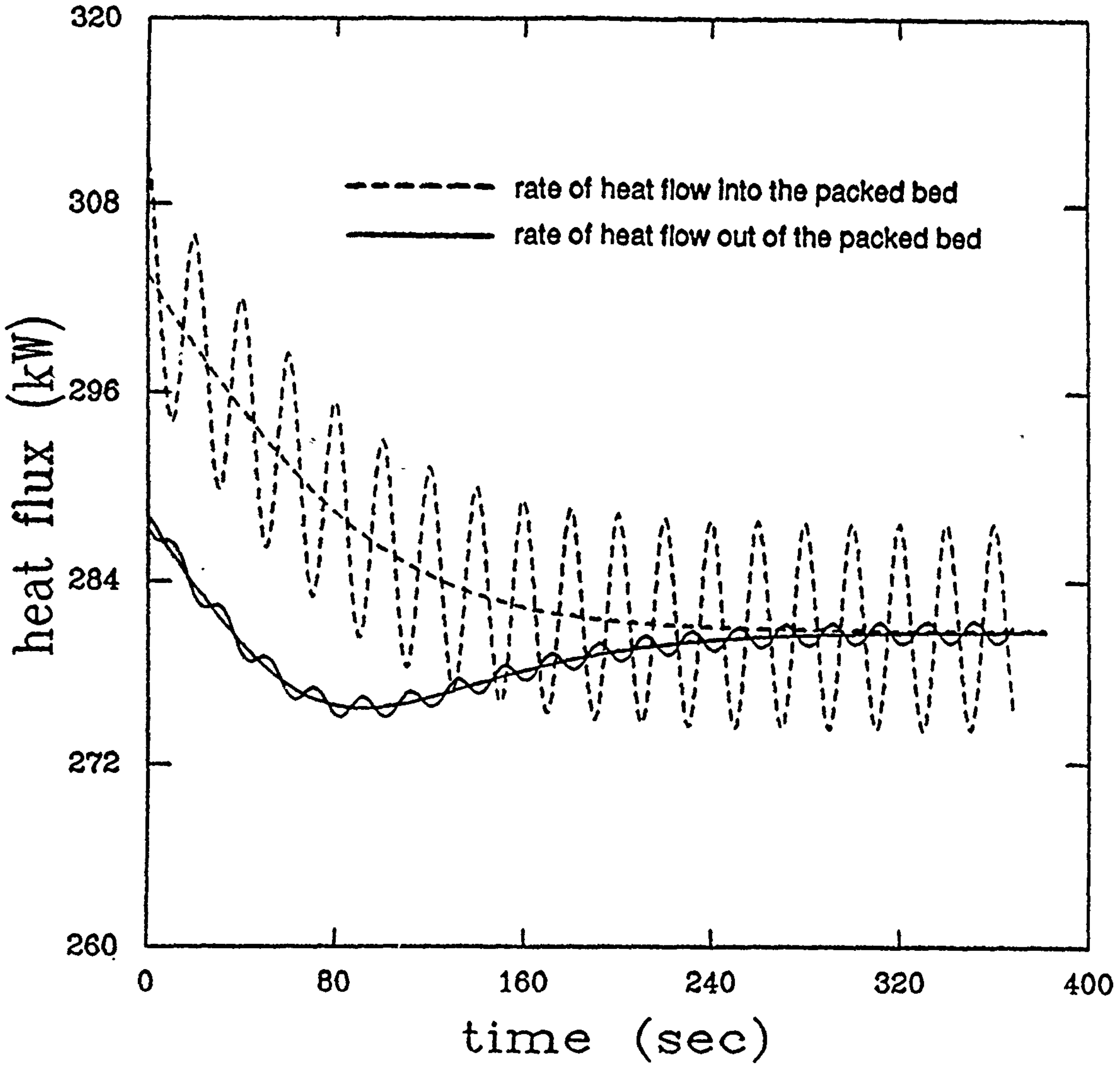

Figure 6.9: Time history of heat flow rates into and out of the packed bed.

the temperature. Thus, the former affects the variation in the gas phase velocity more, causing a more pronounced oscillation in the mass flow rate of the gas phase.

In Case III we cannot talk about the complete thermal charging of the packed bed due to the oscillating inlet temperature boundary condition. Because at the entrance region of the packed bed, due to this oscillation, the solid temperature also oscillates (not necessarily at the same frequency and amplitude, because the heat capacity of the solid phase is much larger than that of the working fluid and, therefore, the temperature of the solid phase cannot follow the temperature of the incoming gas at the same frequency and amplitude). Yet, one can speak of a pseudo-charging of the packed bed. Figure 6.10 depicts this pseudo-charging behavior (representing the net energy stored within the packed bed). This behavior is different from that of Case II. Because in Case II, although the gas phase inlet pressure is oscillating, since the gas phase inlet temperature is kept constant at the highest value that can be attained by the packed bed particles, there is continuous thermal energy storage within the packed bed until the packed bed is thermally fully charged. However, in Case III, due to the variation of the solid temperature in the entrance region, there are alternating energy storage and removal from the packed bed.

In order to find out whether the qualitative behavior of the energy storage characteristics changes with particle Reynolds number (Re_p), cases with different nominal Re_p were investigated. Higher particle Reynolds numbers were obtained by increasing the mean inlet pressure. The results are depicted in Figure 6.11 for three different cases in which the amplitude of the inlet pressure oscillations was the same. As can be seen, the qualitative behavior is similar in each case although higher nominal Reynolds numbers, meaning higher mass flow rates, cause faster charging of the packed bed. The effect of the pressure oscillations is seen most clearly in the case with lowest Re_p since the amplitude of

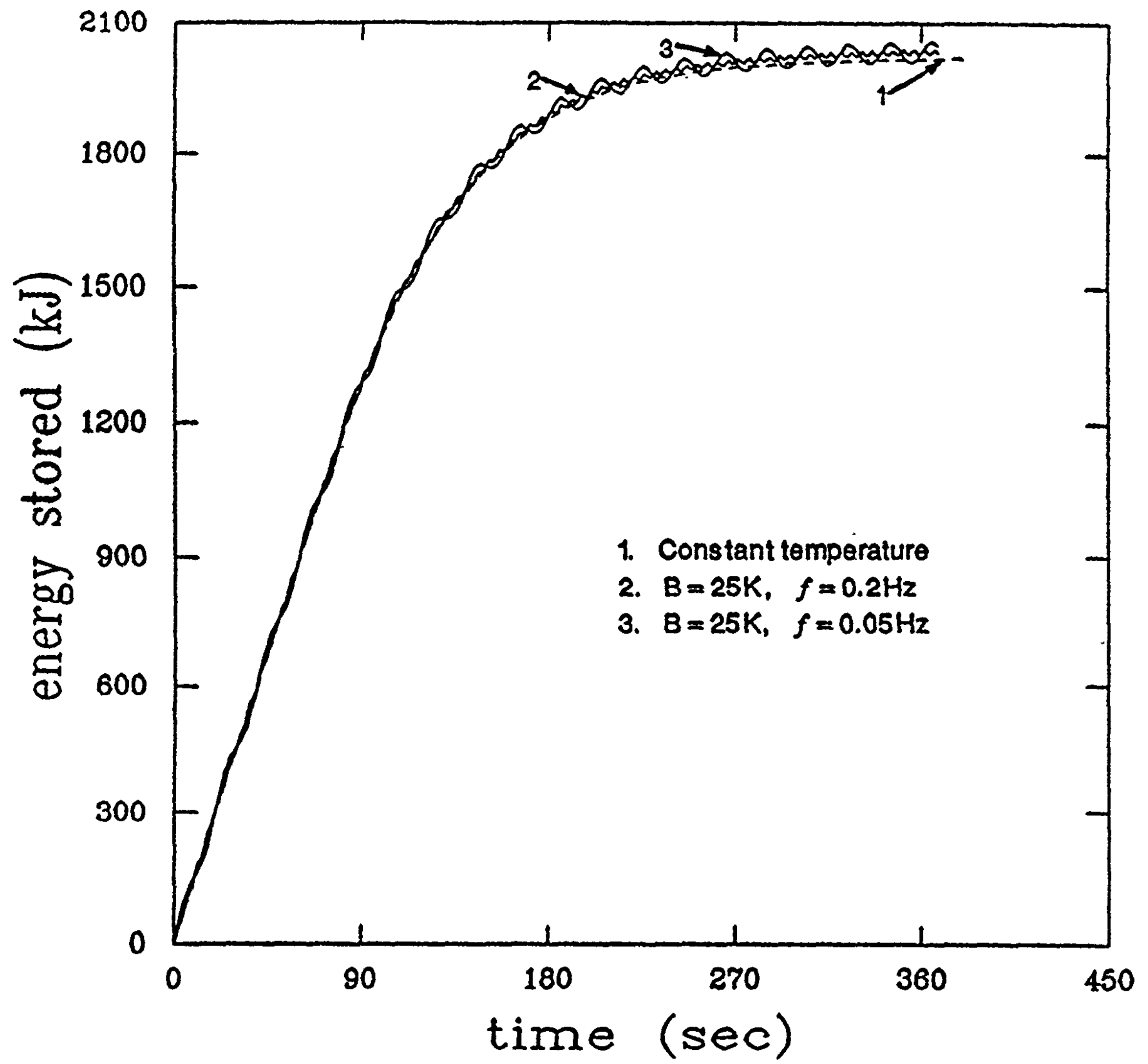

Figure 6.10: Time history of energy storage in the packed bed.

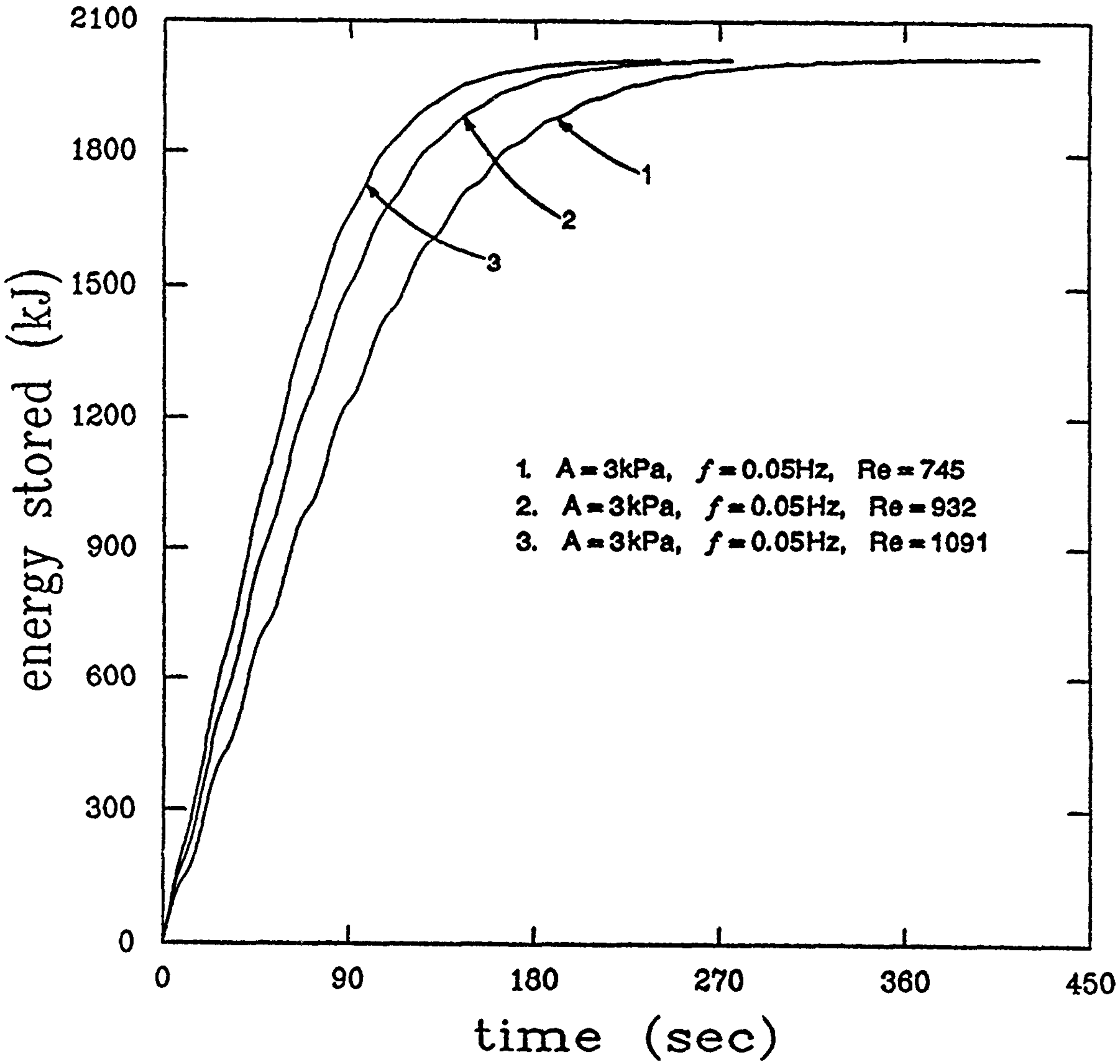

Figure 6.11: Time history of energy storage in the packed bed.

the oscillations is largest relative to the global pressure difference applied across the packed bed for that case.

6.5 Conclusions

The dynamic response of sensible heat storage packed beds with oscillating inlet boundary conditions has been studied numerically for forced convective flow of a compressible fluid. A finite difference scheme with uniform grid size was employed. It was found that the average energy storage behavior did not have major differences in the cases of constant or oscillating inlet boundary conditions although the field variables showed oscillating behavior in cases of oscillating boundary conditions. As expected, the variation of the energy storage was found to become smoother as the amplitude of the oscillation of the inlet condition decreased and/or as the frequency increased. It was also observed that due to the nature of the governing equations the response of the field variables was more sensitive to the amplitude of the fluid pressure variation than to that of the fluid temperature variation at the inlet of the packed bed.

BIBLIOGRAPHY

Ananthanarayanan, V., Sahai, Y., Mobley, C.E., and Rapp, R.A., 1987, "Modeling of Fixed Bed Heat Storage Units Utilizing Phase Change Materials," Metallurgical Transactions B, Vol. 18B, pp. 339-346

Barker, J.J., 1965, "Heat Transfer in Packed Beds," Industrial and Engineering Chemistry, Vol. 57(4), pp. 43-51

Baumeister, E.B., and Bennett, C.O., 1958, "Fluid Particle Heat Transfer in Packed Beds," AIChE Journal, Vol. 4(1), pp. 69-74

Benanati, R.F., and Brosilow, C.B., 1962, "Void Fraction Distribution in Beds of Spheres," AIChE Journal, Vol. 8(3), pp. 359-361

Berger, D., and Pei, D.C.T., 1973, "Drying of Hygroscopic Capillary Porous Solids- A Theoretical Approach," International Journal of Heat and Mass Transfer, Vol. 16, pp. 293-301

Bhattacharyya, D., and Pei, D.C.T., 1975, "Heat Transfer in Fixed Bed Gas-solid Systems," Chemical Engineering Science, Vol. 30, pp. 293-300

Dullien, F.A.L., 1979, *Porous Media Fluid Transport and Pore Structure*, Academic Press, New York

Eckert, E. R. G., and Pfender, E., 1980, "Heat and Mass Transfer in Porous Media with Phase Change," In Proc. 6th International Heat Transfer Conf., Vol. 6, pp.1-12

Ergun, S., 1952, "Fluid Flow Through Packed Columns," Chemical Engineering Progress, Vol. 48, pp. 89-94

Gamson, B.W., Thodos, G., and Hougen, O.A., 1943, "Heat, Mass and Momentum Transfer in the Flow of Gases Through Granular Solids," Transactions AIChE, Vol. 39, pp. 1-35

Goldstein, M.E., and Siegel, R., 1971, "Analysis of Heat Transfer for Compressible Flow in a Two-dimensional Porous Media," International Journal of Heat and Mass Transfer, Vol. 14, pp. 1677-1690

Gray, W.G., 1975, "A Derivation of the Equations for Multi-phase Transport," International Journal of Heat and Mass Transfer, Vol. 30, pp. 229-233

Kaviany, M., and Mittal, M., 1987, "Funicular State in Drying of a Porous Slab," International Journal of Heat and Mass Transfer, Vol. 30, pp. 1407-1418

Kidder, R.E., and La Habra, 1957, "Unsteady Flow of Gas Through a Semi-infinite Porous Medium," Journal of Applied Mechanics, Vol. 24, pp. 329-332

Lane, G. A., 1986, *Solar Heat Storage: Latent Heat Material, Vol. II*, CRC Press, Inc. Boca Raton, FL.

Marianowski, L.G., and Maru, H.C., 1977, "Latent Heat Thermal Energy Storage Systems above 450°C," 12th IECEC, 779090, p. 555

Morrison, F.A, 1972, "Transient Gas Flow in a Porous Column," Industrial and Engineering Chemistry Fundamentals, Vol. 11(2), pp. 191-197

Motakef, S., and El-Masri, M., 1986, "Simultaneous Heat and Mass Transfer with Phase Change in a Porous Slab, " International Journal of Heat and Mass Transfer, Vol. 29, pp. 1503-1512

Nilson, R.H., 1981, "Transient Fluid Flow in Porous Media: Inertia-dominated to Viscous-dominated Transition," ASME Journal of Fluids Engineering, Vol. 103, pp. 339-343

Nilson, R. H., and Montoya, P. C., 1980, "Experiments on Transient Condensing Flow through a Porous Medium," ASME Journal of Heat Transfer, Vol. 102, pp.489-494

Ogniewicz,Y., and Tien, C. L., 1981, "Analysis of Condensation in Porous Insulation," International Journal of Heat and Mass Transfer, Vol. 24, pp. 421-429

Pitts, D.R., and Hong, J. S., 1987, "Analysis of the Transient Thermal Performance of a Latent Heat Storage Packed Bed," in *Multiphase Transport in Porous Media*, ASME FED-Vol. 60, HTD-Vol. 91, pp. 51-54

Plumb, O.A., Spolek, G.A., and Olmstead, B.A., 1985, "Heat and Mass Transfer in Wood During Drying," International Journal of Heat and Mass Transfer, Vol. 28, pp. 1669-1678

Riaz, M., 1977, "Analytical Solution for Single- and Two-phase Models of Packed-bed Thermal Storage Systems," ASME Journal of Heat Transfer, Vol. 99, pp. 489-492

Schumann,T.E.W., 1929, "Heat Transfer: A Liquid Flowing Through a Porous Prism," Journal of the Franklin Institute, Vol. 208, pp. 405-416

Sozen, M., and Vafai, K., 1990, "Analysis of the non-thermal equilibrium condensing flow of a gas through a packed bed," International Journal of Heat Mass Transfer, Vol. 33, pp. 1247-1261

Spiga, G., and Spiga, M., 1981, A rigorous solution to a heat transfer two phase model in porous media and packed beds. International Journal of Heat and Mass Transfer, Vol. 24, pp. 355-364

Torab, H., and Chang, W.S., 1988, "High Temperature Thermal Energy Storage for Power Systems," in *Analysis of Time Dependent Thermal Systems*, ASME AES-Vol. 5, p. 71

Udell, K. S., 1985, "Heat Transfer in Porous Media Considering Phase Change and Capillarity.- Heat Pipe Effect," International Journal of Heat and Mass Transfer, Vol. 28, pp. 485-495

Udell, K.S., and Fitch, J., 1985, "Heat and Mass Transfer in Capillary Porous Media Considering Evaporation, Condensation and Non-Condensible Gas Effects," in *Heat Transfer in Porous Media and Particulate Flows*, ASME HTD-Vol. 46, pp. 103-110

Vafai, K., 1984, "Convective Flow and Heat Transfer in Variable-porosity Media," Journal of Fluid Mechanics, Vol. 147, pp. 233-259

Vafai, K., and Sarkar, S., 1986, "Condensation Effects in a Fibrous Insulation Slab," ASME Journal of Heat Transfer, Vol. 108, pp. 667-675

Vafai, K., and Sozen, M., 1990, "Analysis of energy and momentum transport for a flow of a gas in a porous bed," ASME Journal of Heat Transfer, Vol. 112(3), pp. 690-699

Vafai, K., and Tien, C.L., 1981, "Boundary and Inertia Effects on Flow and Heat Transfer in Porous Media," International Journal of Heat and Mass Transfer, Vol. 24, pp. 195-203

Vafai, K., and Whitaker, S., 1986, "Simultaneous Heat and Mass Transfer Accompanied by Phase Change in Porous Insulation," ASME Journal of Heat transfer, Vol. 108, pp. 132-140

Whitaker, S., 1977, "Simultaneous Heat, Mass, and Momentum Transfer in Porous Media: A Theory of Drying," Advances in Heat Transfer, Vol. 13, pp. 119-203

☆ U.S. GOVERNMENT PRINTING OFFICE: 1992 - 648-127/62179